www.icgst.com

# The International Congress for global Science and Technology

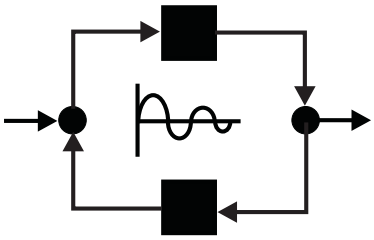

# ICGST International Journal on Automatic Control & System Engineering (ACSE)

**Volume (15), Issue (I)**
**June 2015**

**wwww.icgst.com**
**www.icgst-amc.com**
**www.icgst-ees.com**

ACSE Journal
ISSN:  Print 1687-4811
ISSN Online 1687-482X
ISSN CD-ROM 1687-4838

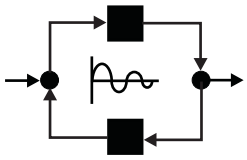

# Table of Contents


| Papers | Pages |
|---|---|
| P1111451356,<br>Mohd Syakirin Ramli and Shigeru Yamamoto,<br>A Lyapunov Function Approach to Dynamic Stable Matching in A Multi-agent system, | 1--13 |
| P1111510361,<br>Vinay S. Prabhavalkar and Vijay R. Ghorpade,<br>A Novel Approach to Reduce the Spectral Ping-Pong Effect for the Mobility Management Framework in a Cognitive Radio Cellular Network., | 15--22 |
| P1111518375,<br>Kottam Pranay Kumar and K.Uday reddy and G.Jithendra Naidu and S.Siva Prasad,<br>DESIGN OF SOLAR POWERED MOBILE CHARGER WITH POWERBANK USING SUPERCAPACITOR AND STORAGE BATTERY FOR FAST CHARGING", | 23--30 |
| P1111521381,<br>N. Krishna Kumari and G. Tulasi Ram Das and M.P.Soni,<br>Online Stator Reference Flux Approach to Torque Ripple Minimization for SPM Drive using Fuzzy and PI Controllers, | 31--38 |
| P1111519376,<br>Ranuva Nageswararao and S.S. Tulasi Ram,<br>Effect of Multiple Particles and Collisions in a 3-Phase Gas Insulated Bus Duct under Switching Impulse Voltage , | 39--45 |
| P1111447354,<br>J.E.Muralidhar and P.Varanasi,<br>An Exotic Robust Performance of PI-Fuzzy Controller Fed BLDC Drive, | 47--53 |

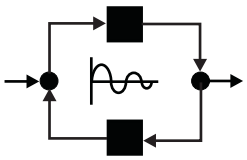

**ICGST International Journal on Automatic Control & System Engineering - (ACSE)**

**A Publication of the International Congress for global Science and Technology - (ICGST)**

**ICGST Editor in Chief: Dr. rer. nat. Ashraf Aboshosha**

**www.icgst.com, www.icgst-amc.com, www.icgst-ees.com**

**editor@icgst.com**

www.icgst.com

# A Lyapunov Function Approach to Dynamic Stable Matching in A Multi-agent System

Mohd Syakirin Ramli[1,3], Shigeru Yamamoto[2]
[1]*Graduate School of Natural Science & Engineering, Kanazawa University, Kakuma-machi, Kanazawa-city, Ishikawa, 920-1192, Japan.*
[2]*Faculty of Electrical and Computer Engineering, Institute of Science and Engineering, Kanazawa University, Kakuma-machi, Kanazawa-city, Ishikawa, 920-1192, Japan.*
[3]*Faculty of Electrical & Electronics Engineering, University Malaysia Pahang, 26600 Pekan, Pahang, Malaysia.*
[1]syakirin@moccos.ec.t.kanazawa-u.ac.jp, [2]shigeru@se.kanazawa-u.ac.jp,

## Abstract

The Stable Marriage Problem (SMP) is a combinatorial optimization problem of finding the stable partnership in a given bipartite graph. In this paper, we investigate the potential of implementing the Lyapunov theory to attain stable matching in a multi-agent system (MAS). In the system, all agents are segregated into two groups, which can be regarded as the men's and women's sets, respectively. A suitable local Lyapunov function is defined for each agent based on a given preference list. A global optimization is formulated by summing the local Lyapunov function of each individual agent. Two control laws (centralized and decentralized) are derived and compared so that dynamic matching between agents is obtained. Current results indicate that the matching and agents formation are stable in the sense of Lyapunov despite the existence of a few blocking pairs.

***Keywords:*** *Stable Marriage Problem, multi-agent system, Gale & Shapley algorithm, Lyapunov function, decentralized control.*

## Nomenclature

| | |
|---|---|
| $\mathcal{E}$ | Set of edges |
| $\mathbb{G}$ | Communication graph |
| $\mathcal{J}_i$ | Set of the same gender agents |
| $\mathcal{K}_i$ | Set of the different gender agents |
| $\mathcal{I}_\mathcal{M}$ | Index set of men |
| $\mathcal{I}_\mathcal{W}$ | Index set of women |
| $\mu$ | Lebesque measure |
| $\mathcal{N}_i$ | Set of neighboring agents to $i$ |
| $\otimes$ | Kronecker product |
| $\overline{\text{co}}$ | Closed convex hull |
| $\mathbb{R}$ | Real numbers |
| $\mathcal{X}$ | Set of agents' positions |
| $a.e.$ | Almost everywhere |
| $B(x,\delta)$ | Closed $\delta$ neighborhood of $x$ |
| $K\{f(\cdot)\}$ | Filippov's differential inclusion |
| $L$ | Laplacian matrix |
| $p_M$ | Partner |

## 1 Introduction

The multi-agents system (MAS) provides a substantial platform in many research areas. Well-established and ongoing discussion topics surrounding MAS vary from formation control (i.e., leader-follower [1], consensus [2], and pursuit [3]) to wireless sensor networks [4], and system tracking [5].

On the other hand, the stable marriage problem (SMP) is a combinatorial optimization problem widely discussed in the area of discrete mathematics. Given a bipartite graph, the ultimate aim of solving a SMP is to find the best match between variables. In 1962, Gale and Shapley [6] were the first to introduce SMP terminology. They proposed an algorithm that, given the preference lists of these sets (i.e., Tables 1 and 2), attained stable matching. The set of pairing is considered stable in the sense of SMP theory if the obtained solution does not indicate the existence of blocking pairs in the matching.

The SMP is widely applied in economic and market studies [7, 8]. Further, it has also been profoundly adopted into computer science [9], engineering [10], and robotics [11]. For a real-case example, see [11] where the authors introduced distributed SMP into autonomous mobile

Table 1: Men's preference list

| | $1^{st}$ | $2^{nd}$ | $3^{rd}$ | $4^{th}$ | $5^{th}$ | $6^{th}$ |
|---|---|---|---|---|---|---|
| $m_1$ | $w_3$ | $w_6$ | $w_5$ | $w_1$ | $w_2$ | $w_4$ |
| $m_2$ | $w_2$ | $w_1$ | $w_5$ | $w_6$ | $w_3$ | $w_4$ |
| $m_3$ | $w_2$ | $w_3$ | $w_1$ | $w_6$ | $w_5$ | $w_4$ |
| $m_4$ | $w_1$ | $w_3$ | $w_2$ | $w_4$ | $w_5$ | $w_6$ |
| $m_5$ | $w_4$ | $w_6$ | $w_2$ | $w_3$ | $w_5$ | $w_1$ |
| $m_6$ | $w_1$ | $w_6$ | $w_4$ | $w_2$ | $w_5$ | $w_3$ |

Table 2: Women's preference list

| | $1^{st}$ | $2^{nd}$ | $3^{rd}$ | $4^{th}$ | $5^{th}$ | $6^{th}$ |
|---|---|---|---|---|---|---|
| $w_1$ | $m_2$ | $m_3$ | $m_5$ | $m_1$ | $m_4$ | $m_6$ |
| $w_2$ | $m_6$ | $m_4$ | $m_2$ | $m_3$ | $m_5$ | $m_1$ |
| $w_3$ | $m_2$ | $m_4$ | $m_3$ | $m_5$ | $m_6$ | $m_1$ |
| $w_4$ | $m_5$ | $m_4$ | $m_1$ | $m_6$ | $m_3$ | $m_2$ |
| $w_5$ | $m_6$ | $m_1$ | $m_5$ | $m_2$ | $m_3$ | $m_4$ |
| $w_6$ | $m_3$ | $m_4$ | $m_2$ | $m_6$ | $m_5$ | $m_1$ |

robots' environments to achieve appropriate matching between robots and their charging stations.

Many proposed methods for solving the SMP are found in the literature. Irving [12] presented an $O(n^2)$ algorithm to determine whether a given problem is an SMP, and if so, to find matching. Conversely, Ehlers [13] presented their main results by following the characterization of Von Neuman Morgenstern stable sets of a one-to-one matching problem. Umeyama [14] analyzed and discussed the weighted matching problem for directed and undirected graphs using eigen-decomposition of the adjacency matrices. Similarly, Almohamad and Duffua [15] proposed a linear programming approach to solve the weighted graph matching problem using the Simplex based algorithm.

The SMP has also been contemplated in heuristic optimization studies. Nakamura *et al.*[16] considered a sex-fair matching in the SMP. Vien and Chung [17] treated SMP as multi-objective fitness functions and solved them using a genetic algorithm. Alternatively, SMP was also solved using Ant Colony Optimization [18], and even elucidation through graphical representation [19, 20].

In a similar fashion to our main objective, Hata and Ishida [21] used the prey-predator strategies based on the Lotka-Volterra model to dynamically obtain stable matching. They designed a set of differential equations that were constructed on the basis of preference lists, each representing the potential pairs in the matching. Then, the stable matching was evaluated based on the exhibitory solutions of the differential equations that give the value of 1.

In contrast, this paper investigates the potential of incorporating the Lyapunov stability theory within the SMP and MAS framework. By designing the suitable control laws to steer the agents' motion so that they dynamically seek their stable partners, we anticipate stable matching through Lyapunov function minimization. The initial proposal presented in [22] considers a simple case of three-pairs SMP. We assume that the agents are segregated into two sets where each represents the men's and women's groups, respectively. Similar to the original SMP [6] where each agent ranks his/her preferred partner in the preference list, we further utilize this information to determine the weighting gains between agents. These gains are then used to define the appropriate Lyapunov function where it exhibits minimum value once the agents are matched with their suitable partners.

In our work, we consider centralized and decentralized control strategies to dynamically attain stable matching between agents. When the centralized control strategy is executed, the total agents dynamics is viewed as a smooth function. Conversely, a non-smooth total agents dynamics is observed when the decentralized control structure is selected. For each strategy, there are two control objectives to be satisfied. First, all agents must rendezvous with their stable partners while maintaining specified distance separation with other agents of the same gender, $\forall\ t > 0$. Second, as $t \to \infty$, the center of the agents' formation must be successfully tracking the desired state trajectory. This is achieved by exerting an additional state feedback control law to all agents. Contrary to stability analysis in the original stable marriage theory where the final objective is to avoid the blocking pairs, we introduce and observe the stability of the agents' formation in dynamical form. This means that we declare that stable matching between agents is reached whenever the whole dynamical system is stable in the sense of Lyapunov. Figure 1 depicts the process flow to achieve dynamic stable matching.

The organization of this paper is as follows. In section 2, we provide the mathematical preliminaries. In sections 3 and 4, we introduce our approach on the dynamic stable matching in the centralized and decentralized control frameworks, respectively. A numerical example is presented in section 5. Finally, we present our conclusions and future work in section 6.

# 2 Backgrounds

## 2.1 Notations

Let $\mathbb{R}$ and $\mathbb{R}^m$ denote the set of real numbers and real vector of dimension $m$, respectively. The superscript $T$ on a matrix is used to represent its transposition. We denote $\mathbf{1}_N$ to imply $\mathbf{1} = [1, \ldots, 1]^T \in \mathbb{R}^N$. The identity matrix with $n \times n$ dimension is denoted as $I_n \in \mathbb{R}^{n\times n}$. The Euclidean 2-norm of a given vector $v \in \mathbb{R}^n$ is denoted as $\|v\| := \|v\|_2 = \sqrt{v^T v} = \sqrt{\sum_{i=1}^{n} |v_i|^2}$. For $A = (a_{ij}) \in \mathbb{R}^{n\times m}$ and $B \in \mathbb{R}^{l\times k}$, the Kronecker product $A \otimes B \in \mathbb{R}^{nl\times mk}$ is defined

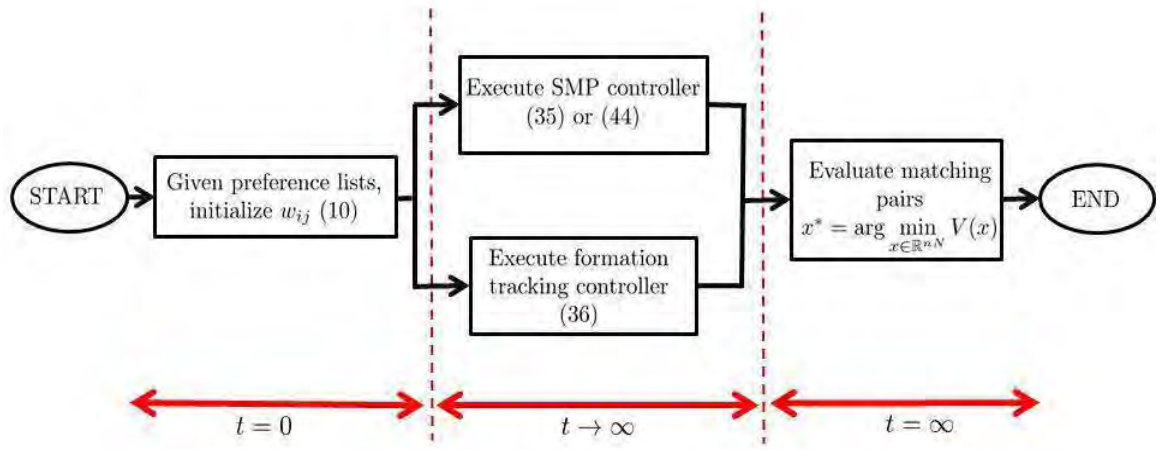


Figure 1: Process flow to achieve dynamic stable matching.

by

$$A \otimes B = \begin{bmatrix} a_{11}B & \dots & a_{1m}B \\ \vdots & \ddots & \vdots \\ a_{n1}B & \dots & a_{nm}B \end{bmatrix}.$$

We say that a function $V$ satisfies a Lipschitz condition on a set of $D$ if there is a constant $C \geq 0$ such that

$$|V(u) - V(v)| \leq C|u - v|, \ \forall (u, v) \in D.$$

## 2.2 Agents Dynamics

We consider $N$ agents moving in an $n$ dimensional Euclidean space. Each of the agents is described by a single integrator as

$$\dot{x}_i = u_i, \tag{1}$$

where $x_i \in \mathbb{R}^n$ is the position vector of agent $i$ and $u_i \in \mathbb{R}^n$ is the (velocity) control input to be designed. To represent $N$ agents, the total state and control vectors are defined as

$$x = \begin{bmatrix} x_1 \\ \vdots \\ x_N \end{bmatrix} \in \mathbb{R}^{nN} \ \text{ and } \ u = \begin{bmatrix} u_1 \\ \vdots \\ u_N \end{bmatrix} \in \mathbb{R}^{nN}, \tag{2}$$

respectively. We can further rewrite the total system dynamic in the form

$$\dot{x} = u. \tag{3}$$

The group center that is the virtual center state can be obtained by considering the average of all positions as

$$x_c = \frac{1}{N} \sum_{i=1}^{N} x_i. \tag{4}$$

It is also assumed that the desired state trajectory $x_d \in \mathbb{R}^n$ for the group center $x_c$ can be achieved by $u_d \in \mathbb{R}^n$, that is

$$\dot{x}_d = u_d. \tag{5}$$

## 2.3 Graph Theory

In this section, we introduce some terminologies and notations, which are more or less standard in the field of graph theory as discussed in [23].

For $N$ number of agents, a graph $\mathbb{G}$ is built upon a finite set called a *vertex set* represented by $\mathcal{X} = \{x_1, x_2, \dots, x_N\}$ and the *edge set* of $\mathcal{E}$. If $(x_i, x_j) \in \mathcal{E}$, there is a communication link between them. We denote the cardinality of agent $x_i$ as $|x_i|$ where cardinality is the number of edges connecting $x_i$ to other agents. For a graph $\mathbb{G}$ with associated weight $W_{ij} \geq 0$, we define the graph Laplacian $L := (l_{ij})_{N \times N}$ as

$$l_{ij} = \begin{cases} \sum_j W_{ij} \text{ if } j = i \\ -W_{ij} \quad \text{if } j \neq i \end{cases} \tag{6}$$

The Laplacian matrix is positive semi-definite with non-positive off-diagonal elements. When $\mathbb{G}$ is a balanced graph, then the matrix $L$ always satisfies $L\mathbf{1} = \mathbf{1}^T L = \mathbf{0}$.

## 2.4 Stable Marriage Problem

In this section, we discuss the methodology used for finding the stable pairs from the given preference list. We first describe the seminal algorithm by Gale and Shapley [6] on establishing the stable pairs between any bi-partite sets. Definitions 1 to 5 are adopted from Gusfield and Irving [24], and they are asserted here for clarity.

**Definition 1** (Preferred partner)**.** Person $p$ prefers $q$ to $r$ where $q$ and $r$ are in the opposite sex to $p$, if and only if $q$ precedes $r$ on $p$'s preference list.

**Definition 2** (Matching)**.** A matching $M$ is a one-one correspondence between men and women. If man $m$ and woman $w$ are matched in $M$, then $m$ and $w$ are called *partners* in $M$, and can be written as $m = p_M(w), w = p_M(m)$ where $p_M(w)$ and $p_M(w)$ are the $M$-partners of $m$ and $w$, respectively.

**Definition 3** (Blocking Pairs)**.** A man $m$ and woman $w$ are said to *block* a matching $M$, or to be a *blocking pair* of

$M$, if $m$ and $w$ are not partners in $M$, but $m$ prefers $w$ to his current partners $p_M(w)$ and $w$ prefers $m$ to her current partners $p_M(m)$.

**Definition 4** (Stability in SMP)**.** A matching for which there is at least one blocking pair is called *unstable*, otherwise the matching is *stable*.

**Definition 5** (Stable Pair)**.** A man $m$ and woman $w$ constitute a *stable pair* if and only if $m$ and $w$ are partners in some stable matching; in these circumstances $m$ is a *stable partner* of $w$, and vice versa.

#### 2.4.1 Gale and Shapley Algorithm

Let us assume that there exist sets of men $\mathcal{M} := \{m_1, m_2, \ldots, m_P\}$, and women $\mathcal{W} := \{w_1, w_2, \ldots, w_P\}$ with $P$ as the number of pairs. Each of the individuals in these two sets rank their preferred partners in the preference lists. Let us denote the man $m$ as the current man proposing to the woman $w$ in his preference list. Also, if the proposed woman $w$ is already engaged, we denote her current partner as $m'$. We denote $w'$ as the next-woman to be proposed to from the man $m$'s preference list. The procedure of the Gale and Shapley algorithm [6] is presented in Algorithm 1.

This algorithm is guaranteed to terminate at $O(P \log P)$ iterations[25], and upon termination, stable pairs $M$ will be established. The stable pairs established in $M$ are said to be *Men-Optimal, Women-Pessimal* since the men are proposing first. The results will be opposite if the women are the first to propose [6, 24].

**Algorithm 1** Gale & Shapley Algorithm (Men-proposer)

```
procedure StableMatching(m, w)
    Initialize all men and women to be free
    while ∃ free m do
        w = m's highest ranked woman to whom he has not yet proposed
        if w is free then
            m = p_M(w) & w = p_M(m)
            (m, w) → M                          ▷ become partner
        else if w is already engaged with m' then
            if m precedes m' in w's preference list then
                w = p_M(m)
                (m, w) → M                      ▷ choose new partner
                m' becomes free
            else
                w = p_M(m') remain engaged
                (m', w) → M                     ▷ remain partner
                m proposes to w' in his preference list
            end if
        end if
    end while
end procedure
```

# 3 Dynamic Stable Matching

Motivated by Gale and Shapley [6] in establishing stable pairs, given the bipartite graph with preference list, we consider a matching problem in MAS on finding the stable pairs. We introduce the proper cost function satisfying the G-S algorithm that generates optimum results.

We consider a group of agents $\mathcal{I} = \{1, 2, \ldots, N\}$ and their corresponding positions $\mathcal{X} = \{x_1, x_2 \ldots, x_N\}$, where $x_i$ defined in (1). We assume that $\mathcal{I} = \mathcal{M} \cup \mathcal{W}$ and $\mathcal{M} \cap \mathcal{W} = \emptyset$. Furthermore, we assume that $P$ satisfies $N = 2P$. In addition, let the odd numbering agents belong to the men set and the even numbering agents belong to the women set, respectively. That is,

$$\begin{aligned} i \in \mathcal{M} &\leftrightarrow i \in \mathcal{I}_M := \{1, 3, \ldots, N-1\} \\ i \in \mathcal{W} &\leftrightarrow i \in \mathcal{I}_W := \{2, 4, \ldots, N\}. \end{aligned} \tag{7}$$

**Definition 6** (Dynamic Stable Matching)**.** For the agent $x_i$, we define an index set denoting opposite gender and same gender as follows:-

$$\mathcal{J}_i = \begin{cases} \mathcal{I}_W & \text{if } i \in \mathcal{M} \\ \mathcal{I}_M & \text{if } i \in \mathcal{W}, \end{cases} \tag{8}$$

$$\mathcal{K}_i = \begin{cases} \mathcal{I}_M & \text{if } i \in \mathcal{M} \\ \mathcal{I}_W & \text{if } i \in \mathcal{W}. \end{cases} \tag{9}$$

The agents $i \in \mathcal{I}$ are said to dynamically achieve stable matching if

(a) for the stable partner $j^* \in \mathcal{J}_i$ of $i$ (i.e., $j^* := p_M(i) \mapsto (i, j^*) \in M$), $\lim_{t\to\infty} \|x_{j^*}(t) - x_i(t)\| = 0$.

(b) for $k \in \mathcal{K}_i$ there exists $t_0 > 0$ such that $\|x_k(t) - x_i(t)\| \geq d$ for all $t > t_0$.

(c) the center trajectory $x_c$ satisfies $\lim_{t\to\infty} \|x_c(t) - x_d(t)\| = 0$ for the desired trajectory $x_d$.

To achieve the dynamic stable matching, we use the preference rank $p_{ij}$ and the weighted degree $w_{ij}$.

**Definition 7** (Preference Rank)**.** The preference rank $p_{ij} \in \{1, 2, \ldots, N\}$ of the agent $i$ towards $j \in \mathcal{J}_i$ is defined as the order of the agent $j$ in the $i$'s preference list (i.e., $p_{ij} = 1$ means most preferred and $p_{ij} = 2$ second most preferred). In addition, for $j \in \mathcal{K}_i$, $p_{ij} := 0$.

**Definition 8** (Weighted Degree)**.** The weighted degree $w_{ij}$ is defined by the preference rank $p_{ij}$ as

$$w_{ij} = \begin{cases} \dfrac{2}{|\mathcal{J}_i|\,(|\mathcal{J}_i| + 1)} \left(|\mathcal{J}_i| - p_{ij} + 1\right) & \text{if } j \in \mathcal{J}_i \\ 0 & \text{otherwise} \end{cases} \tag{10}$$

where $|\mathcal{J}_i|$ is the cardinality of $\mathcal{J}_i$.

**Example 1.** When we have a preference list in Table 1, $w_1$ (agent 2) is ranked second in the $m_2$'s (agent 3) preference list, thus $p_{32} = p_{m_2 w_1} = 2$. Then, from Tables 1 and 2, the

preference rank matrix is

$$\mathfrak{P} = (p_{ij})_{12\times 12} = \begin{bmatrix} 0 & 4 & 0 & 5 & 0 & 1 & 0 & 6 & 0 & 3 & 0 & 2 \\ 4 & 0 & 1 & 0 & 2 & 0 & 5 & 0 & 3 & 0 & 6 & 0 \\ 0 & 2 & 0 & 1 & 0 & 5 & 0 & 6 & 0 & 3 & 0 & 4 \\ 6 & 0 & 3 & 0 & 4 & 0 & 2 & 0 & 5 & 0 & 1 & 0 \\ 0 & 3 & 0 & 1 & 0 & 2 & 0 & 6 & 0 & 5 & 0 & 4 \\ 6 & 0 & 1 & 0 & 3 & 0 & 2 & 0 & 4 & 0 & 5 & 0 \\ 0 & 1 & 0 & 3 & 0 & 2 & 0 & 4 & 0 & 5 & 0 & 6 \\ 3 & 0 & 6 & 0 & 5 & 0 & 2 & 0 & 1 & 0 & 4 & 0 \\ 0 & 6 & 0 & 3 & 0 & 4 & 0 & 1 & 0 & 5 & 0 & 2 \\ 2 & 0 & 4 & 0 & 5 & 0 & 6 & 0 & 3 & 0 & 1 & 0 \\ 0 & 1 & 0 & 4 & 0 & 6 & 0 & 3 & 0 & 5 & 0 & 2 \\ 6 & 0 & 3 & 0 & 1 & 0 & 2 & 0 & 5 & 0 & 4 & 0 \end{bmatrix}$$

and the weighted degree matrix is

$$\mathfrak{W} = (w_{ij})_{12\times 12} = \frac{1}{21}\begin{bmatrix} 0 & 3 & 0 & 2 & 0 & 6 & 0 & 1 & 0 & 4 & 0 & 5 \\ 3 & 0 & 6 & 0 & 5 & 0 & 2 & 0 & 4 & 0 & 1 & 0 \\ 0 & 5 & 0 & 6 & 0 & 2 & 0 & 1 & 0 & 4 & 0 & 3 \\ 1 & 0 & 4 & 0 & 3 & 0 & 5 & 0 & 2 & 0 & 6 & 0 \\ 0 & 4 & 0 & 6 & 0 & 5 & 0 & 1 & 0 & 2 & 0 & 3 \\ 1 & 0 & 6 & 0 & 4 & 0 & 5 & 0 & 3 & 0 & 2 & 0 \\ 0 & 6 & 0 & 4 & 0 & 5 & 0 & 3 & 0 & 2 & 0 & 1 \\ 4 & 0 & 1 & 0 & 2 & 0 & 5 & 0 & 6 & 0 & 3 & 0 \\ 0 & 1 & 0 & 4 & 0 & 3 & 0 & 6 & 0 & 2 & 0 & 5 \\ 5 & 0 & 3 & 0 & 2 & 0 & 1 & 0 & 4 & 0 & 6 & 0 \\ 0 & 6 & 0 & 3 & 0 & 1 & 0 & 4 & 0 & 2 & 0 & 5 \\ 1 & 0 & 4 & 0 & 6 & 0 & 5 & 0 & 2 & 0 & 3 & 0 \end{bmatrix}.$$

The following lemma is crucial in our analysis and will be used throughout the text.

**Lemma 1.** Given the Euclidean norm $h(x) := \|x(t)\|$ with $x \in \mathbb{R}^n$, its derivative with respect to $t$ is

$$\frac{d}{dt}\|x\| = (\partial h(x))^T \frac{dx}{dt} \tag{11}$$

with subdifferential of $h(x)$ with respect to $x$

$$\partial h(x) = \begin{cases} \dfrac{x}{\|x\|} & \text{if } x \neq 0 \\ \{g \in \mathbb{R}^n \mid \|g\| \leq 1\} & \text{if } x = 0. \end{cases} \tag{12}$$

*Proof:* First, consider the part when $x \neq 0$. By defining $s(x) := r^2 = \|x\|^2 = x^T x$ and differentiating it by $t$, we have $\frac{ds}{dt} = 2x^T \dot{x}$. With this in mind, we can calculate the derivative of $\|x\|$ with respect to $t$ by applying the chain rule such that

$$\frac{d}{dt}\|x\| = \frac{dr}{dt} = \frac{dr}{ds}\frac{ds}{dt} = \frac{1}{2}s^{-\frac{1}{2}}\frac{ds}{dt} = \frac{x^T}{\|x\|}\dot{x}$$

which is valid $\forall x \neq 0$. Next, we consider the part when $x = 0$. Since $h(x)$ is non-smooth at $x = 0$, then we define a subgradient $g$ which is any element of $[-1, 1]$ to ensure the continuity of the $\partial h(x)$, that is

$$\frac{d}{dt}\|x\| = g^T \dot{x}.$$

■

**Assumption 1.** The Euclidean norm $h(x)$ defined in Lemma 1 is a $C^0$ function and is not differentiable at point $x = 0$. By introducing the subdifferential (12) with subgradients $x/\|x\|$ and $g$, we assume this function becomes smooth at $x = 0$.

Now, consider the dynamic equation (3). Suppose the control law $u$ takes the form of $u = f(x, t)$, then we can rewrite (3) as an autonomous system

$$\dot{x} = f(x, t) \tag{13}$$

where $f : D \to \mathbb{R}^{nN}$ is a locally Lipschitz map from domain $D \subset \mathbb{R}^{nN}$ into $\mathbb{R}^{nN}$. Comparatively, when $u$ takes the discontinuous form so that $f(x, t)$ is discontinuous, (3) can be written as

$$\dot{x} \in^{a.e.} K\{f(x, t)\}, \tag{14}$$

where $K\{f(x, t)\}$ is the Filippov's differential inclusion and *a.e.* is the abbreviation for "almost everywhere".

**Definition 9** (Filippov solution [26, 27])**.** A vector function $x(\cdot)$ is a solution of (14) on $[t_0, t_1]$ if $x(\cdot)$ is absolutely continuous on $[t_0, t_1]$ and for almost all $t \in [t_0, t_1]$

$$\dot{x} \in K\{f(x, t)\} \tag{15}$$

where

$$K\{f(x, t)\} = \bigcap_{\delta>0}\bigcap_{\mu(D)=0} \overline{\text{co}}\, f(B(x, \delta) - D, t) \tag{16}$$

where $\overline{\text{co}}$ means the closed convex hull; $B(x, \delta)$ is a closed $\delta$ neighborhood of $x$; $D$ is an arbitrary set in $R^{nN}$; $\mu$ is $nN$ dimensional Lebesgue measure. Hence, $\cap_{\mu(N)=0}$ means the intersection over all sets $D$ of Lebesgue measure zero. We use the notation in (14) or (15) to denote the differential equation with a discontinuous right-hand side.

For each $x_0 \in \mathbb{R}^{nN}$, there exists at least one solution of differential inclusion with the initial condition $x(0) = x_0$.

**Definition 10** (Stability of the equilibrium point [28, 29])**.** Let $x_0 \in D$ be the equilibrium points of either (13) or (14). Then the equilibrium point $x = x_0$ is

- stable, if for any $\epsilon > 0$ there exists $\delta = \delta(\epsilon) > 0$ such that

$$\|x(0)\| < \delta \Rightarrow \|x(t)\| < \epsilon, \ \forall\, t \geq 0,$$

- asymptotically stable, if it is stable and $\delta$ can be chosen such that

$$\|x(0)\| < \delta \Rightarrow \lim_{t\to\infty} x(t) = x_0.$$

**Lemma 2** (Lyapunov's second method for stability)**.** Assume that the system (13) has an equilibrium point at $x = x_0$. Then, the system is *globally asymptotically stable* in the sense of Lyapunov if and only if, there exists a Lyapunov function $V(x) : \mathbb{R}^n \to \mathbb{R}$ such that

- $V(x) > 0$ for all $x \neq x_0$ and $V(x_0) = 0$,
- $\dot{V}(x) < 0$ for all $x \neq x_0$ and $\dot{V}(x_0) = 0$.

Lemma 2 provides strong conditions to ensure state convergence to the equilibrium point. However, it is not suitable for analyzing a non-smooth Lyapunov function. This can be remedied by the following lemma:

**Lemma 3** (Generalized Lyapunov Theorem)**.** Given that (14) is discontinuous on the right-hand-side, and has an equilibrium point $x = x_0$. If there exists a $V : \mathbb{R}^n \to \mathbb{R}$, such that

- $V(x_0) = 0,\ V(x) > 0,\ \forall x \neq 0$, and $V(x(t))$ is absolutely continuous on $[t, \infty)$,
- with $\dfrac{d}{dt}[V(x(t))] < -\epsilon < 0$ a.e. on $\{t \mid x(t) \neq x_0\}$,

then $x$ converges to $x_0$ in finite time. Thus, the system (14) is *generally asymptotically stable* in the sense of Lyapunov.

*Proof:* See Theorem 2 in [27] for completing the proof. ■

To derive a suitable control law for the dynamic stable matching, we design a Lyapunov function to be minimized as

$$V(x) = V_T(x) + V_c(x), \tag{17}$$

where $V_T(x) > 0 : \mathbb{R}^{nN} \to \mathbb{R}$ and $V_c(x) > 0 : \mathbb{R}^n \to \mathbb{R}$ are defined to use a multiplier constant $\nu_{ik} > 0 \in \mathbb{R}$ and the weighted degree $w_{ij}$ as

$$V_T(x) = \sum_{i=1}^{N} V_i(x), \tag{18}$$

$$V_i(x) = \exp \sum_{j \in \mathcal{J}_i} w_{ij}\|x_j - x_i\| + \sum_{k \in \mathcal{K}_i} \nu_{ik}\left(d - \|x_k - x_i\|\right)^2 - 1 \tag{19}$$

$$V_c(x) = \frac{1}{2}\|x_c - x_d\|^2. \tag{20}$$

The Lyapunov candidate $V_T$ is designed to take (a) and (b) in Definition 6 into consideration. Minimizing $V_T$ implies to solve an optimization problem:

$$\begin{aligned} &\text{minimize} && \exp \sum_{j \in \mathcal{J}_i} w_{ij}\|x_j - x_i\| \\ &\text{subject to} && \|x_k - x_i\| \geq d,\ \forall k \in \mathcal{K}_i, i = 1, 2, \ldots, N. \end{aligned} \tag{21}$$

Meanwhile, the Lyapunov candidate $V_c$ is designed as the energy dissipation function corresponding to the $x_c$ and $x_d$ to take (c) into consideration in Definition 6.

**Theorem 1.** (Fixed network stable matching) For fixed network agents, starting from $\Omega = \{x : V(x) \leq \gamma\}$, the dynamic stable matching is achieved under the state feedback control

$$u_i = u_i^{SM} + u_i^c, \tag{22}$$

$$u_i^{SM} = u_i^a + u_i^r, \tag{23}$$

$$u_i^c = -k^c(x_i - x_d) + u_d, \tag{24}$$

where $u_i^a$ is the attraction of agent $i$ with $j \in \mathcal{J}_i$

$$u_i^a = \sum_{j \in \mathcal{J}_i} (a_i b_{ij} + a_j b_{ji})(x_j - x_i) \tag{25}$$

and $u_i^r$ is the repulsion between agent $i$ with $k \in \mathcal{K}_i$

$$u_i^r = \sum_{k \in \mathcal{K}_i} (c_{ik} + c_{ki})(x_k - x_i), \tag{26}$$

and $k^c > 0$ is an appropriate control gain and[1]

$$\begin{aligned} a_i &= \exp \sum_{j' \in \mathcal{J}_i} w_{ij'}\|x_{j'} - x_i\| \\ b_{ij} &= \frac{w_{ij}}{\|x_j - x_i\|} \\ c_{ik} &= 2\nu_{ik}\left(1 - \frac{d}{\|x_k - x_i\|}\right). \end{aligned} \tag{27}$$

*Proof:* We first prove Theorem 1 by investigating $V(x) = V_T(x) + V_c(x) \geq 0$ where the $V_T(x)$ in (18) is non-negative except when $x_i, x_j, x_k$ satisfying $x_j = x_i, \|x_k - x_i\| = d$. Obviously, $V_c(x) \geq 0$ and $V_c(x) = 0$ when $x_c = x_d$. Clearly, $V(x)$ satisfies the first condition in Lemma 2.

Next, we show that $V(x)$ satisfies the second condition in Lemma 2. From (17), its time derivative is obtained as

$$\dot{V}(x) = \dot{V}_T(x) + \dot{V}_c(x). \tag{28}$$

By using (1) and Lemma 1, the derivative of (18) with respect to $t$ is calculated as

$$\begin{aligned} \dot{V}_T &= \sum_{i=1}^{N} \dot{V}_i, \\ \dot{V}_i &= a_i \sum_{j \in \mathcal{J}_i} b_{ij}(x_j - x_i)^T(u_j - u_i) + \sum_{k \in \mathcal{K}_i} c_{ik}(x_k - x_i)^T(u_k - u_i). \end{aligned} \tag{29}$$

Note that in (29), the terms $b_{ij}(x_j - x_i)$ and $c_{ik}(x_k - x_i)$ require us to apply Lemma 1 to ensure continuity at the non-differentiable points. This implies

$$b_{ij}\, x_{ji} = \begin{cases} w_{ij}\dfrac{x_{ji}}{\|x_{ji}\|} & \text{if } \|x_{ji}\| \neq 0 \\ w_{ij}\, g & \text{if } \|x_{ji}\| = 0 \end{cases}$$

$$c_{ik}\, x_{ki} = \begin{cases} 2\nu_{ik}\left(1 - \dfrac{d}{\|x_{ki}\|}\right)(x_{ki}) & \text{if } \|x_{ki}\| \neq 0 \\ 2\nu_{ik}\,(x_{ki} - dg) & \text{if } \|x_{ki}\| = 0 \end{cases}$$

where $x_{ji} := x_j - x_i,\ x_{ki} := x_k - x_i$ and the subgradient $g$ satisfying $\|g\| \leq 1$. For simplicity, we can always choose the subgradient $g$ to be a zero vector, i.e., $g = \mathbf{0}$. Hence,

$$\begin{aligned} \dot{V}_T &= \sum_{i=1}^{N} \dot{V}_i(x) \\ &= -u_1^T \sum_{j \in \mathcal{J}_1} (a_1 b_{1j} + a_j b_{j1})(x_j - x_1) \\ &\quad -u_1^T \sum_{k \in \mathcal{K}_1} (c_{1k} + c_{k1})(x_k - x_1) \\ &\quad \cdots \\ &\quad - u_N^T \sum_{j \in \mathcal{J}_N} (a_N b_{Nj} + a_j b_{jN})(x_j - x_N) \\ &\quad -u_N^T \sum_{k \in \mathcal{K}_N} (c_{Nk} + c_{kN})(x_k - x_N). \end{aligned} \tag{30}$$

[1]Note that $j$ and $j'$ refer to two different variables.

By introducing

$$L = L^a + L^r, \tag{31}$$

with $L^a := (l^a_{ij})_{N\times N}$ and $L^r := (l^r_{ik})_{N\times N}$ are defined as[2]

$$(l^a)_{ij} = \begin{cases} \sum_{j'\in\mathcal{J}_i} (a_i b_{ij'} + a_{j'} b_{j'i}) & \text{if } j = i \\ -(a_i b_{ij} + a_j b_{ji}) & \text{if } j \neq i,\ j \in \mathcal{J}_i \\ 0 & \text{otherwise,} \end{cases}$$

$$(l^r)_{ik} = \begin{cases} \sum_{k'\in\mathcal{K}_i} (c_{ik'} + c_{k'i}) & \text{if } k = i \\ -(c_{ik} + c_{ki}) & \text{if } k \neq i, k \in \mathcal{K}_i \\ 0 & \text{otherwise,} \end{cases}$$

we can rewrite (30) as

$$\dot{V}_T = u^T (L \otimes I_n)\, x. \tag{32}$$

In addition,

$$\dot{V}_c = (x_c - x_d)^T(\dot{x}_c - \dot{x}_d) = (x_c - x_d)^T \left(\frac{1}{N}\sum_{i=1}^{N} u_i - u_d\right). \tag{33}$$

To (32) and (33), we apply feedback control (22), (23) and (24) with the vector form

$$u = u^{SM} + u^c, \tag{34}$$

$$u^{SM} = -(L \otimes I_n)x, \tag{35}$$

$$u^c = -(I_N \otimes \mathbf{k}^c)(x - \mathbf{1}_N \otimes x_d) + \mathbf{1}_N \otimes u_d, \tag{36}$$

where $\mathbf{k}^c = k^c I_n$ is the diagonal feedback gain matrix.

The equation (32) is rewritten as

$$\begin{aligned} \dot{V}_T &= (u^{SM} + u^c)^T (L \otimes I_n)\, x = (u^{SM} + u^c)^T(-u^{SM}) \\ &= -\|u^{SM}\|^2 - (u^c)^T u^{SM}. \end{aligned} \tag{37}$$

The second term in (37) can be rewritten as

$$\begin{aligned} -(u^c)^T u^{SM} = &-(x^T - \mathbf{1}_N^T \otimes x_d^T)(I_N \otimes \mathbf{k}^c)(L \otimes I_n)x \\ &+(\mathbf{1}_N^T \otimes u_d^T)(L \otimes I_n)x. \end{aligned}$$

Furthermore, we have

$$(I_N \otimes \mathbf{k}^c)(L \otimes I_n) = (I_N L) \otimes (\mathbf{k}^c I_n) = L \otimes \mathbf{k}^c$$

and due to the matrix gains $L$ is symmetric and have columns/rows sum equal to zero, that is

$$(\mathbf{1}_N^T \otimes u_d^T)(L \otimes I_n) = (\mathbf{1}_N^T L) \otimes (u_d^T I_n) = 0.$$

Then, we can show that

$$\begin{aligned} -(u^c)^T u^{SM} &= x^T (L \otimes \mathbf{k}^c)x + (\mathbf{1}_N^T \otimes x_d)(L \otimes \mathbf{k}^c)x \\ &= -\|x\|^2_{L\otimes\mathbf{k}^c} + (\mathbf{1}_N^T L) \otimes (x_d^T \mathbf{k}^c)x \\ &= -\|x\|^2_{L\otimes\mathbf{k}^c} \leq 0. \end{aligned} \tag{38}$$

[2]Similarly, $k$ and $k'$ refer to two different variables.

Next, since

$$\begin{aligned} \sum_{i=1}^{N} u_i^{SM} &= \mathbf{1}_{nN}^T u^{SM} = -(\mathbf{1}_N^T \otimes \mathbf{1}_n^T)(L \otimes I_n)x \\ &= -(\mathbf{1}_N^T L) \otimes (\mathbf{1}_n^T I_n)x = 0, \end{aligned}$$

and (24), we have

$$\begin{aligned} \frac{1}{N}\sum_{i=1}^{N} u_i - u_d &= \frac{1}{N}\sum_{i=1}^{N}(u_i^{SM} + u_i^c) - u_d \\ &= \frac{1}{N}\sum_{i=1}^{N} u_i^c - u_d \\ &= \frac{1}{N}\sum_{i=1}^{N} -k^c(x_i - x_d) \\ &= -k^c(x_c - x_d). \end{aligned} \tag{39}$$

By substituting (39) in (33), we obtain

$$\dot{V}_c = -k^c(x_c - x_d)^T(x_c - x_d) = -k^c\|x_c - x_d\|^2 \leq 0. \tag{40}$$

To sum up, combining results (37) and (40), we show that $\dot{V}(x) \leq 0$.

The above results clearly indicate that $V(x)$ is monotonically decreasing $\forall t \geq 0$. From LaSalle's invariance principle [28], all states starting in $\Omega$ converge to the largest invariant set $E = \{x \in \Omega : \dot{V} = 0\}$. When $\dot{V} = 0, u^{SM} = 0, \|x\|_{L\otimes\mathbf{k}^c} = 0$ and $x_c = x_d$. Therefore, all states asymptotically converges to the largest invariant set $E = \{x \in \Omega : x_c = x_d, \dot{x}_i = \dot{x}_c, \|x_{j^*} - x_i\| = 0\}$. That is to say, all agents' speed asymptotically converges to the formation center's speed while the formation's center converges to the desired trajectory. At this point, each agent $i$ is matched with his/her best *partner* such that $\{i = p_M(j^*), j^* = p_M(i) \mid (i, j^*) \to M\}$. ■

# 4 Decentralized Structure

## 4.1 Decentralized Control Law

The proposed control law (23) for each agent $i$ presented in Section 3 utilizes the information from all agents. Due to the excess information, the calculated control action tends to be very large, as shown in Figure 2. Hence, to overcome this problem, we allow each agent $i$ to communicate only with its neighboring agents. As all agents tend to follow the desired trajectory to achieve condition (c) in Definition 6, there will be more agents within $i$'s sensing range, thus permitting for wider selection of potentially matching agents.

**Definition 11** (Neighboring Agents)**.** Let $R$ be the distance sensing range of agent $i$. Agent $j$ is called a neighbor of agent $i$ if it belongs to the set

$$\mathcal{N}_i = \left\{j \in \mathcal{I} \mid r_{ij} = \|x_j - x_i\| \leq R\right\}. \tag{41}$$

Due to limited communication to achieve control objectives (1)-(3), we propose the decentralized control of the same form as (22), given as

$$u_i = u_{i_N}^{SM} + u_i^c \tag{42}$$

and in the vector form as

$$u = u_N^{SM} + u^c \tag{43}$$

where $u_N^{SM}$ is defined in (44) and $u^c$ is given in (36), respectively. The control law $u_{i_N}^{SM}$ in (42) is due to SMP and has the same form as (23), but with different control gains due to time-varying communication topology. In the vector form, it is recurrently defined as

$$u_N^{SM} = -(L^N \otimes I_n)x \tag{44}$$

where $L^N = L_N^a + L_N^r$ with

$$L_N^a := (l_{ij}^{a,N})_{N\times N} = \begin{cases} \sum_{j'\in\mathcal{J}_i\cap\mathcal{N}_i} (a_i^N b_{ij'}^N + a_{j'}^N b_{j'i}^N) & \text{if } j = i \\ -(a_i^N b_{ij}^N + a_j^N b_{ji}^N) & \text{if } j \neq i, \\ & j \in \mathcal{J}_i \cap \mathcal{N}_i \\ 0 & \text{otherwise} \end{cases}$$

$$L_N^r := (l_{ij}^{r,N})_{N\times N} = \begin{cases} \sum_{k'\in\mathcal{K}_i\cap\mathcal{N}_i} (c_{ik'}^N + c_{k'i}^N) & \text{if } k = i, \\ -(c_{ik}^N + c_{ki}^N) & \text{if } k \neq i, \\ & k \in \mathcal{K}_i \cap \mathcal{N}_i \\ 0 & \text{otherwise.} \end{cases}$$

The variables $a_i^N, b_{ij}^N$, and $c_{ik}^N$ of each agent $i$ take the form of equation (27) but only their neighboring agents are taken into account. Hence, we redefine (27) as

$$\begin{aligned} a_i^N &= \exp\left(\sum_{j'\in\mathcal{J}_i\cap\mathcal{N}_i} w_{ij'}\|x_{j'} - x_i\|\right) \\ b_{ij}^N &= \frac{w_{ij}}{\|x_j - x_i\|} \\ c_{ik}^N &= 2\nu_{ik}\left(1 - \frac{d}{\|x_k - x_i\|}\right). \end{aligned} \tag{45}$$

## 4.2 Discontinuous Dynamics

Because of the selection of control law (44), the total control dynamic (3) has a discontinuous right-hand side; hence, it takes the differential form of (15). Based on Definition 9 and using (43) where $f(x,t) = u = u_N^{SM} + u^c$, the differential inclusion defined in (16) for the discontinuous differential equation of (15) can be calculated using the calculus in [27]. Hence, the total dynamic is obtained as

$$\begin{aligned} \dot{x} \in K\{f(x,t)\} &= K\{u\} = K\{u^{SM}\} + K\{u^c\} \\ &= \begin{cases} u_N^{SM} + u^c & \text{if } \exists \\ u^c & \text{otherwise,} \end{cases} \end{aligned} \tag{46}$$

where $\exists \triangleq \{\forall i, \exists j \in \mathcal{J}_i \cap \mathcal{N}_i, \exists k \in \mathcal{K}_i \cap \mathcal{N}_i\}$.

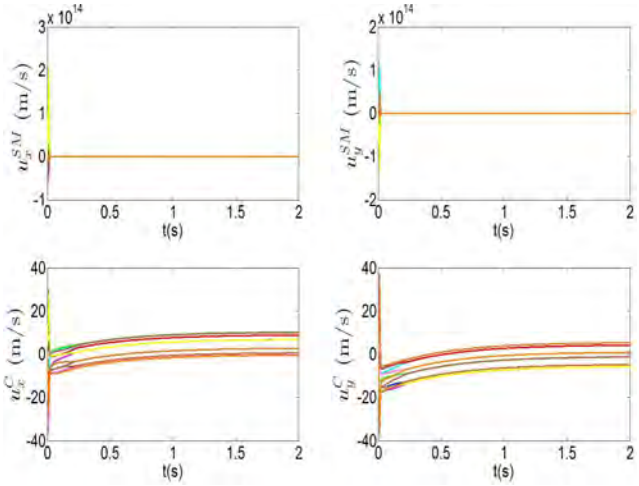


Figure 2: Control signals due to centralized control structure.

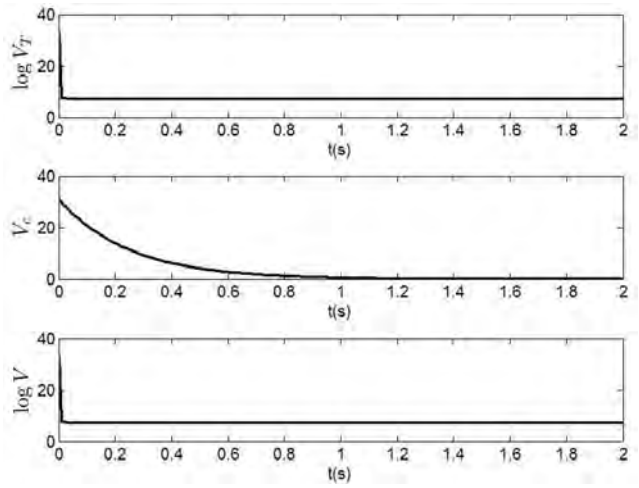


Figure 3: Lyapunov function (centralized control).

## 4.3 Nonsmooth Stability Analysis

In the form similar to (17), we use a suitable Lyapunov function candidate for the non-smooth system

$$V(x) = V_T(x) + V_c(x) \tag{47}$$

where

$$V_T(x) = \sum_{i=1}^{N} V_i(x) \tag{48}$$

and $V_c(x)$ is defined in (20). However, a slight modification in $V_i$ is needed so that $\mathcal{J}_i$ is divided into two groups: neighbor $\mathcal{J}_i \cap \mathcal{N}_i$ and not neighbor $\mathcal{J}_i \backslash \mathcal{N}_i$, and $\mathcal{K}_i$ is divided into into $\mathcal{K}_i \cap \mathcal{N}_i$ and $\mathcal{K}_i \backslash \mathcal{N}_i$, as well. That is,

$$\begin{aligned} V_i(x) = \exp\left(\sum_{j\in\mathcal{J}_i\cap\mathcal{N}_i} w_{ij}\|x_j - x_i\|\right) + \exp\left(\sum_{j\in\mathcal{J}_i\backslash\mathcal{N}_i} w_{ij}R\right) \\ + \sum_{k\in\mathcal{K}_i\cap\mathcal{N}_i} \nu_{ik}\left(d - \|x_k - x_i\|\right)^2 + \sum_{k\in\mathcal{K}_i\backslash\mathcal{N}_i} \nu_{ik}\left(d - R\right)^2 - 1 \end{aligned}$$

where $V_i(\cdot) \in C^0$ corresponds to the local Lyapunov function of agent $i$.

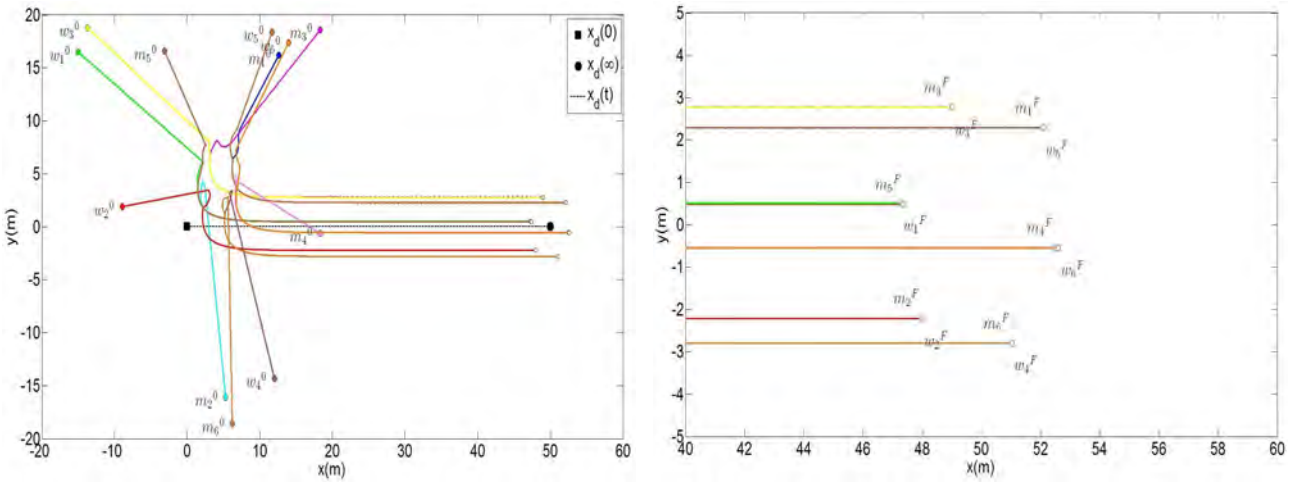


(a) Trajectories (b) Final positions (enlarged)

Figure 4: Trajectories of agents with centralized control law (22).

Since the chosen Lyapunov function (47) is non-smooth, classical notion of gradients is not appropriate. Provided that the function is locally Lipschitz, Clarke's generalized gradient can be put to use to analyze the non-smooth stability [30]. The generalized gradient at point $x$ can be evaluated as a set-valued map equal to convex closure of the limiting gradient near $x$ [31]. We provide the formal definition of Clarke's generalized gradient and set-valued derivative adopted from Gu *et al*. [31] as follows.

**Definition 12** (Clarke's generalized gradient)**.** For a locally Lipschitz function $V : \mathbb{R}^m \to \mathbb{R}$, the generalized gradient of $V$ at $x$ is defined as

$$\partial V(x) = \overline{\text{co}}\left\{\lim_{x_t \to x} \nabla V(x_t) \mid x_t \notin \Omega_v \cup D\right\} \tag{49}$$

where $\Omega_v$ is the set of Lebesgue measure zero where the gradient $\nabla V$ does not exist and $D$ is an arbitrary set of zero measure.

**Definition 13** (Set-valued derivative)**.** The set-valued derivative of $V$ is defined as

$$\dot{\overline{V}}(x) = \{a = p^T v \in \mathbb{R} \mid \exists v \in K\{f(x,t)\}, \forall p \in \partial V(x)\}. \tag{50}$$

For the function $V(x)$ that is differentiable at $x$, the appropriate set-valued derivative is $\dot{\overline{V}} = \{(\nabla V(x))^T v \mid v \in K\{f(x,t)\}\}$.

The generalized version of LaSalle's invariance principle [32] for regular Lyapunov function [29] in non-smooth analysis is to be employed in the stability analysis.

**Definition 14** (Weakly invariant set definition)**.** A set $\Omega_m$ is called a weakly invariant set for (14) if through each point $x \in \Omega_m$, there exists a maximal solution of (14) lying in $\Omega_m$.

**Lemma 4** (Adopted from Lemma 2 in Gu *et al*. [31])**.** Let $x$ be a solution of differential inclusions (15) and let $V$ be a locally Lipshitz continuous and regular function. Then, $(d/dt)V(x)$ exists almost everywhere and $(d/dt)V(x) \in \dot{\overline{V}}(x)$ almost everywhere.

To achieve dynamic stable matching between agents with time-varying communication topology, we propose the following theorem:

**Theorem 2.** (Time-varying network stable matching) For time-varying network agents, starting from $\Omega = \{x : V(x) \leq \gamma\}$, the dynamic stable matching between agents as defined in Definition 6 is *generally* asymptotically stable under the state feedback control $u_i$ (42) with appropriate control gain $k^c$.

*Proof:* In (47), it is trivial that $V_T(x)$ and $V_c(x)$ are positive definite functions. Thus, it can be deduced that the first condition of Lemma 3 is satisfied due to the fact that $V(x)$ in (47) is positive definite.

Next, we show that the generalized gradient of the selected Lyapunov function (47) will satisfy the second condition in Lemma 3. By Lemma 4, if $x$ is a solution of differential inclusion (14) and $V(x)$ defined in (47) is a locally Lipschitz continuous and regular function, then $(d/dt)V(x)$ exists almost everywhere and $(d/dt)V(x) \in \dot{\overline{V}}(x)$ almost everywhere.

The generalized gradient of $V(x)$ in (47) is derived as

$$\partial V(x) = \partial V_T(x) + \partial V_c(x). \tag{51}$$

where, for the first component in (51), the generalized gradient of $V_i(x)$ is calculated as

$$\partial V_i(\cdot) = \begin{cases} 0 & \text{if } \mathcal{J}_i \cap \mathcal{N}_i = \emptyset \\ & \text{and } \mathcal{K}_i \cap \mathcal{N}_i = \emptyset \\ a_i^{\mathcal{N}} \sum\limits_{j \in \mathcal{J}_i \cap \mathcal{N}_i} b_{ij}^{\mathcal{N}}(x_j - x_i) & \\ + \sum\limits_{k \in \mathcal{K}_i \cap \mathcal{N}_i} c_{ik}(x_k - x_i) & \text{otherwise.} \end{cases} \tag{52}$$

Similarly, we apply Lemma 1 to $b_{ij}^{\mathcal{N}}(x_j - x_i)$ and $c_{ik}^{\mathcal{N}}(x_k - x_i)$ in (52) to imply

$$b_{ij}^{\mathcal{N}}\, x_{ji} = \begin{cases} w_{ij}\dfrac{x_{ji}}{\|x_{ji}\|} & \text{if } \|x_{ji}\| \neq 0 \\ w_{ij}\, g & \text{if } \|x_{ji}\| = 0 \end{cases}$$

$$c_{ik}^{\mathcal{N}}\, x_{ki} = \begin{cases} 2\nu_{ik}\left(1 - \dfrac{d}{\|x_{ki}\|}\right)(x_{ki}) & \text{if } \|x_{ki}\| \neq 0 \\ 2\nu_{ik}\,(x_{ki} - dg) & \text{if } \|x_{ki}\| = 0 \end{cases}$$

where $x_{ji} := x_j - x_i$ , $x_{ki} := x_k - x_i$ and $\|g\| \leq 1$. The calculated set-valued derivative for the differential inclusion (14) is obtained as

$$\begin{aligned} \dot{\overline{V}}_T(x) &= \bigcap_{\xi \in \partial V_T} \xi^T K\{f(x,t)\} = \sum_{i=1}^{N} \bigcap_{\xi_i} \xi_i^T \dot{x}_i \\ &= -\sum_{i=1}^{N} \sum_{j \in \mathcal{J}_i \cap \mathcal{N}_i} (a_i^{\mathcal{N}} b_{ij}^{\mathcal{N}} + a_j^{\mathcal{N}} b_{ji}^{\mathcal{N}})(x_j - x_i)^T \dot{x}_i \\ &\quad - \sum_{i=1}^{N} \sum_{j \in \mathcal{K}_i \cap \mathcal{N}_i} (c_{ik}^{\mathcal{N}} + c_{ki}^{\mathcal{N}})(x_k - x_i)^T \dot{x}_i \\ &= -(u_{\mathcal{N}}^{SM})^T (u_{\mathcal{N}}^{SM} + u_c) \\ &= -\|u_{\mathcal{N}}^{SM}\|^2 - \|x\|^2_{L^{\mathcal{N}} \otimes \mathbf{k}^c} \end{aligned} \tag{53}$$

where $\xi_i \in \partial V_i(x)$.

Likewise, to the centralized control, the generalized gradient of the second component in (51) can be obtained by re-using (39) and (33). Thus, we reach

$$\partial Vc(x) = \dot{V}_c(x,t) = -\|x_c - x_d\|^2_{\mathbf{k}^c} \leq 0. \tag{54}$$

Combining (53) and (54), we obtain the set-valued derivative for the generalized gradient of (51) given by

$$\dot{\overline{V}}(x) = -\|u_{\mathcal{N}}^{SM}\|^2 - \|x\|^2_{L^{\mathcal{N}} \otimes \mathbf{k}^c} - \|x_c - x_d\|^2_{\mathbf{k}^c} \tag{55}$$

To use the generalized version of LaSalle's invariance principle (see Theorem 3 in [29] ), let

$$X_V = \{x \in \mathbb{R}^{nN} : 0 \in \dot{\overline{V}}(x)\} \tag{56}$$

The largest weakly invariant subset of $\overline{X_V}$ is $\{\|u_{\mathcal{N}}^{SM}\|^2 = 0, \|x\|^2_{L^{\mathcal{N}} \otimes \mathbf{k}^c} = 0, \|x_c - x_d\|^2_{\mathbf{k}^c} = 0\}$. Thus, for all states starting in $\Omega$, the Filippov's trajectories of the system converge to the largest weakly invariant set $E = \{x \in \Omega : x_c = x_d, \dot{x}_i = \dot{x}_c,\ \|x_{j^*} - x_i\| = 0\}$. All agents are matched with their best partners that yield to stable matching i.e., $\{i = p_M(j^*), j^* = p_M(i) \mid (i, j^*) \rightarrow M\}$. ■

# 5 Numerical Example

## 5.1 Achieving Matching

Consider that the MAS consists of 12 agents to constitute a 6 pairs SMP. The odd and even numbering agents are clustered into men's and women's sets, respectively (i.e., $\mathcal{I}_{\mathcal{M}} = \{x_1, x_3, \ldots, x_{11}\} = \{m_1, m_2, \ldots, m_6\}$ and $\mathcal{I}_{\mathcal{W}} = \{x_2, x_4, \ldots, x_{12}\} = \{w_1, w_2, \ldots, w_6\}$). We use the same preference lists as in Tables 1 and 2. It is assumed that each agent can access the preference list of other agents. This means that $i$ knows his/her rank in $j$'s list, and vice versa. We consider the motions of agents in the Euclidean space such that $n = 2$.

The initial positions of all agents are randomly generated within $[-20, 20]$m in both x-y coordinates. All agents are set to be stationary at $t = 0$ (i.e., $\dot{x}_i(0) = 0,\ \forall i \in \mathcal{I}$). Meanwhile, the desired state trajectory is chosen as a straight line governed by $x_d(t) = \begin{bmatrix} 5t & 0 \end{bmatrix}^T$. We specify the desired distance separation between stable pairs to be $d = 5$ m. The state feedback control gain and the multiplier constant are chosen as $k_c = 2$ and $\nu_i = 10$, respectively. The simulation time interval is $t = [0, 10]$s. For clarity, in figures where the horizontal axis is the time-axis, we use the time scale $t = [0, 2]$s.

We first investigate the overall system's behavior due to the centralized control law (22). Figure 4 shows the trajectories of the agents when (22) is exerted. It can be seen that the formation centers converge to the desired trajectory which yields the final matching of $M = \{m_1w_5, m_2w_2, m_3w_3, m_4w_6, m_5w_1, m_6w_4\}$, satisfying all conditions in Definition 6. Since the stable matching control law (23) uses the information from all agents, the calculated control values tend to be large, as embodied in Figure 2. This consequently yields a large global Lyapunov cost at $t = 0$, and instantaneously decreases as $t \rightarrow \infty$ as illustrated in the first plot of Figure 3. Furthermore, when we consider the energy dissipation function (20) for the formation center's trajectory tracking as in the second plot of Figure 3, it can be seen that the energy is monotonically decreasing as $t \rightarrow \infty$.

Next, we analyze the performance of decentralized control law (42) to achieve stable matching in the MAS. Contrary to the centralized control structure, each of the agents calculate its control action based on the information obtained from its neighboring agents. In this case, we specify the sensing range of each agent $i$ as $R = 10$ m.

Figure 5 shows the agents' trajectories and their final positions when we use (42). Comparing the magnitude of control between centralized and decentralized controllers (Figures 2 and 6, respectively), it can be observed that there is a significant amount of signal reduction in the decentralized case. The final matching established by this control action is $M = \{m_1w_6, m_2w_1, m_3w_5, m_4w_4, m_5w_3, m_6w_2\}$, which also satisfies all conditions in Definition 6.

In Figure 7, we presented the trajectory of the global Lyapunov function (47) and the cost function due the formation tracking $V_c$. For ease of illustration, the normalized scale is used in these plots. It can be seen that the cost $V_c$ due to formation tracking is monotonically decreasing even though the cost function due to SMP is non-smooth. Thus, the minimization of the cost function indicates that the control objectives (a)-(c) in Definition 6 are achieved.


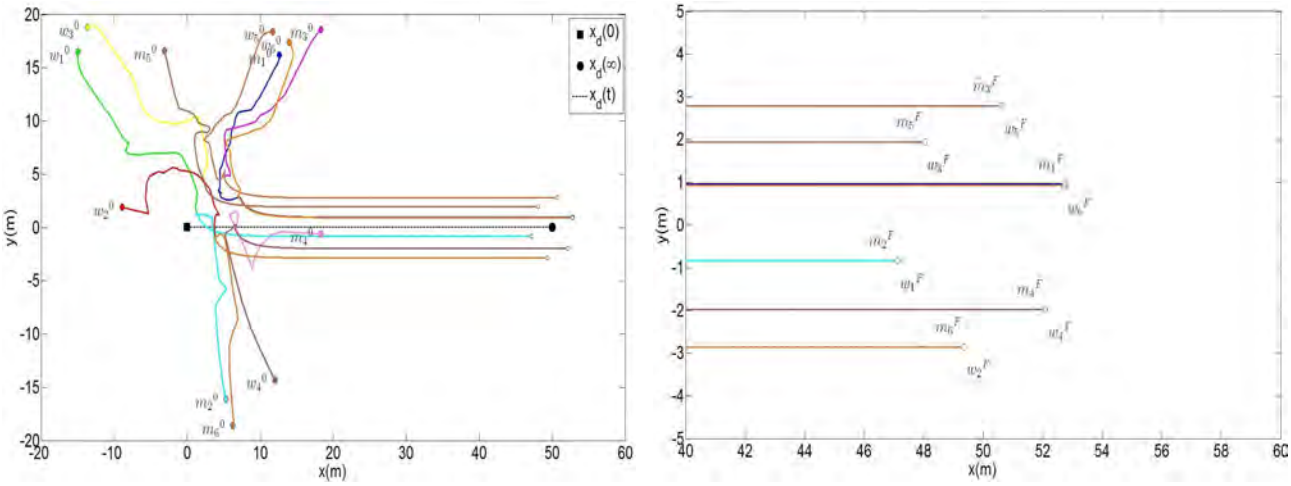


(a) Trajectories (b) Final positions (enlarged)

Figure 5: Trajectories of agents with decentralized control law (42).

## 5.2 Blocking Pairs and Stability Analysis

In the original SMP, the stability of the final matching is determined on the basis of the number of blocking pairs that exist in the solution [6, 12]. An obtained matching is said to be stable if it satisfies Definition 4. Meanwhile, in the case of dynamic SMP, we redefined stability of dynamic SMP based on the conditions in Definition 6. Meaning that the obtained matching is said to be stable if the overall system satisfies stability in the sense of Lyapunov.

Table 3 presents the results of final matching and the number of blocking pairs due to Gale & Shapley algorithm and the proposed controllers. It can be seen that that final matching obtained by the proposed controllers still exhibits a number of blocking pairs; hence, they are unstable in the sense of SMP theory. In fact, the number of blocking pairs are even higher on the decentralized control case. However, when analyzing these result in the sense of Lyapunov stability theory, we concluded through observation of the final trajectory of the agents as illustrated in Figures 4 and 5 that the final matchings are all stable matchings.

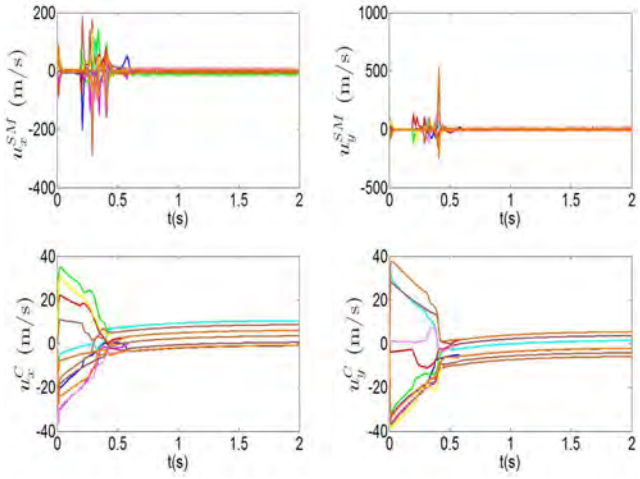


Figure 6: Control signals due to decentralized control structure.

Table 3: Final Matching and Blocking Pairs

| **Matching,** M | **GS** | **CC** | **DC** |
|---|---|---|---|
| ***Proposer*** | $p_M(m_i)$ | | |
| $m_1$ | $w_5$ | $w_5$ | $w_6$ |
| $m_2$ | $w_2$ | $w_2$ | $w_1$ |
| $m_3$ | $w_3$ | $w_3$ | $w_5$ |
| $m_4$ | $w_1$ | $w_6$ | $w_4$ |
| $m_5$ | $w_4$ | $w_1$ | $w_3$ |
| $m_6$ | $w_6$ | $w_4$ | $w_2$ |
| **BP** | 0 | 4 | 6 |

**BP** -: Total number of blocking pairs
**GS** -: Gale & Shapley algorithm
**CC** -: Centralized Control
**DC** -: Decentralized Control

In our attempt to redefine the SMP in terms of Lyapunov stability, we can see that there always exist blocking pairs in the solutions. Hence, our results suggest that the proposed control algorithm does not necessarily guarantee a Lyapunov minimization in the global sense. The trajectory solutions of the agents may trap into the local minima of the Lyapunov function, thus, yielding solutions with blocking pairs.

# 6 Conclusion

Motivated by the Gale & Shapley seminal work, we investigated the potential of acquainting the SMP theory into MAS. Two control algorithms have been presented: the

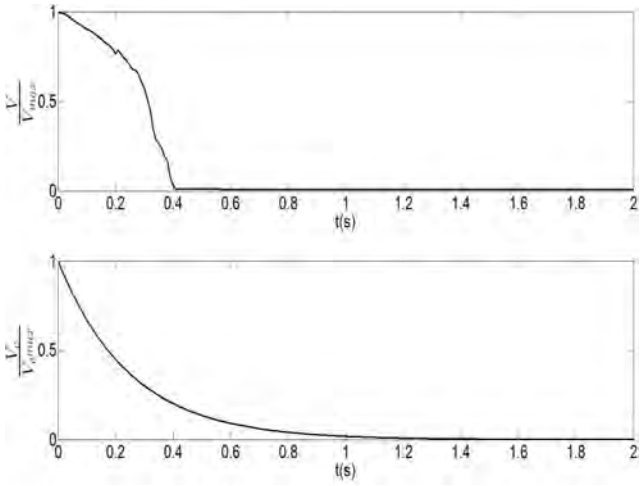


Figure 7: Lyapunov function response (decentralized control).

centralized and decentralized control structures. Our results indicated that the total system is asymptotically stable in the sense of Lyapunov, but the final matching exhibited a number of blocking pairs. Hence, the final matching is unstable in terms of SMP stability theory.

Future work in this study will include appropriate cost function incorporating the blocking pairs phenomenon in the global Lyapunov cost function. As avoiding blocking pairs is essence of stability analysis in the original SMP theory, it has been omitted in this paper due to the nonexistence of such cost function. By taking blocking pairs into account, it is expected that the derived control law can guarantee asymptotic convergence of the agents' trajectories such that their final matching shall satisfy both the Lyapunov stability and SMP theories.

## Acknowledgement

The first author gratefully acknowledges Ministry of Education Malaysia for their financial support in this work.

## References

[1] Z. Lin, W. Ding, G. Yan, C. Yu, and A. Giua, "Leader-follower formation via complex Laplacian," *Automatica*, vol. 49, pp. 1900–1906, June 2013.

[2] J. Wu and Y. Shi, "Consensus in multi-agent systems with random delays governed by a Markov chain," *Systems & Control Letters*, vol. 60, pp. 863–870, Oct. 2011.

[3] W. Ding, G. Yan, and Z. Lin, "Collective motions and formations under pursuit strategies on directed acyclic graphs," *Automatica*, vol. 46, pp. 174–181, Jan. 2010.

[4] J. Wu, S. Yuan, S. Ji, G. Zhou, Y. Wang, and Z. Wang, "Multi-agent system design and evaluation for collaborative wireless sensor network in large structure health monitoring," *Expert Systems with Applications*, vol. 37, pp. 2028–2036, Mar. 2010.

[5] Y. . Khalifa, E. Okoene, and N. Paltz, "Autonomous intelligent agent-based tracking systems, recent developments," *ICGST-Journal of Automatic Control and System Engineering*, vol. 7, no. 1, pp. 21–31, 2007.

[6] D. Gale and L. Shapley, "College admissions and the stability of marriage," *The American Mathematical Monthly*, vol. 69, no. 1, pp. 9–15, 1962.

[7] A. Roth and J. Vate, "Random paths to stability in two-sided matching," *Econometrica*, vol. 58, no. 6, pp. 1475–1480, 1990.

[8] E. Arcaute and S. Vassilvitskii, "Social networks and stable matchings in the job market," in *Internet and Network Economics*, vol. 5929 of *Lecture Notes in Computer Science*, pp. 220–231, Springer Berlin Heidelberg, 2009.

[9] P. Biró, D. F. Manlove, and E. J. McDermid, "Almost StableMatchings in the Roommates Problem," *Theoretical Computer Science*, vol. 432, pp. 10–20, May 2012.

[10] Nitin and A. Subramanian, "Efficient algorithms and methods to solve dynamic MINs stability problem using stable matching with complete ties," *Journal of Discrete Algorithms*, vol. 6, pp. 353–380, Sept. 2008.

[11] M. Nakamura, H. Kino, and K. Onaga, "Distributed Stable Marriage Problem and Its Application to Autonomous Mobile Robots Environments," *Technical report of IEICE. CST*, vol. 96, pp. 15–20, May 1996.

[12] R. W. Irving, "An efficient algorithm for the stable roommates problem," *Journal of Algorithms*, vol. 595, no. 6, pp. 577–595, 1985.

[13] L. Ehlers, "Von Neumann-Morgenstern stable sets in matching problems," *Journal of Economic Theory*, vol. 134, pp. 537–547, May 2007.

[14] S. Umeyama, "An Eigendecomposition Approach to W e ighted G raph Matching Problems," *IEEE Transactions on Pattern Analysis and Machine Intelligeence*, vol. 10, no. 5, pp. 695–703, 1988.

[15] A. Almohamad, "A linear programming approach for the weighted graph matching problem," *IEEE Transaction on Patten Analysis and Machine Intelligence*, vol. 15, no. 5, pp. 522–525, 1993.

[16] M. Nakamura, K. Onaga, S. Kyan, and M. Silva, "Genetic Algorithm for Sex-fair Stable Marriage Problem," *International Symposium on Circuits and Systems*, vol. 1, pp. 509–512, 1995.

[17] N. A. Vien and T. Chung, "Multiobjective Fitness Functions for Stable Marriage Problem using Genetic Algorithm," *SICE-ICASE International Joint Conference*, pp. 5500–5503, 2006.

[18] Y. Liu, Q. Chang, and H. Xiong, "An Improved Ant Colony Algorithm for Multi-Attribute Stable Bilateral Matching Problem," *International Conference on Logistics Engineering and Intelligent Transportation Systems*, pp. 1–4, Nov. 2010.

[19] Y. Morizumi, T. Hayashi, and Y. Ishida, "A Network Visualization of Stable Matching in The Stable Marriage Problem," *Artificial Life and Robotics*, vol. 16, pp. 40–43, June 2011.

[20] T. Hayashi, Y. Hata, and Y. Ishida, "A Diagrammatic Classification in A Combinatorial Problem: The Case of The Stable Marriage Problem," *Artificial Life and Robotics*, vol. 16, pp. 575–579, Feb. 2012.

[21] Y. Hata and Y. Ishida, "A dynamical model of stable marriage problem based on Lotka Volterra model," in *Proceedings of the International Conference on Management of Emergent Digital EcoSystems - MEDES '11*, (New York, USA), pp. 272–278, ACM Press, 2011.

[22] M. S. Ramli and S. Yamamoto, "Control of multiagent dynamic systems toward stable matching," in *Proceedings of the MJIIT-JUC Joint International Symposium 2013*, no. 4, pp. 1–4, 2013.

[23] M. Mesbahi and M. Egerstedt, *Graph Theoretic Methods in Multiagent Networks*. Princeton series in applied mathematics, Princeton University Press, 2010.

[24] D. Gusfield and R. W. Irving, *The stable marriage problem: structure and algorithms*. The MIT Press, 1989.

[25] L. B. Wilson, "An analysis of the stable marriage assignment algorithm," *BIT Numerical Mathematics*, vol. 12, pp. 569–575, Dec. 1972.

[26] T. Ito, "A Filippov solution of a system of differential equations with discontinuous right-hand sides," *Economics Letters*, vol. 4, no. 4, pp. 349–354, 1979.

[27] B. Paden and S. Sastry, "A calculus for computing Filippov's differential inclusion with application to the variable structure control of robot manipulators," *IEEE Transactions on Circuits and Systems*, vol. 34, pp. 73–82, Jan. 1987.

[28] H. Khalil, *Nonlinear Systems*. Prentice Hall, 3rd ed., 2002.

[29] A. Bacciotti and F. Ceragioli, "Stability and stabilization of discontinuous systems and nonsmooth Lyapunov functions," *Control Optimisation and Calculus of Variations*, vol. 4, no. June, pp. 361–376, 1999.

[30] F. Clarke, "Generalized gradients and applications," *Transactions of the American Mathematical Society*, vol. 205, no. 1970, pp. 247–262, 1975.

[31] D. Gu and H. Hu, "Using fuzzy logic to design separation function in flocking algorithms," *IEEE Transactions on Fuzzy Systems*, vol. 16, pp. 826–838, Aug. 2008.

[32] M. Di Marco, M. Forti, M. Grazzini, and L. Pancioni, "Set-valued derivative and Lyapunov method for full-range cellular neural networks," in *2009 IEEE International Symposium on Circuits and Systems*, pp. 2705–2708, May 2009.

# Biographies

**Mohd Syakirin Ramli** received the B. Sc. degree from Purdue University, USA and M.E. degree from Universiti Teknologi Malaysia, Skudai, Malaysia in 2005 and 2007, respectively. His research interest includes control system design, multi-agent formation control, and tele-operation. He is currently a Ph.D candidate of Graduate School of Natural Science and Technology, Kanazawa University, Japan. He is also affiliated with Faculty of Electrical & Electronics Engineering, Universiti Malaysia Pahang and currently on study leave status. He is a student member of IEEE and member of Institution of Engineers (IEM), Malaysia.

**Shigeru Yamamoto** received the B.S, M.S. and Ph.D. degrees from Osaka University, Osaka, Japan, in 1987, 1989, and 1996, respectively. In 1989, he joined the Faculty of Engineering of Osaka University as an Assistant Professor. In 1994, he joined the Faculty of Engineering Science of Osaka University, and he served there as Lecturer and Associate Professor. In 2007, he joined Kanazawa University as a Professor. His research interests include networked control systems, data-oriented controller tuning, and human support control systems. He is also a member of IEEE, JSME, SICE and ISCIE.



ICGST-ACSE Journal, ISSN: 1687-4811, Volume 15, Issue 1, Delaware, USA, June 2015

www.icgst.com

# A Novel Approach to Reduce the Spectral Ping-Pong Effect for the Mobility Management Framework in a Cognitive Radio Cellular Network.

Vinay S. Prabhavalkar and Vijay R. Ghorpade
*Department of Technology, Shivaji University Kolhapur, Maharashtra, India*
*D.Y.Patil College of Engineering & Technology Kolhapur, Maharashtra, India*
vinay.prabhavalkar@gmail.com, vijayghorpade@rediffmail.com

## Abstract

Cognitive radio devices use the unutilized spectrum i.e. the unutilized frequency resource from the underlying technology in that region. When a primary user appears in a channel, the cognitive radio (CR) devices switch to a different channel which leads to spectral handoff. When this switching happens in a very quick succession, the CR device barely gets chance to carry out its work and is forced to account the spectral handoff's leading to the spectral ping-pong effect. In this paper, two load based algorithms are devised that consider the current load on the system to allocate the frequency resources to the CR devices. CR_resource_allocation algorithm allocates resources when a CR device enters the coverage area of a base station (BS), and CR_handoff algorithm allocates resources to the CR device when it undergoes a handoff process. Simulations show that, the proposed algorithms significantly reduce the number of handoff for the CR device thereby reducing the spectral ping-pong effect.

***Keywords:*** *Cognitive radio, spectrum hole, spectral handoff, ping-pong, proactive handoff.*

***Nomenclature:***

| | |
|---|---|
| CR | Cognitve Radio |
| BS | Base Station |
| FCC | Federal Communication Commission |
| SU | Secondary User |
| PU | Primary User |
| PRP M/G/1 | Preemptive Resume Priority Queuing |
| OSAB | Opportunistic Spectrum Access with Backup |
| BA | Base Area |
| EA | Extended Area |
| CRCN | Cognitive Radio Cellular Network |
| QoS | Quality of Service |

## 1. Introduction

Cognitive radio is a cutting edge technology that allows the cognitive radio devices to utilize the unused frequency channels of the underlying technology without interfering the working of the registered users.

Figure 1 shows Cognitive Radio Network [1] in which two licensed and one unlicensed band are shown.

[1]This work is being implemented on the Java platform at the Shivaji University Kolhapur, Maharashtra, India as a M.Tech research work.

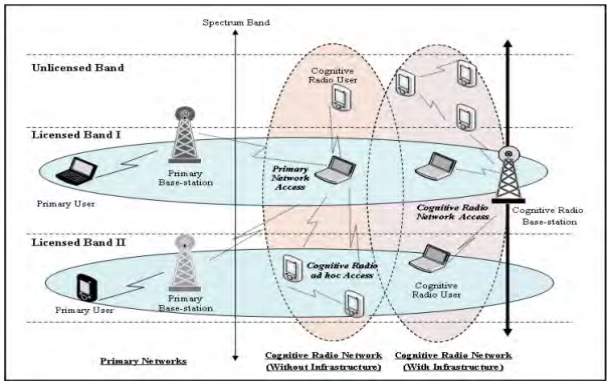


Figure1: A sample Cognitive Radio Network

Cognitive radio base station can access all the three bands and provide services to CR users, where as primary base stations operate in licensed band and provide services to the PUs. Thus, when a cognitive radio network is deployed in an area, the cognitive radio base station senses all the available frequency channels falling in different technologies in its coverage area, and allows the CR devices to utilize those channels that go unused. This utilization is as per the recommendation of the FCC [2]. Here the registered users are the primary users of the underlying technology called as PUs and the secondary users are the cognitive radio devices called as secondary users (SUs) or CR devices. The PUs holds the higher priority over the SUs for the
frequency resource contention. Thus when the PUs demand a channel already occupied by the SU, the SU vacates that channel immediately and finds a different channel in the same or different frequency pool. This scenario is called as the spectral handoff scenario.

When a SU find a new frequency channel (finds a spectrum hole [3]) for its use, there incurs the reconfiguration of the radio frequency circuitry of the SU device. This reconfiguration consumes some time which makes the problem more worst if the frequency pools are far apart. To add to this problem, if the SU is moving at a faster speed the situation deteriorates even more. To solve this problem, a mobility supporting cell structure [4] is used which is explained in 3 ahead in this paper. Based on this structure, load based algorithms are devised that intelligently allocate frequency resources to the CR devices in such a way that they account for less number of handoff.

The remainder of the paper is organised as follows: In section 2 a brief review of handoff in cognitive radio networks is presented. In section 3 the spectrum pool structure is described. In section 4 the mobility supporting cell structure is described. In section 5 handoffs and their types are described. In section 6 integrated mobility and handoff management method is described. In section 7 frequency allocation method is described. In section 8 load based frequency allocation and handoff algorithms for the CR devices are described. In section 9 the simulation setup is given. In section 10 the simulation results are discussed, and finally in section 11 the conclusion is given.

## 2. Review of handoffs in cognitive radio networks

A lot of research has been carried out by various researchers regarding the handoffs in the cognitive radio networks.

Li-Chun Wang and Chung-Wei Wang, [5] has proposed and analyzed a PRP M/G/1 queuing network model based on which, the proactive or reactive handoff is to be done is decided.

C.-W. Wang, L.-C. Wang, and F. Adachi, [6] has proposed a Markov transition model in which a secondary user has a series of target channels which can be utilized sequentially when required.

M. Kalil, H. Al-Mahdi, A. Mitschele, [7] has proposed a OSAB channel where the unlicensed channels are used as backup for handoffs in addition to the licensed channels.

Soumaya Dahi, Sami Tabbane, [8] have proposed a sigmoid (S-shaped curve) based method of channel selection which considers the highest channel idle time.

Lu Li, Yanming Shen, Keqiu Li, Kai Lin, [9] has proposed a time based method for spectral handoff consisting of two probabilities namely- busy-to-idle and idle-to-busy to determine the target channel.

J. Guo, H. Ji, Y. Li, X. Li, [10] has proposed a support vector machine (SVM) based model to predict the point of handoff, so that the SU can get some time to prepare for the handoff before the channel is occupied by the PU.

Mrs. R. S. Kale (Sandikar), Dr. Vijay M. Wadhai, Dr. Jagdish B. Helonde, [11] has proposed a spectrum handoff based on efficient spectrum sensing and proper handoff decision. Here a fuzzy logic based decision is made to take a proper handoff decision.

Vinay S. Prabhavalkar, Dr. Vijay R. Ghorpade [12] gives a survey on the spectral handoffs for the Cognitive Radio Networks.

Venkatesan.D, Sathishkumar. S [13] has proposed a PRP M/G/1 queuing network model based Real Time Spectrum Handoff method. Here, the latency performance of the secondary connections was studied. The proposed model accurately estimates the extended data delivery time of different proactively designed target channel sequences.

Samad Nejatian, Sharifah K. Syed-Yusof, Nurul M. Abdul-Latiff [14], has used neural networks, fuzzy logic to devise intelligent-based (IB) cognitive radio learning for spectrum mobility in cognitive radio network.

The proposed approach is a novel method and is different from the existing once in that the load based allocation of frequency resource is considered while initial resource allocation and also during the handoff process. It has been proved that the load based allocation of frequency resource incurs less number of handoffs for the CR devices.

## 3. Spectrum pool structure

Spectrum pool is a core component of the cognitive radio network. Figure 2 shows the spectrum pool structure:-

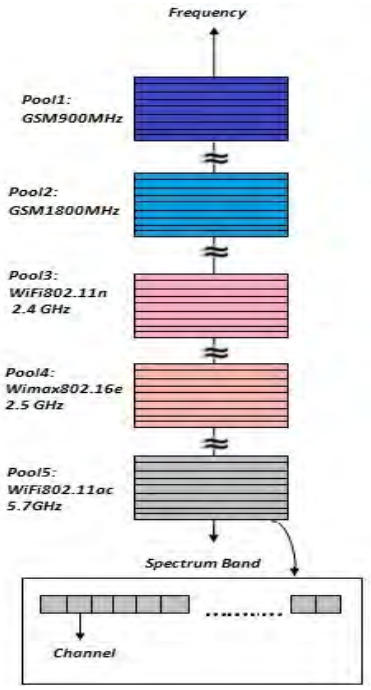


Figure 2: Spectrum Pool Structure

***Frequency pool:*** It is a bunch of contiguous frequency bands available in a technology.

***Frequency band:*** A frequency band is nothing but a basic bandwidth required for operating a wireless technology.

***Frequency channel:*** A channel is the minimum logical unit of wireless frequency resource required by a mobile user to access the technology.

## 4. Cell Structure

In the cognitive radio network each base station is assigned spectrum pools [15] based on the predetermined frequency reuse factor considering the neighbouring cells. Each base station is divided into two parts namely- BA and EA [15].

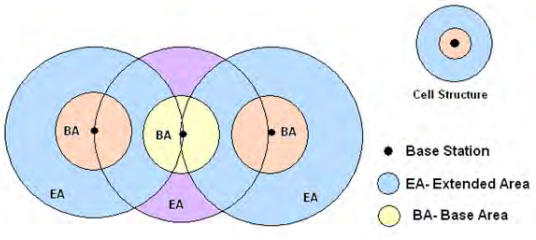


Figure 3. Cell structure with spectrum pool allocation

The BA consists of the entire frequency bands except one band and is the inner covering ring whereas the EA is the

outer covering ring of frequency resource and consists of only one frequency band. Figure 3 gives the cell structure with the spectrum pool allocation:
In figure 2, the different colours of the base stations denote the frequency pools of different frequency. It is worth to note that, no two pool of same frequency can be places besides each other but can be placed with a gap of a base station as depicted. This type of frequency pool allocation is as per the frequency reuse factor mentioned above.

## 5. Handoff Types

In a traditional cellular network, there exists only one handoff which occurs when there is a change in the cell by the mobile user due to mobility. But in the case of the cognitive radio device, there exist two types of handoffs- a traditional handoff when there is a change in the cell due to mobility and second is the spectral handoff [15] due to the spectral mobility of the cognitive radio device. Thus based on the spectral mobility and the pool allocation structure there exists four handoff types as follows;

1. ***Intracell–Intrapool handoff (type 1):*** A handoff that occurs within the same cell and same frequency pool.
2. ***Intracell–Interpool handoff (type 2):*** A handoff that occurs within the same cell but different frequency pool.
3. ***Intercell–Intrapool handoff (type 3):*** A handoff that occurs between two cells but same frequency pool.
4. ***Intercell–Interpool handoff (type 4):*** A handoff that occurs between two cells and different frequency pool.

## 6. Integrated mobility and handoff management

Figure 4 shows the integrated mobility and handoff management method [14]. Physical layer continuously monitors the SU mobility and PU activity, the MAC layer provides the channel access method and the network layer monitors the packet traffic. The handoff management framework thus, not only monitors the SU mobility and PU activity, but also analyzes the available spectrum and accounts for decision making for handoff. This is where the CR_Resource_Allocation and CR_Handoff algorithms come into picture. These algorithms are explained in detail in section 8 of this paper.

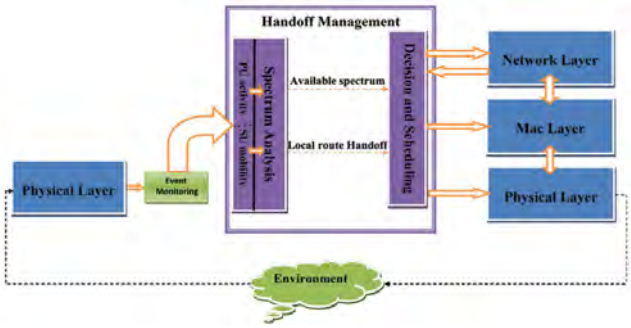


Figure 4 Integrated mobility and handoff management

## 7. Frequency Allocation Method

All the cognitive radio devices are considered to acquire the channels through the centralized sensing technique [16][17][18]. In the centralized sensing technique, the BSs collect the sensing information from the CR devices and control the handoff procedure. Figure 5 shows how the PUs and SUs are allocated the frequency resource. The PUs are allocated the frequency resource directly from the frequency pool, where as the SUs are allocated the frequency resource through the load based frequency resource algorithms.

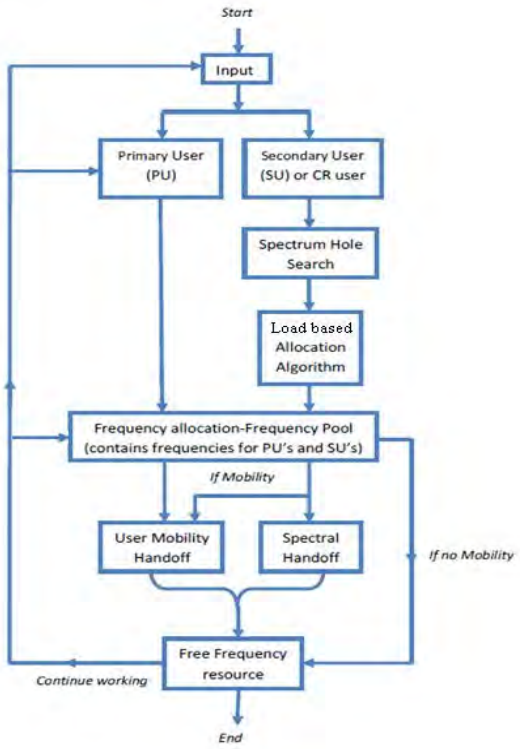


Figure 5. Frequency allocation method for PUs & SUs.

## 8. Algorithms

**Algorithm: CR_Resource_Allocation**

This algorithm is called as 'CR_resource_allocation' is used by the BS to allocate the frequency resource when the CR user (CR node) enters into the coverage range of that BS. It takes the CR node, frequency pool and their channels as input and either returns the frequency resource in a channel of a pool or NA if there is no frequency resource to allocate to the CR node as output.
The algorithm starts with the load calculation of each channel in the pool. Here two threshold values are maintained namely- minimum threshold and a maximum threshold [20]. The minimum threshold signifies those channels that are below the 30 % usage level and the maximum threshold signifies those channels that are above the 80 % usage level. After the load for the channel is calculated, it first checks whether the channel is below the minimum threshold level. If the channel falls below this level, it is directly allocated to the CR node. This makes sure that even if at some later time a PU arrives and asks for the frequency resource in that channel, it gets it without forcing the CR node to go for a spectral handoff [21]. Further, if the channels load is greater that minimum

threshold and less than the maximum threshold value, the algorithm selects that frequency channel whose load value is the lowest among all the channels load above the minimum threshold and below the maximum threshold. Further if the channels load is more than the maximum threshold but the channel is not utilized full, that channel is allocated. Now, in case the channel utilization is full, the channel is discarded as it cannot allocate any frequency resource to the CR node. This is where the algorithm returns a NA value.

```
I/P:  CR node, channel (ch), pool
O/P:      1. Allocated frequency resource (pool, ch)
          2. Resource not available (NA)

ch_with lowest_load=Φ
lowest_load=Φ
for each ch of pool
        load = pool.get_resource_used (ch)
        if load<= min_threshold
                Return pool,ch;
        else if load > min_threshold and
load<max_threshold      //80%
                if lowest_load= Φ
                        lowest_load=load
                        ch_with_ lowest_load= ch
                else if load< lowest_load
                        lowest_load= load
                        ch_with_ lowest_load= ch
                    end if
                end if
        end if
        end if
end for

if ch_with_ lowest_load != Φ
        return pool, ch_with_ lowest_load
else
        for each ch' of pool
                 load' = pool.get_resource_used (ch')
                if load'==100
                        Continue to for
                end if
                if lowest_load== Φ
                        lowest_load= load'
                        ch_with_lowest_load=ch'
                else if  load< lowest_load
                        lowest_load= load'
                        ch_with_ lowest_load= ch'
                end if
                end if
        end for each
end if
if ch_with_lowest_use!= Φ
        return pool, ch_with_ lowest_load
end if;
return NA
```

**Algorithm: - CR_Handoff**

This algorithm is called as 'CR_handoff' accounts for the actual handoff procedure. Here it considers the load on the system before allocating the frequency resource in the same or new pool in the same or adjacent BS. The algorithm takes the CR node as input and gives the new channel and or pool as output. Thus depending upon the new channel and pool, the handoff type is determined as mentioned above in this paper. The algorithm considers the current channel and pool of the CR device and calculates the load for that channel.

```
I/P: CRnode
O/P: reallocated channel within a pool

step1:
        pool = CRnode.allocated_pool
        ch = CRnode.allocated_ch
step2:          load = pool.get_resource_used (ch)
        if load > max_threshold    //80%
                lowest_load = Φ
                lowest_loaded_ch = Φ
                for each ch' of pool
                  load'= pool.get_resource_used (ch')
                  if load' < max_threshold
                        if    lowest_load==    Φ       ||
load'<lowest_load
                        lowest_load=load'
                        lowest_loaded_ch=ch'
                        end if
                   end if
                if lowest_load!= Φ CRnode.handoff to
(lowest_loaded_ch)      //Intra Cell Intra Pool
                        Return;
                end if
step3:  lowest_avg_load = Φ
        lowest_avg_loaded_pool = Φ
step4:   for each pool' of BS
                avg_load' = pool'.get_avg_load
                if avg_load'<max_threshold
step5:                  if    lowest_avg_load==    Φ    ||
avg_load' < lowest_avg_load
                lowest_avg_load = avg_load'
                lowest_avg_loaded_pool = pool'
                        end if
                end if
        end for
step6:   if(lowest_avg_loaded_pool != Φ )
                CR.node.handoff                         to
(lowest_avg_loaded_pool)//IntraCellInter Pool
                Return;
        end if
        end for
        end if
step7:  for each BS         //inter cell intra pool and inter
cell inter pool
          perform step 2 - step 6.
```

If the load is above the maximum threshold value then, it calculates the load for all the channels in that pool and finds a channel with the lowest load and makes the CR device to switch that channel thus accounting for the intracell-intrapool handoff. If it doesn't find any channel in that pool, then the algorithm finds a channel in another pool. At this point, the algorithm calculates the average load for each pool available under that BS and selects one with lowest average load below the maximum threshold now accounting for the intracell-interpool handoff.


Further, if the algorithm dosen't finds any pool's average load below the threshold value, it finds a channel in same pool of another BS thus accounting for the intercell-intrapool. Finally if the same pool in the new BS is also not satisfying the load condition, it performs the intercell-interpool handoff making the CR device to move to a new pool of the new BS.

## 9. Simulation Setup

This project is implemented in Java using the Net beans integrated development environment (IDE). A cognitive radio network simulation environment is designed to carry out the simulation as per the following parameters

**Base Station:**

The experimental setup consists of 4 BS. Given below are some common parameters that describe BS in detail:-

1. Each BS has a unique identifier called as 'cell ID'.
2. BS's base area covers a distance of 2 km and the extended area covers a distance of 4 km. That is, EA is considered to double the coverage area compared to BA.
3. Each BS is assigned two frequency spectrum pools.

**Frequency Pools:**

Five frequency pools in three different technologies are considered in this project, namely- GSM (900MHz & 1800 MHz), Wi-Fi (802.11ac & 802.11n), and Wimax (802.16e). The uplink and downlink frequencies of the GSM 900 are- 935 MHz to 945 MHz and 890 MHz to 900 MHz respectively. For the GSM 1800 the uplink and downlink frequencies are – 1710 MHz to 1720 MHz and 1805 MHz to 1815 MHz respectively. Further each GSM pool is considered to have maximum 5 frequency bands. These bands are divided into eight logical channels called as time slots. Thus as per the TDMA/FDMA channel access method of GSM, a maximum of 40 users per pool can be allocated the frequency slots simultaneously. The Wi-Fi 802.11n band start frequency is 2401 MHz and end frequency is 2472 MHz It has a total of 13 channels as per the standard channelization in this band. The Wi-Fi 802.11ac band start frequency is 5735 MHz and end frequency is 5815 MHz This pool has a total of 5 Wi-Fi channels. The Wimax 802.16e frequency pool has starting frequency 2500 MHz and end frequency is 2600 MHz Here the Wimax pool has a total of 5 frequency channels.

**Node:**

All the primary nodes- Wi-Fi, Wimax and GSM and also all the secondary nodes- CR devices are considered to move at a distance of 60 kmph, 70 kmph, 80 kmph. The nodes are chosen randomly to get any one speed out of the three variations available. Further each node is assigned a direction randomly. The node continues to move in only that direction. There are four power levels set to each node in this project as per the energy model-transmission power (Tx), reception power (Rx), idle mode power (Ix), and sleep mode power (Sx). The values of these levels are- Tx=1.33 Rx=0.97, IX=0.84, and Sx=0.07. Also it is considered that each node is a battery powered device and has a battery of 2500mAh as its power source.

**Network:**

The network layer is considered to have the following parameters for the packet creation-

Source and destination address-it is an IP address chosen randomly. Each packet [10] is considered to have a hop count of 10, a payload size of 1KB and the header of 128 bytes. Each base station is considered having different network address ranges. Further, a packet is generated every 500ms to consider the QoS parameter for the mobile nodes.

Each node is given a random MAC address and a queue of length 50 is maintained at each node. Also each packet is considered to have a sequence number which is maintained at the logical link layer (LL).

At the physical layer, the propagation model called as 'shadowing' based on Friis's Equation is derived with following values:-

Received power at distance'd' = Pr(d). This Pr(d) is based on the transmission power from the base station. $G_r$ and $G_t$ are the gains at the transmitter and the receiver which are considered to be 1. Further the wavelength ($\lambda$) is derived based on the values of the frequency signal and the speed of light. The path loss coefficient is considered to be 1.

**Simulation Scenario:**

Frequency pools allocated to each BS and the number of mobile nodes deployed in this scenario, are as follows:

BS1: Wi-Fi 802.11n and Wimax 802.11e
BS2: GSM900 and Wi-Fi 802.11ac
BS3: Wi-Fi 802.11n and Wimax 802.11e
BS4: GSM1800 and WiFi802.11ac
Number of GSM, Wi-Fi, Wimax, and CR nodes is 60 each.

## 10. Simulation Results

The simulation is run for 180 seconds, first without the inclusion of the algorithm and second with the algorithms and the following results were obtained which are compared with each other to draw the conclusion. The simulation results contains the graph generated for the number of handoff's on Y-axis against the four types of handoffs at the speed of 60, 70, and, 80 KMPH on X-axis. Figure 6 shows a summary graph for the whole system for the simulation without any algorithm. This is followed by the individual BS graph shown in figure 7,8,9,10. Next, figure 11 shows the summary graph for the whole system for the simulation with the algorithms. This is followed by the individual BS graph shown in figure 12,13,14,15. The summary graph contains the aggregated values of individual BS graphs for the algorithms use and unused run instances of the simulation respectively.

In this simulation, the emphasis is on measuring the number of handoff that take place across all the BS's in the system rather than measuring the QoS and energy efficiency parameters. In the traditional environment, it is observed that, whenever any CR device is needed the frequency resource, it is allocated as per the availability i.e. as soon as any frequency channel is found vacant, it is allocated. In this situation, whenever there comes a PU and demands the channel, the CR devices has to switch to

a different channel. Such a switch is observed to happen frequently giving rise to the spectral ping-pong effect. Specifically, the effect can be seen in the type 1 handoff (intracell-intrapool) as per the simulation setup.

This effect is seen to be minimized with the inclusion of the algorithms in the system. When the algorithms are added to the same scenario, they yield better results which can be easily verified in the graphs above. A comparative study of figure 11 and figure 6 shows that, the total number of handoff considerably go down when the load on each pool of each BS is considered to allocate the frequency resource. In figure 6, where the total number of handoffs of type 1 occur for several hundreds and type 2,3,4 handoff occur for few more than a hundred, are considerably reduced in figure 11, where type 1 handoff occurs somewhat over hundred and type 2,3,4 handoff occur for atmost 30. Also it is worth to note that the spectral handoff are done on a priority basis, i.e. firstly intracell-intrapool (type1) is checked for frequency allocation, then followed by intracell-interpool (type2), intercell-intrapool(type3) and intercell-interpool (type4) respectively. It is also worth noticing that, these handoffs also depend upon the location of the CR device in the BS. Depending upon the location, the handoff type changes which depend upon the frequency channels they sense. This is how the uneven or sporadic utilization of the frequency resource is now optimized to accommodate the CR nodes and account for less number of handoff to reduce the spectral ping-pong effect.

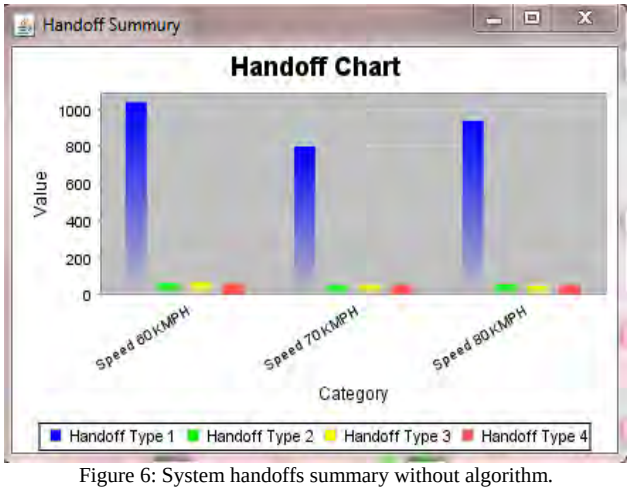


Figure 6: System handoffs summary without algorithm.

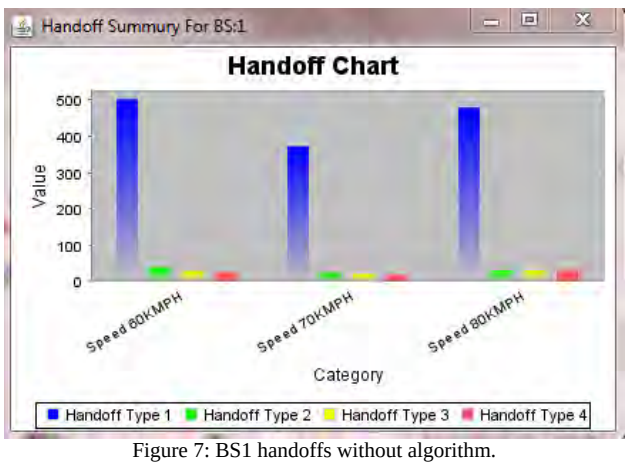


Figure 7: BS1 handoffs without algorithm.

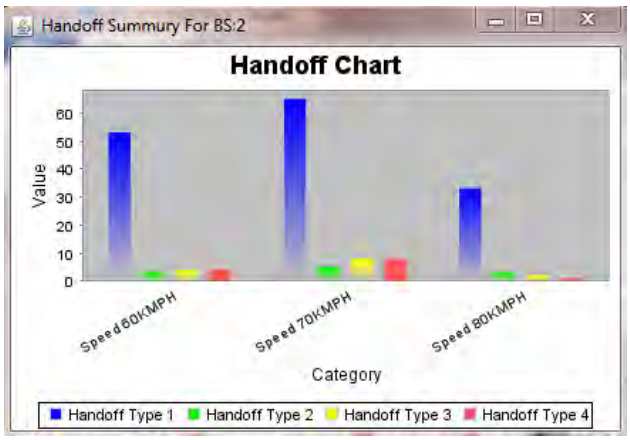


Figure 8: BS2 handoffs without algorithm.

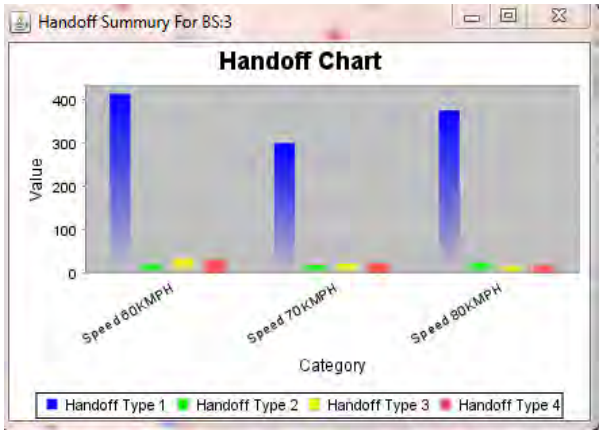


Figure 9: BS3 handoffs without algorithm.

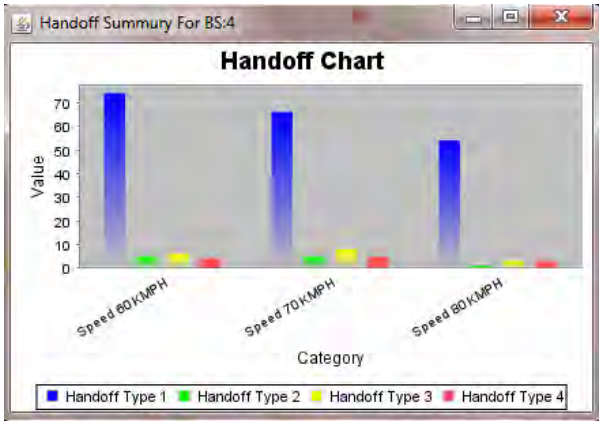


Figure 10: BS4 handoffs without algorithm.

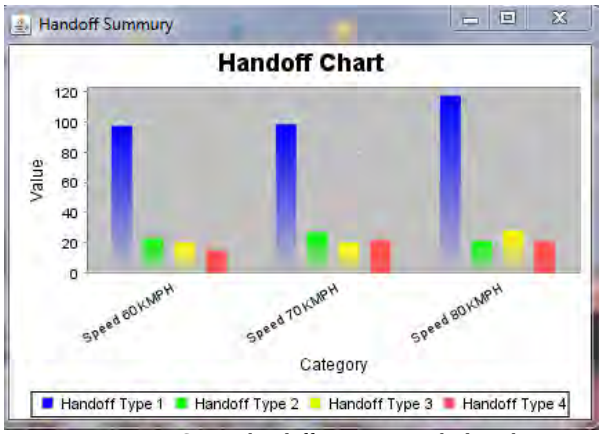


Figure 11: System handoffs summary with algorithm.

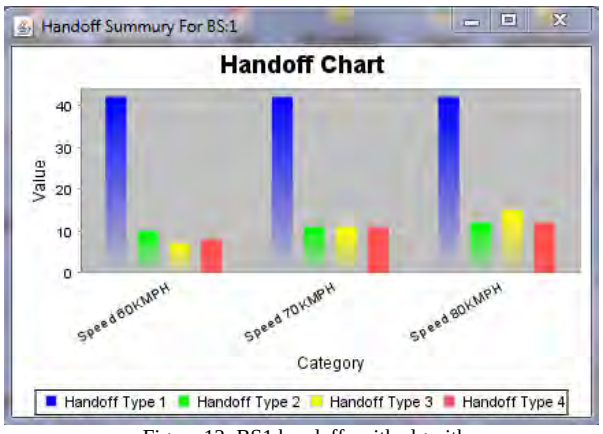


Figure 12: BS1 handoffs with algorithm.

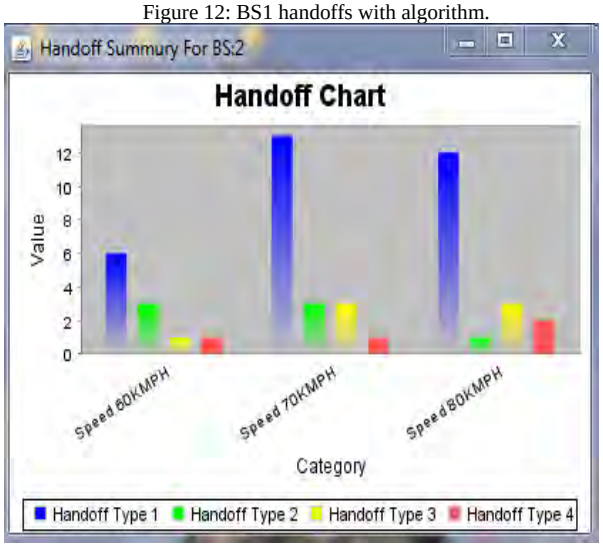


Figure 13: BS2 handoffs with algorithm.

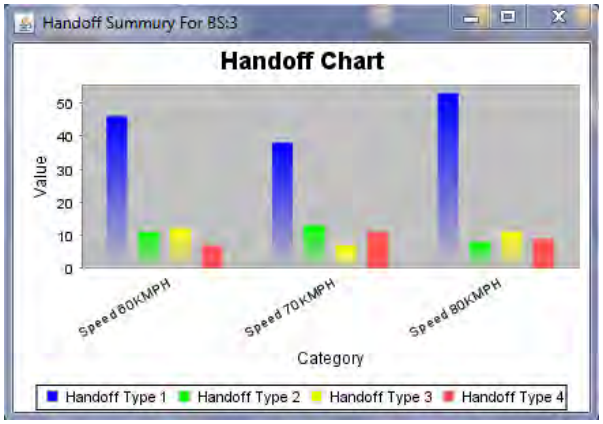


Figure 14: BS3 handoffs with algorithm.

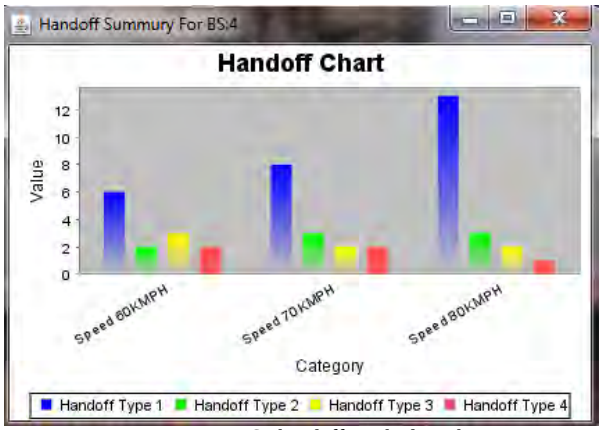


Figure 15: BS4 handoffs with algorithm.

## 11. Conclusion

Frequent frequency handoffs are a cause of spectral ping-pong effect for the CR devices. In this paper, a novel method to reduce the spectral ping-pong effect in a cognitive radio cellular network is proposed. To reduce this effect i.e. to lower the number of handoffs in the system, algorithms that consider the current load on the system have been devised. These algorithms calculate the current load on each pool before allocating resource to the CR device, and allocate a channel in that pool which has lowest load.

In this paper, results of the cognitive radio network without the use of algorithms were compared against the cognitive radio network with the use of load based algorithms. Simulation results show that there is 85% decrease in the number of handoff in the system. From the simulation results, it has been concluded that the load based approach to allocate the resources to the CR devices proves very beneficial to reduce the spectral ping-pong effect as it accounts for less number of handoffs.

## References

[1] http://howdoesinternetwork.com/2012/cognitive-networks/cognitive-radio-system

[2] FCC, ET Docket No 03-222 Notice of proposed rulemaking and order, December2003.

[3] Ian F. Akyildiz, Won-Yeol Lee, Mehmet C. Vuran, Shantidev Mohanty, “NeXt generation/dynamic spectrum access/cognitive radio wireless networks: A survey”, Computer Networks 50 (2006) Elsevier 2127–2159

[4] T.A. Weiss and F.K. Jondral, “Spectrum Pooling: An Innovative Strategy for the Enhancement of Spectrum Efficiency”, IEEE Comm. Magazine, vol. 42, no. 3, pp. 8-14, Mar. 2004.

[5] Li-Chun Wang¤ and Chung-Wei Wang “Spectrum Hando® for Cognitive Radio Networks: Reactive-Sensing or Proactive-Sensing?”, IEEE 2008.

[6] C.-W. Wang, L.-C. Wang, and F. Adachi, “Modeling and analysis for reactive-decision spectrum handoff in cognitive radio networks,” IEEE Globecom, 2010.

[7] M. Kalil, H. Al-Mahdi, A. Mitschele-Thiel, “Spectrum Handoff Reduction for Cognitive Radio Ad Hoc Networks”, IEEE ISWCS, 2010.

[8] Soumaya Dahi, Sami Tabbane “Sigmoid Utility function Formulation for Handoff Reducing Access model in Cognitive Radio”, IEEE 2013.

[9] Lu Li, Yanming Shen, Keqiu Li, Kai Lin, “TPSH: A Novel Spectrum Handoff Approach Based on Time Estimation in Dynamic Spectrum Networks”,IEEE 2011.

[10] J. Guo, H. Ji, Y. Li, X. Li, “A Novel Spectrum Handoff Management Scheme based on SVM in Cognitive Radio Networks”, in Proc of 6th International ICST Conference on Communications and Networking(CHINACOM), IEEE2011.

[11] Mrs. R. S. Kale (Sandikar), Dr. Vijay M. Wadhai, Dr. Jagdish B. Helonde, “Optimized Spectrum Handoff Delay in Cognitive Radio through Efficient Spectrum Sensing and Proper Decision of Handoff”, International Journal of Research in Advent Technology, Vol.2, No.4, April 2014 . E-ISSN: 2321-

9637
[12] Vinay S. Prabhavalkar, Dr. Vijay R. Ghorpade, “A Survey on Spectral Handoff Mechanisms for the Cognitive Radio Network”, International Journal on Recent and Innovation Trends in Computing and Communication Volume: 3 Issue: 1 ISSN: 2321-8169.
[13] Venkatesan.D, Sathishkumar.S, “A Novel Approach to Real Time Spectrum Handoff”, OSR Journal of Computer Engineering (IOSR-JCE) e-ISSN: 2278-0661, p- ISSN: 2278-8727Volume 9, Issue 2 (Jan. - Feb. 2013)
[14] Samad Nejatian, Sharifah K. Syed-Yusof, Nurul M. Abdul-Latiff, Ali Farzamnia, “Self-organizing intelligent-based cognitive radio learning system for proactive pre-emptive unified spectrum handoff: a conceptual framework”, Fifth International Conference on Intelligent Systems, Modelling and Simulation, 2014 IEEE.
[15] Won-Yeol Lee, Student Member, IEEE, and Ian F. Akyildiz, Fellow, IEEE “Spectrum-Aware Mobility Management in Cognitive Radio Cellular Networks “,IEEE TRANSACTIONS ON MOBILE COMPUTING, VOL. 11, NO. 4, APRIL 2012.
[16] Li-Chun Wang¤ and Chung-Wei Wang “Spectrum Handoff® for Cognitive Radio Networks: Reactive-Sensing or Proactive-Sensing?”, IEEE IPCCC 2008
[17] Chung-Wei Wang¤+, Li-Chun Wang¤, and Fumiyuki Adachi, “Modeling and Analysis for Proactive-decision Spectrum Handoff in Cognitive Radio Networks”, IEEE International Conference on Communications (2009)
[18] Tevfik Y¨ucek and H¨useyin Arslan “A Survey of Spectrum Sensing Algorithms for Cognitive Radio Applications”, IEEE COMMUNICATIONS SURVEYS & TUTORIALS, VOL. 11, NO. 1, FIRST QUARTER 2009.
[19] V. R. Ghorpade Y. V. Joshi and R. R. Manthalkar, “Fuzzy Logic based Trust Management Framework for MANET, ICGST DSP Journal, Volume 8, Issue 1,December, 2008.
[20] Jiang Zhu, Zhengguang Xu, Furong Wang, Benxiong Huang, Bo Zhang, “Double Threshold Energy Detection of Cooperative Spectrum Sensing in Cognitive Radio”, in Proc IEEE CrownCom 2008.
[21] Suk-Un Yoon and Eylem Ekici, “Voluntary Spectrum Handoff: A Novel Approach to Spectrum Management in CRNs”, IEEE ICC 2010

## Biographies

**Vinay Sudhir Prabhavalkar** has received the Bachelor of Engineering in Computer Science & Engineering Degree from Shivaji University Kolhapur in the year 2008. Currently he is pursuing the M.Tech at the Shivaji University, Kolhapur, Maharashtra, India. His areas of interest include- Cognitive Radio Cellular Network and their handoffs.

**Dr. Vijay R. Ghorpade** has completed his PhD in Computer Science & Engineering in 2008. He is presently working as Principal/Professor at the D. Y. Patil College of Engineering & Technology, Kolhapur, Maharashtra, India. He is guiding 8 PhD students and several PG students. He has published papers in various national and international journals. His area of interest is network security, and ad-hoc networks.

www.icgst.com

# DESIGN OF SOLAR POWERED MOBILE CHARGER WITH POWERBANK USING SUPERCAPACITOR AND STORAGE BATTERY FOR FAST CHARGING

Kottam Pranay Kumar[1], K.Uday reddy[2], G.Jithendra Naidu[3], S.Siva Prasad[4]
[1, 3&4]*Department of Electrical Engineering, J.B Institute of Technology, Hyderabad, India.*
[2]*Department of Mechanical Engineering, SRM University,Chennai,India.*
E- Mail: [1]Pranay829reddy@gmail.com,
[2]udaykottam@gmail.com,[3]jithu10920821@gmail.com,[4]sshivprasadeee@gmail.com

## ABSTRACT

In this paper a new method is proposed and investigated the performance that can make use of the Supercapacitor connected in series with a storage battery for quick charging, controlled with MoSFETs and Op-Amps. The main advantage of the proposed method is that we can integrate the whole set up into the mobile pouch so we can charge the power bank on the go and we can use the stored energy in power bank to charge the gadgets battery.

***Keywords:****Energy storage, Supercapacitor, MoSFET, Op- Amp, Power bank, charging time.*

**Nomenclature**

| | |
|---|---|
| MoSFET | Metal Oxide Semiconductor Field Effect Transistor |
| Op- Amp | Operational Amplifier |
| mAh | milliampere hour |
| PV | Photovoltaic |
| A.B | Auxiliary Battery |
| C | Supercapacitor |
| M.B | Mobile Battery |
| $D_i$ (i=1…..n) | Diodes |

## 1. Introduction

The scientific development over the past century paved ways to utilize natural resources and converting them according to our use. Out of different renewable energy conversions available, Photo voltaic conversion provides us a great advantage of availability of solar energy, mobility and less dynamic losses.Modern mobile electronic devices operate with electrical energy which is stored in form of chemical energy in rechargeable batteries and supply to these devices when needed. But the capacity of these batteries is limited, so under prolonged operation, battery may not be able to provide enough energy especially at remote places where there is no supply of electric power. Instead of depending on external power source we can generate power from renewable solar power on board and also store the generated energy in battery[1] and supercapacitorfor recharging. With the available solar power banks in market it will take 5-6 hours of time to charge it completely. The portable solar chargers available in the market such as Changers®, SolarJoos®, Sunjack® make use of batteries and control electronics to power up the mobile battery using solar panel and they are promising it will take 4-6 hours of time to charge a mobile battery based on the panel size, sun shine and alignment of panel towards sun. Even at high power generation by the solar panel, the power(in watts) intake capability of power bank battery is limited by the electrode materials of the battery due to limitation of electron transfer across phase boundary. But in case of supercapacitor the phase changing process during charge and discharge is not presentand charge accumulation takes along the surface of electrodes, result in fast charging and discharging. By making use of Supercapacitor we can bring down the charging time(in hours) nearly to half of it. For this problem, we have introduced a method that can make use of supercapacitor in conjunction with auxiliary battery which helps to charge faster and store more energy enough to supply mobile device battery and quickly charging it. In this paper we have designed a system which uses a supercapacitor and an auxiliary battery in conjunction so they can be used to charge fast during charging mode and supply the charge to the mobile battery during supply mode continuously.

The remainder of the paper is organized as follows: Section (2) focuses on working principle of the proposed method, Section (3) emphasizes on

detailed explanation of the proposed method, Section (4) explains the advantages of the proposed method over the existing technologyand Section (5) focuses on the experimental analysis.

## 2. Working Principle

Electrochemical capacitors, also known as supercapacitors, store energy in an electric field within an electrochemical double layer. The so-called nonfaradaic mechanism[2], is a principle for electrochemical capacitor operation. The non faradic mechanism is quick process unlike insertion or conversion mechanism applied in batteries. So we can charge and discharge the supercapacitor quickly [3]. At the electrode/electrolyte interface a capacitor with an electrical double layer is formed. It is composed of charges on a metal surface and ions of opposite charge in the solution directly adjacent to the electrode surfaceas shown in Figure.1. Using electrodes with a developed surface such as graphite allows obtaining high capacitance values[4][5][6].In the process ofcapacitor charging or discharging an internal change of electrode potential(in volts) is continuously observed. Since for mobile Battery charging we need voltage which is approximately constant and higher than

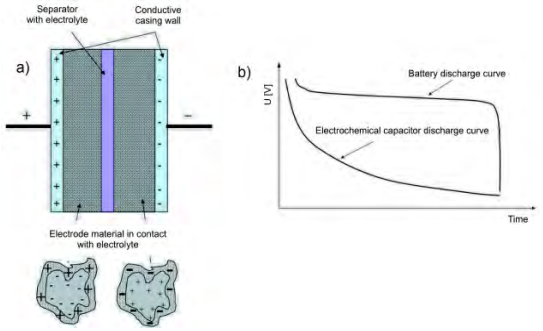


Figure 1. a) Electrode and electrolyte arrangement in a supercapacitor, b) discharge curves of a battery and a supercapacitor

its operating voltage using only a supercapacitor for charging is not sufficient. Also the energy density(inKilo Watt-hour) is less for Supercapacitor[5] which is not enough for electronic devices to operate for longer time. So to provide higher operating voltages and high Energy storage[7] in conjunction with fast charging we are connecting Supercapacitor(or supercap) in series with auxiliary battery [8] for discharge operation by and charging them using a PV solar panel. For control operation in order to control battery and supercapoperation in series when needed and for activation of secondary circuit for charging when supercap is fully discharged we are using a set of MOSFETs. Also we use Mechanical switching mechanism to switch charging mode and operation mode manually as shown in Figure.7. A micro controller is programmed to switch the voltage supply to the Gate terminals in between two types of MoSFETswhich are assigned for controlling flow of charge through different circuits in the system.

## 3. Proposed Method

The solar energy obtained from Photo voltaic(PV) solar panel can be stored in Supercapacitor and auxiliary battery. Both of these devices can be charged parallel or individually by switching the supply point to the respective positions(c,b; c; b) mechanically as shown in Figure.3. The stored energy in both of these devices can be used to charge Mobile battery when needed by mechanically switching from charging mode to supply mode. This can be done by connecting the supercap and auxiliary battery in series. Since, during discharge supercap voltage reduces to zero, so after full discharge of supercap we have to isolate it from the circuit inorder to provide continuous operation to the charging of Mobile battery[9][10]. This can be done by controlling the MoSFET gate signals. The whole system operates in two modes.

1. Charging mode 2. Supply mode.

***Charging mode***

In this Mode the system works as a power bank which store energy and provide it for later use.During the Charging Mode the Supercapacitor(C) and the Auxiliary Battery (A.B) can be charged by PV solar panel either in parallel or individually by switching the supply point Mechanical switches (Ms1 & Ms2) to the point terminals(c,b;c;b).If we want to charge the Supercap alone then the PV panel is connected along Ms1,c - P and Ms2,c - Q. In the same way to charge Auxiliary Battery the panel is connected along Ms1,b - R and Ms2,b – S shown in Figure.3. To charge both supercapacitor and Auxiliary battery the charge flow will be along Ms1,c,b – P,R and Ms2,c,b – Q,S. In this mode(c,b) we are making use of supercapacitor to charge the auxiliary battery quickly. For this operation we are making use of MoSFETs (Type A, Type B) for switching operation[11] and a microcontroller to provide required logic operation. Initially when Type A MoSFETs are activated result in flow of charge through circuit Ms1,c,b – P,R and Ms2,c,b – Q,S result in charging of battery and supercapacitor in parallel. Since the supercapacitor can be charged quickly, once it reaches its rated value of voltage result in shifting of gate current to Type 2 MoSFETs. Now the current flow will be along the path Ms2,c,b –S-R-P-Q-Ms1,c,b. This logic can be

done by using a microcontroller provided an input of supercapacitor voltage as a measure. Now the PV panel and supercapacitor are in series which provide charge(in coulombs) to the battery. Since the supercapacitor can be discharged quickly so that we can recharge the auxiliary battery at high rate resulting in quick charging. After full discharge of supercapacitor (i.e. at 0 volt) again the gate signals are switched to Type AMoSFET result in charging of supercapacitor and battery in parallel. This process repeats. Under no availability of solar power or during night times we can charge the power bank with an alternate 5v plug in supply. Diodes D1 and D2 are connected across PV Panel to prevent the backflow of charge when an alternate supply is connected as it damages the panel. Diodes D3 and D4 are placed to prevent current flow to supercapacitor when we connect switches to the terminals where we need to charge only the auxiliary battery. Diode D5 is placed at the supercapacitor terminal to prevent backflow of charge from supercapacitor to A.B since the negative potential of supercapacitorat full charge is higher compared to battery as shown in Figure2.

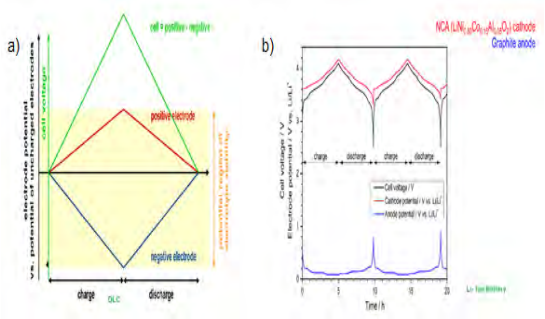


Figure 2: Variation of anode and cathode voltages while charging and discharging in a) Double layer capacitor (DLC)b) Li ion battery

The Maximum output voltage of Supercap is 2.7V whereas for Auxiliary Battery (Li-Ion Type) is 3.6-4.2V. Also for Auxiliary battery the overcharge protection circuit needs to be placed as shown in Figure.4 since it cannot be overcharged as it lead to side reactions whereas the overcharge protection is not needed for supercapacitor[12] since there is not electrochemical reaction involved.

During charging Mode the charge has to be supplied from the PV solar panel. Since the solar panel cannot provide constant current(in Amps) as the energy provided by it depend on incoming sun radiation which varies with time so we need a constant current charger circuit[13] as shown in Figure.4 which is placed across the auxiliary battery charging circuit ( Ms1,b-R-S-Ms2,b).

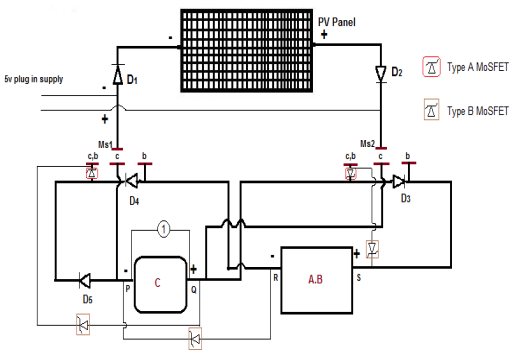


Figure 3: Set up of the PV panel Mobile charger in charging mode

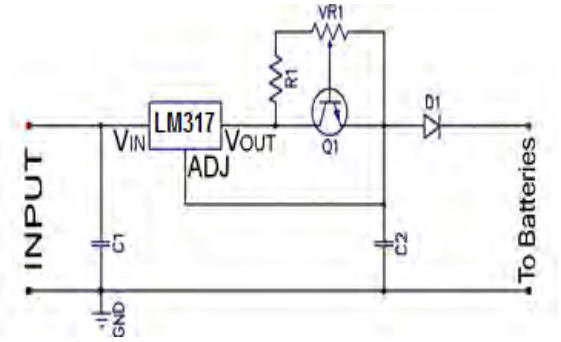


Figure 4: Diagram of a constant current charging circuit connected across auxiliary battery

***Supply mode***

In this Mode, the system works as a power supply to the Mobile battery. During the supply operation the supercapacitor(C) and the Auxiliary Battery (A.B) are connected in series and the output terminals from them are connected to the Mobile Battery for charging. This can be done by providing gate supply to the MoSFET (F3) so that it will conduct and provide short circuit path so that both (A.B) and (C) are in contact electrically and connected in series. When the supercapacitor and Battery are connected in series the charge from supercapacitor is provided to Mobile battery (M.B) by providing Gate supply to the MoSFETs (F2 and F6) and the charge flow path will be along P-T-U-S-R-Q-P as shown in Figure.5 So the MoSFETsF3, F2 and F6 (Type 1 MoSFETs) have to be switched ON at the same time. During the supply operation the charge in Supercap Keeps on decreasing so the voltage of Supercap also decreases. After a limited discharge operation the Supercap voltage reduces to zero (Zero charge). At this point the supply operation is interrupted since there is no charge available in Supercap to supply. In order to avoid interruption to the supply we have to isolate the supercap from the charging circuit and connect the PV Panel in series to the auxiliary battery so that in this case the PV panel and (A.B) in series work as

supply to the Mobile battery[14]. This can be done by removing Gate supply to the Type 1 MoSFETs and providing supply to the Type 2 MoSFETs ($F_1$, $F_4$, $F_5$ and $F_7$). In this case the charge flow will be along (S1-S-R-T-U-S2) as shown in Figure.5.a).MoSFET $F_5$ is activated to recharge the supercapacitor from the Auxiliary battery and the charge flow will be along (S-Q-P-R). The voltage values across supercapacitor (C) and Auxiliary battery (A.B) have to be provided to the Op-Amp adder as shown in Figure.5.b). The output of the Op- Amp is provided to the Microcontroller which is programmed to switch the gate signal to the MoSFETsat a defined Op-Amp output voltage values.

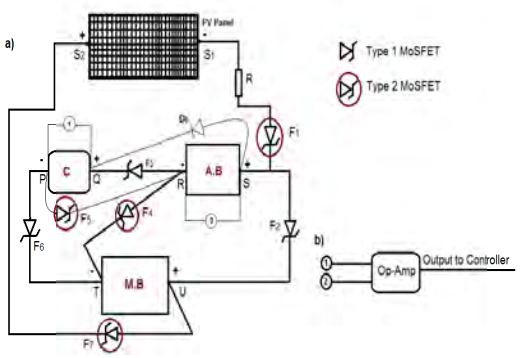


Figure 5: a) Set up of the PV panel Mobile charger in supply mode, b) Op-Amp as an adder providing voltage value to the microcontroller

The switching Mechanism of Gate triggering for Type1 MoSFETs to Type 2 MoSFETs has to be done in reference to boundary voltage conditions which is depicted in Figure.6. When the Op- Amp output is at a voltage value $V_1(V_C+V_{A.B})$ Type 1 MoSFETs are activated so that both supercapacitor and Auxiliary battery are in series and provide supply to the Mobile battery.

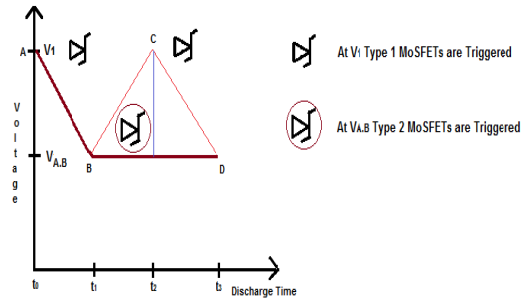


Figure 6: Showing the switching mechanism of the MoSFETs controlled by a microcontroller

During discharge the voltage of supercapacitor decreases as shown in Figure.6 form A-B. At the end of discharge the voltage of supercapacitor is zero so we left over with the voltage of Auxiliary battery ($V_{A.B}$). At this point of time $t_1$(in hours) the Op- amp provides only $V_{A.B}$(in volts)to the microcontroller which is a switching predefined voltage for the Microcontroller and the micro controller switches Gate signals from Type 1 MoSFETs to Type 2 MoSFETs. Now due to recharge operation of Supercap from MoSFET $F_5$ conduction the voltage of supercapacitor again increases as shown in Figure.6 from B-C. Also the supply operation to the Mobile battery is working(due to Type 2 MoSFETs) in parallel to the supercapacitor recharging so there will be no interruption to the supply. When the Voltage is reached to $V_1$(in volts) again (i.e.supercapacitor is recharged fully) the microcontroller switches the gate supply from Type 2 MoSFETs to Type 1 MoSFETs ($V_1$ is microcontroller switching predefined value). Again the Type1 MoSFETs are in conduction and the voltage decreases again (from C-D). This cycle is repeated along the discharge operation.

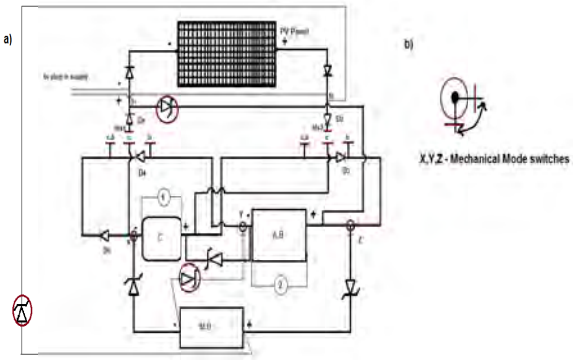


Figure 7: a) wholesetup of the power bankwith b) Mechanical mode switches

## 4. Advantages of the proposed method

The advantage of the proposed method over the existing technology is that the current power banks available in market use battery as energy storage device charged from a solar panel and the stored energy(in Kilowatt-hour) is supplied to the mobile battery, where as in the proposed method we use a supercapacitor which stores energy initially in parallel with auxiliary battery.Since the supercapacitor can be charged quickly, after full charge it is turned as a supply to the auxiliary battery in series with solar panel resulting in quick charge of the auxiliary battery since the supercapacitor can also be discharged quickly resulting in high current provided to auxiliary battery. This is done by the microcontroller with input reference as the voltage of the supercapacitor. During the supply to the mobile battery, the supercapacitor is in series with the auxiliary battery resulting in high voltage and current

provided to the mobile battery that provides quick charging facility.

## 5. Experimental Analysis

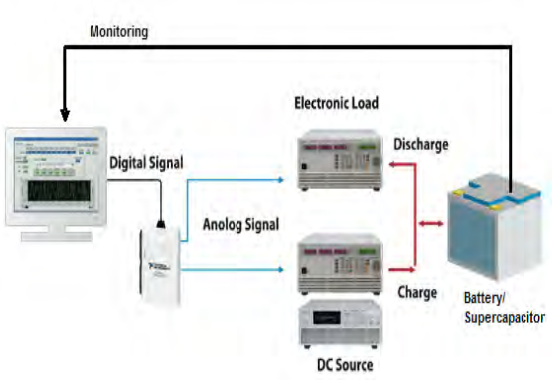


Figure 8: Schematic of the hardware used for charge/discharge test

Figure 8: Schematic of the hardware used for charge/discharge test

Figure.8 shows the schematic of the experimental setup of the Battery and supercapacitor charge and discharge test consist of Power source integrated with an electronic load which can supply power for batteries andsupercapacitor and can act as a load during their discharge operation.

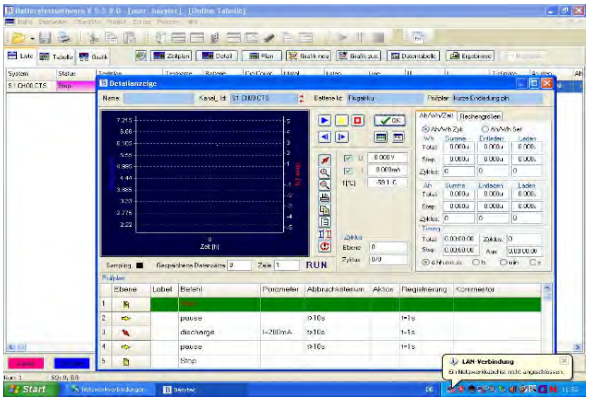

Figure 9: Photocopy of the BASYTEC software interface

The variation of electrical parameters such as current(in Amps) and voltage(in volts) of the battery and supercapacitor along the charge and discharge operation which follow the command process given by the input through software interface can be monitored on a computer screen through BASYTEC software as shown in Figure9..Using this software we can provide commands for the charge and discharge operation of storage devices which is generated as a digital signal converted to analog signal and provided to the electronic load. Commandswritten for the battery capacity check is shown in Figure.11.

Experiment has been done on the charging time of Battery of capacity 1000 mAh using Battery test software at constant current supply (at 2 Amps) during constant current charge and the values are drawn into a graph as shown. From the Figure.12, the blue graph indicates the variation of battery voltage between terminal ($V_T$) and cut-off ($V_c$) voltage with the operating time(in hours) and the red graph indicates the variation of current(in Amps) during charging and discharging operation of battery. Initially at time $t_1$ the battery is charged at constant current charge (CC charge) until the voltage of the battery reaches the terminal value($V_T$).After CC charge, constant voltage charge(CV charge) is used to fully charge the battery until the time $t_2$(in hours). After time $t_2$ battery is discharged at constant output current of 2 Amps. At constant current discharge the voltage of the battery decreases and reaches the cut-off value ($V_c$) at time $t_3$. From the graph, the time taken to charge a battery to its rated voltage (3.6 V) is about 1 hour and to charge it to its full capacity it will take 2.5 hours (from $t_1$ to $t_2$).

Figure 10: Photocopy of the hardware used for charge/discharge test of Battery

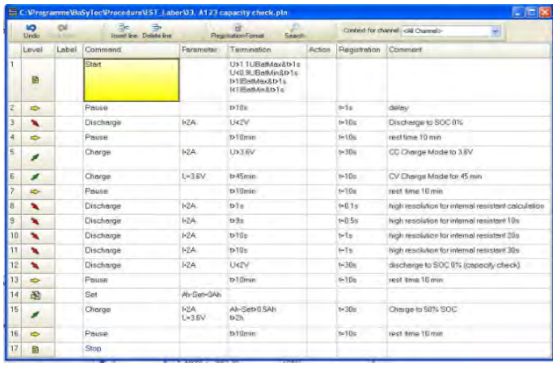

Figure 11: Written programme for the Battery Capacity check

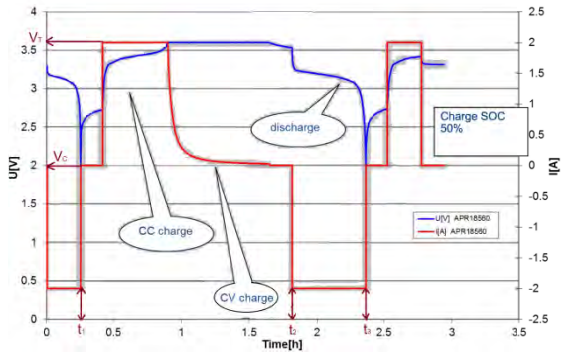


Figure 12: Output charge/Discharge cycles of a battery capacity check experiment.

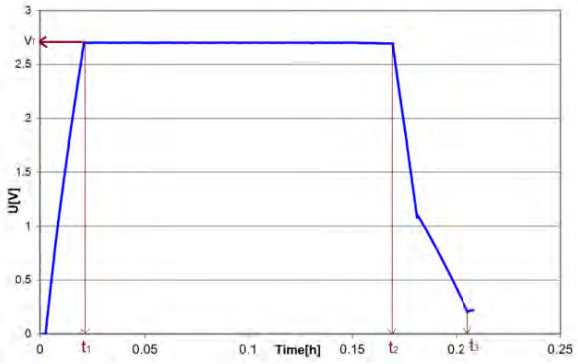


Figure 14: Output charge/Discharge cycles of a Supercapacitorcapacity check experiment

Figure.14indicates the variation of voltage of a supercapacitor of capacity 50 Farads along the charge and discharge operation at constant current of 2 amps. From the graph, the voltage during charge operation increases linearly up to its terminal voltage $V_T$ until time $t_1$. After time $t_1$, the supercapacitor is charged to its full capacity where the voltage of the supercapacitor is constant until time $t_2$. From the graph, time taken to charge a supercapacitor to its rated voltage ($V_T$=2.7V) is 0.05 hours where as to charge it to its full capacity it will take 9 minutes for the same constant current supply.

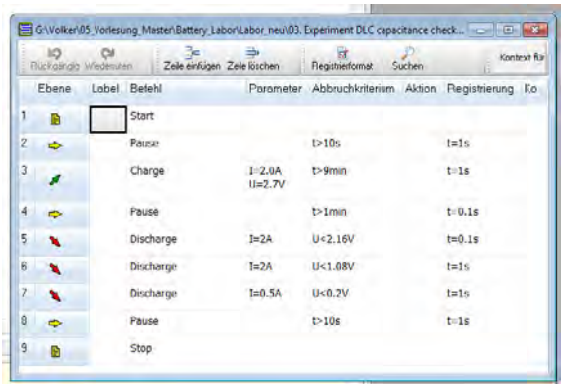


Figure 13: Written programme for the Supercapacitor Capacity check

After time $t_2$ supercap is discharged at constant output current of 1.5 Amps. At constant current discharge the voltage of the supercap decreases and reaches up to zero at time $t_3$During discharge operation of the supercapacitor it takes almost 3 minutes(from time $t_2$ to $t_3$) to discharge (at 1.5 Amps) as shown from the Figure. 14.By connecting the supercapacitor and battery in series the supercapacitor, allowing auxiliary battery for quick discharge result in fast charging of the Mobile battery. During charging the supercapacitor acts as a temporary storage.

## 6.Conclusion

The proposed method which stores electrical energy, generated through a solar PV panel and provides it for the Mobile electronic devices at high rate is to use a supercapacitor in conjunction with an auxiliary battery. The power generated from the solar PV panel is not high enough to charge the power bank (only with batteries) quickly resulting in high charge completion time. So in order to reduce the charging time we have introduced a method which make use of supercapacitor in combination with an auxiliary battery as a power bank with electronic switching mechanism and a microcontroller to charge it quickly along with high capacity well enough to provide energy to the mobile battery. Also the system which is used to storegeneratedelectric energy stated above is used to supply the power to the mobile battery at high rate with change in electronic switching and microcontroller operation. In this mechanism the supercapacitor and auxiliary battery connected in series provide high power to the mobile battery well enough to charge it quickly. Implementation aspect focuses on the practical work carried out in the field of energy storage and supply in power banks that can efficiently store generated electrical energy and provide it to the mobile battery at high rate. The advantage of the above proposed method over other methods of energy conversion [15][16] and storage is that we can integrate the whole system on to a mobile pouch,provided easy to carry and less charging time needed. This idea of energy storage mechanism efficiently solves the problems of taking long hours to charge the powerbank and mobile battery and limited power availability.

## 7. Future work

Future work will be to write an embedded programme for the microcontroller for performing the required logic operation and testing it with battery and

supercapacitorwith charge /discharge curves observed and comparing with expected values.

## 8. Acknowledgement

The author would like to thank the WeiterbildungszentrumBrennstoffzelle Ulm e.V. (WBZU) for helping to perform the experimental work.

## 9. References

[1] Jen-HaoTeng, Shang-Wen Luan, Dong-Jing Lee, and Yong-Qing Huang“Optimal Charging/ Discharging Scheduling of Battery Storage Systems for Distribution Systems Interconnected with Sizeable PV Generation Systems”; IEEE transaction on power systems, VOL. 28, NO. 2, MAY 2013.

[2] Lisowska-OleksiakA.,Nowak A.P“Supercapacitors as energy storage devices”;Journal of Power Sources, vol. 173, 2007, pg. 829.

[3] Kótz R. and Carlen M. “Principles and applications of electrochemical capacitors”. Electrochem. Acta, vol. 45, 2000, p. 2483.

[4] Frąckowiak E. and Bequin F“Carbon materials for the electrochemical storage of energy in capacitors”, Carbon, vol. 39, 2001, p. 937.

[5] Plitz I., Dupasquier A., Badway F, Gural J., Pereira N., Gmitter A., Amatucci G.G“The design of alternative nonaqueous high power chemistries”; Appl. Phys. A, vol. 82, 2006, p. 615.

[6] Lota G., Lota K., Frąckowiak E., “Electrochem. Commun” vol. 53, 2008, p. 2210.

[7] Shukla A.K., Arico A.S., Antonucci V. “An appraisal of electric automobile power sources”Renewable Sustainable Energy Rev., vol. 5, 2001, p. 137.

[8] “Lithium-ion Batteries for Hybrid and All-Electric Vehicles”: the U.S. Value Chain, October 5, 2010.Center on Globalization, Governance & Competitiveness, Duke University.

[9] Carla-FabianaChiasserini, Ramesh R. Rao“Energy Efficient Battery Management”; IEEE Journal on selected areas in communications, VOL. 19, NO. 7, JULY 2001.

[10] Luca Benini, DavideBruni, Alberto Macii, Enrico Macii, Massimo Poncino; “Discharge Current Steering for Battery Lifetime Optimization”, IEEE transactions on computers, VOL. 52, NO. 8, AUGUST 2003.

[11] Linden Harrison “An Introduction to Depletion Mode MoSFETs”

[12] www.dailyreckoning.com.au/supercapacitors/2008/02/28/

[13] http://www.electronicecircuits.com/electronic-circuits/ni-mh-ni-cd-adjustable-constant current-charger

[14] D. Linden, “Handbook of Batteries”, second. ed. Hightstown, N.J.: McGraw-Hill, 1995.

[15] G.Jithendra Naidu, k.Pranay kumar reddy &S. Siva Prasad “Piezo based electric power generation using 3- dimensional mechanical vibrations produced in vehicles”,(IJEEE) ISSN (PRINT): 2231 – 5284, Vol-2, Iss-1, 2012.

[16] K. Pranay kumar reddy, G. Jithendra Naidu and S. Siva Prasad “Energy harvesting and control of vehicle tire pressure using transducers”(IJMRAE), ISSN 0975-7074, Vol. 5, No. III (July 2013), pp. 69-84.

## Biographies

**Kottam Pranay kumar**received his B.Tech From J.B Institute of technology in Electrical and Electronics Engineering, India. Currently he is pursuing MSc in Energy science and Technology from Ulm University, Germany.His previous works include design of 3 Dimensional energy harvester from vibrations and pressure in the vehicle tires using piezoelectric materials. His research interests include implementation of Energy conversion and storage mechanisms.

**K. Udayreddy** is currently pursuing B. Tech in Mechanical engineering from SRM University,India. He is the member of Society of Automotive Engineers His interests include designing of electromechanical energy conversion systems.

**G. Jithendra Naidu** received his B.Tech From J.B Institute of technology in Electrical and Electronics Engineering, India.His previous works include design of 3 Dimensional energy harvester from vibrations and pressure in the vehicle tires using piezoelectric materials.His research interests includethe development of embedded programming

**Dr. S. Siva Prasad**is currently Professor and Head of the department of Electrical and Electronics Engineering in J. B institute of Engineering and Technology (Autonomous). He is the Life member of IndianSociety for Technical Education.He is also the Fellow of the Institute of Electrical and Electronics Engineers. His previous works include design of 6 Phase Induction motor. His main research interests are Energy systems designing using modern Power electronics.

.

www.icgst.com

# Online Stator Reference Flux Approach to Torque Ripple Minimization for SPM Drive using Fuzzy and PI Controllers

N. Krishna Kumari, G. Tulasi Ram Das, and M.P.Soni
*Assoc.Prof, EEE Dept.,, Engineering, VNR VJIET, Hyderabad, A.P, India*
*Prof , EEE Dept.,, JNTUCE, Hyderabad, Prof and HOD, EEE Dept.,MJCET, Hyderabad, India*
nkkpsg@gmail.com, das_tulasiram@yahoo.co.in, drmpsoni@yahoo.com

## Abstract
In this paper different DTC space vectors with online stator flux reference for surface mounted permanent magnet synchronous motor (SPM) drive is carried out using fuzzy and PI speed regulators. The stator reference flux is calculated offline by using the machine parameters conventionally. In the proposed method "A Maximum Torque per Ampere (MTPA)" principle is applied, wherein the online stator reference flux is calculated from torque reference, direct stator flux and quadrature stator flux instead of stator flux linkage. Three sets of DTC space vectors are considered with MTPA operation for analysis purpose and the performance of the three control schemes are evaluated in terms of torque ripple, flux ripple and transient response to step variations in torque and speed control commands. Simulation results using MATLAB/SIMULINK show the effectiveness of the proposed method.

***Keywords :*** *SPM, MTPA, PI Controller, Fuzzy Logic Controller*

**Nomenclature**

| | |
|---|---|
| $v_d$ | direct axis stator voltage, V |
| $v_q$ | quadrature axis stator voltage, V |
| $i_d$ | direct axis stator current, A |
| $i_q$ | quadrature axis stator current, A |
| $R_s$ | stator armature resistance, Ω |
| $L_d$ | direct axis inductances, H |
| $L_q$ | quadrature axis inductances, H |
| $\omega_r$ | rotor speed in electrical rad/s |
| $T_e$ | electromagnetic torque, Nm |
| P | no. of poles |
| $\lambda_f$ | magnetic flux linkage, wb |
| $\lambda_s$ | stator flux linkage, wb |
| $\lambda_d$ | direct axis flux linkage, wb |
| $\lambda_q$ | quadrature axis flux linkage, wb |
| $T_L$ | J moment of inertia in $Kg.m^2$ |
| Θ | angle between stator and rotor flux linkage |
| SPM | Surface mounted permanent magnet synchronous Motor |
| MTPA | maximum torque per ampere |

## 1. Introduction
Surface mounted permanent-magnet synchronous motor (SPM) also known as Axial flux permanent magnet motor where in the permanent magnets are placed on the surface of a cylindrical iron-laminated rotor body and the stator possesses three phase winding [1]. The absence of rotor winding and related losses results in high efficiency, high torque/weight ratio, and reduced cooling requirements [2]. Also the armature reaction effect on pole flux of SPM is low due to high equivalent magnetic air gap when compared with other machines of similar size results in a very low synchronous inductance. [3] [4]. To overcome the disadvantages caused by the conventional DTC [5] [6][7], this paper focuses on the torque ripple minimization of SPM with online stator flux reference approach with three different space vector DTC schemes. To determine on line stator flux, Maximum Torque per Ampere (MTPA) principle is used. From reference flux, optimum voltage space vector can be obtained such that the flux error can be fully compensated which results in flux and torque ripple minimization [8].
As MTPA system being very sensitive to parameter variations, load disturbances etc. the controller parameters have to be continually adapted to update the exact value of on line stator reference flux which can be resolved by several adaptive control techniques [9]. In this paper, online stator reference flux estimation based on MTPA in rotor reference frame of SPM drive is implemented with three different space vector DTC schemes using Fuzzy and PI controllers and the results are compared.
The organization of the paper is as follows: section 2 describes the modeling of SPM. Section 3 explains the concept of basic DTC. Section 4 introduces the proposed DTCs with on line reference stator flux generation using the application of MTPA. Section 5 deals with the application of PI and Fuzzy speed regulator to find reference torque and reference flux Section 6 discusses the comparative results obtained by the proposed DTCs with reference stator flux using PI and Fuzzy controllers. Section 7 concludes the outcome of the paper.

## 2. Modelling of SPM

The SPM is modelled using various DTC space vectors (CDTC, DTCI and DTCII) contains a speed control loop with PI and Fuzzy logic controller to obtain a reference electromagnetic torque. In the rotor reference frame [10]-[12], the voltage equation and the torque equation of SPM are expressed as follows.

$$V_d = R_s i_d + L_d \frac{di_d}{dt} - (\omega_r) L_q i_q \quad (1)$$

$$V_q = R_s i_q + L_q \frac{di_q}{dt} + (\omega_r) L_d i_d + (\omega_r)\lambda_f \quad (2)$$

Assuming a linear magnetic circuit, the *d* and *q*-axis flux linkages are represented as

$$\lambda_d = L_d i_d + \lambda_f \quad (3)$$

$$\lambda_q = L_q i_q \quad (4)$$

The electromagnetic torque is an important output variable that determines mechanical dynamics of the machine as the rotor position and speed varies, which is represented by the following equation

$$T_e = \frac{3}{2}\frac{P}{2}[L_d i_q i_d + \lambda_f i_q - L_q i_q i_d] \quad (5)$$

As indicated in [1] stable torque control can be achieved if

$$\lambda_s \le \frac{1}{2}\lambda_f \quad (6)$$

The amplitude of stator flux linkage should be chosen according to the equation (6) if fast dynamic response is desired. Equation (5) consists of the excitation torque which is produced by permanent magnet flux and the reluctance torque. In SPM because of the large air gap, the armature reaction effect on pole flux is insignificant. Hence in SPM the d-axis and q-axis inductances namely $L_d$ and $L_q$ are equal [3] [12] to synchronous inductance (Ls) without saliency, therefore the reluctance torque becomes zero and torque is simplified as

$$T_e = \frac{3}{2}\frac{P}{2}[\lambda_f i_q] \quad (7)$$

Also a motor model is designed to generate four internal feedback signals namely stator flux ( $\lambda_s$ ), electromagnetic torque ($T_e$), rotor speed ( $\omega_r$ ), phase angle between stator flux linkage ($\theta$). The equations are given below.

$$\lambda_s = \sqrt{\lambda_d^{\,2} + \lambda_q^{\,2}} \quad (8)$$

$$T_e - T_L = \frac{2}{p} J \frac{d\omega_r}{dt} \quad (9)$$

$$\theta = Tan^{-1}\left[\frac{\lambda_{qs}}{\lambda_{ds}}\right] \quad (10)$$

The gate signals of the inverter are obtained by using switching functions $S_a$, $S_b$ and $S_c$ for which value is either 1 or 0; the primary voltage vector $v$ is represented as [13]

$$v(S_a, S_b, S_c) = \sqrt{\frac{2}{3}} V_{dc}\left[S_a + S_b \exp\left(j\frac{2\pi}{3}\right) + S_c \exp\left(j\frac{4\pi}{3}\right)\right] \quad (11)$$

By using this instantaneous vector (11), the behavior of a machine can be conveniently expressed not only in the steady state but also in the transient state. The machine voltages corresponding to the switching states can be calculated by using the following relations

$$\left.\begin{aligned} v_{ab} &= v_a - v_b \\ v_{bc} &= v_b - v_c \\ v_{ca} &= v_c - v_a \end{aligned}\right\} \quad (12)$$

Machine phase voltages for a balanced system are represented by

$$\left.\begin{aligned} v_{as} &= \frac{v_{ab} - v_{ca}}{3} \\ v_{bs} &= \frac{v_{bc} - v_{ab}}{3} \\ v_{cs} &= \frac{v_{ca} - v_{bc}}{3} \end{aligned}\right\} \quad (13)$$

The qs and ds axes voltages are given by

$$\left.\begin{aligned} v_{qs} &= v_{as} \\ v_{ds} &= \frac{1}{\sqrt{3}}(v_{cs} - v_{bs}) = \frac{1}{\sqrt{3}} v_{cb} \end{aligned}\right\} \quad (14)$$

Converting the phase voltages variables *Vabc* to *Vqdso* variables in stationary reference frame, the relation between dqso and abc voltages are represented as [13]

$$\begin{bmatrix} v_{qs} \\ v_{ds} \\ o \end{bmatrix} = \frac{2}{3}\begin{bmatrix} 1 & \frac{-1}{2} & \frac{-1}{2} \\ 0 & \frac{-\sqrt{3}}{2} & \frac{\sqrt{3}}{2} \\ \frac{1}{2} & \frac{1}{2} & \frac{1}{2} \end{bmatrix}\begin{bmatrix} v_{as} \\ v_{bs} \\ v_{cs} \end{bmatrix} \quad (15)$$

## 3. Direct Torque Control

The figure 1 shows the complete block diagram of DTC fed SPM, where in direct control of the electromagnetic torque and stator flux linkages using an optimal voltage switching look up table scheme is considered. The principle goal is to select voltage switching vectors and there by yielding the fastest electromagnetic torque response. The stator flux linkage and the electromagnetic torque are controlled directly by applying optimum voltage switching vectors of the inverter. The electromagnetic torque error and the stator flux linkage error are inputs to the respective flux and torque hysteresis controllers. The flux controller controls the machine operating flux to maintain the magnitude of the operating flux at the rated value till the rated speed and at a value decided by the field weakening block for speeds above the rated speeds. Torque control loop maintains the torque to the torque demand. The outputs of these controllers are depending on the instantaneous position of flux vector. The flux hysteresis comparator is a two level comparator and the torque comparator is a three level comparator.

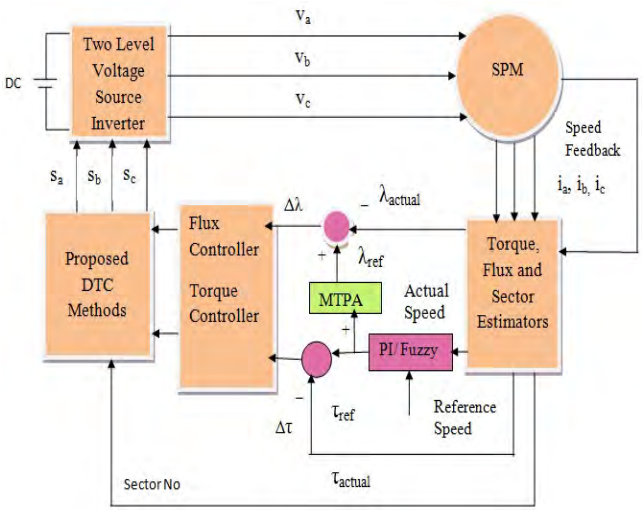


Figure 1. Block diagram of the SPM Drive with on line stator Estimation

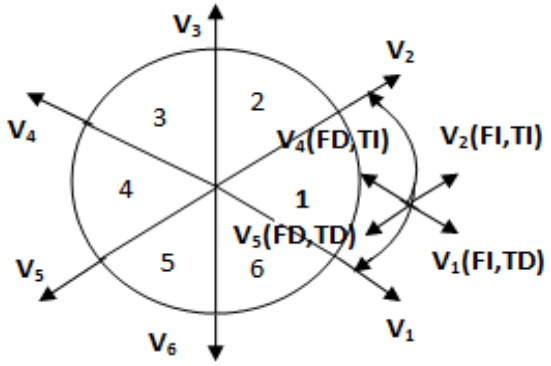


Figure 2. Conventional DTC (CDTC) and its sectors

Table 1: Voltage Vector Selection based on reference flux and torque demand

| In the "K" Sector | Increase | Decrease |
|---|---|---|
| Stator Flux | K, K+1, K-1 | K+2, K-2, K+3 |
| Torque | K+1, K+2 | K-1, K-2 |

Table 2: Space Vector Division

| Sector No. | CDTC (Conventional DTC) | DTCI | DTCII |
|---|---|---|---|
| 1 | $-30^0$ to $+30^0$ | $0^0$ to $60^0$ | $-45^0$ to $+15^0$ |
| 2 | $+30^0$ to $90^0$ | $60^0$ to $120^0$ | $15^0$ to $75^0$ |
| 3 | $90^0$ to $150^0$ | $120^0$ to $180^0$ | $75^0$ to $135^0$ |
| 4 | $150^0$ to $210^0$ | $180^0$ to $240^0$ | $135^0$ to $195^0$ |
| 5 | $210^0$ to $270^0$ | $240^0$ to $300^0$ | $195^0$ to $255^0$ |
| 6 | $270^0$ to $330^0$ | $300^0$ to $360^0$ | $255^0$ to $315^0$ |

## 4. Proposed DTCs With on Line Reference Stator Flux Generation

The outputs of the hysteresis comparators and the information to the position of the stator flux vector are the inputs to the optimum voltage switching selection look up table (Table 1). It can be seen that each sector is 60 electrical degrees apart and for a six step inverter the minimum number of sectors are six. In this work, three different space vector DTCs (CDTC, DTCI and DTCII) are considered to analyze the dynamic performance of the SPM drive. In CDTC first sector is taken from $-30^o$ to $+30^o$, the second sector is from $30^o$ to $90^o$ and so on as shown in figure 2. In DTCI instead of taking the first sector from $-30^o$ to $+30^o$ it is taken from $0^o$ to $60^o$, the second sector is from $60^o$ to $120^o$ and so on. In DTCII the first sector from $-45^o$ to $+15^o$, second sector is from $15^o$ to $75^o$ and so on (refer Table 2).

In the Proposed DTCs up to rated speed of the drive**,** **"**Maximum Torque per unit Current/Ampere (MTPA)" principle is used to find the stator reference flux which in turn is obtained from the reference torque. This ensures minimum stator ohmic losses resulting in maximum efficiency. In other words the desired electromagnetic torque should be achieved with minimum stator current, thus $i_d$ is forced to zero by the appropriate switching vectors. "Maximum Torque per unit Flux (MTPF)" principle is used to find the reference flux for above rated speed of the drive. Further on the torque error and flux errors are calculated to choose appropriate switching voltage vector [14]. The reference flux with the application of MTPA is obtained as follows:

$$\lambda_s = \sqrt{(L_d i_d + \lambda_f)^2 + (L_q i_q)^2} \quad (16)$$

With $i_d$=0

$$\lambda_s = \sqrt{\lambda_f^{\,2} + L_q^{\,2} i_q^{\,2}} \quad (17)$$

then electromagnetic torque is given by

$$T_e = \frac{3}{2} p[\lambda_f i_q] \quad (18)$$

From equation (17), $i_q$ is given by

$$i_q = \frac{2T_e}{(3p\lambda_f)} \quad (19)$$

Substituting $i_q$ in equation (17) yields

$$\lambda_s = \sqrt{\left[\lambda_f^{\,2} + L_q^{\,2}\left[\frac{2T_e}{(3p\lambda_f)}\right]^2\right]} \quad (20)$$

Then the required function for the reference flux can be obtained as

$$\lambda_{ref} = \sqrt{\left[\lambda_f^{\,2} + L_q^{\,2}\left[\frac{2T_{eref}}{(3p\lambda_f)}\right]^2\right]} \quad (21)$$

Here the stator reference flux is calculated in the online by considering the instantaneous reference torque from the equation (21),where in the reference torque is obtained by converting the rotor speed error into instantaneous torque using PI and Fuzzy controllers which is shown in figure 1 [14].

## 5. PI and Fuzzy Logic Controller

***PI Controller:*** The dynamic responses of the SPM transformed to the estimated rotor frame, observer and observer error are nonlinear. The stability of control system is analyzed as a linearized error model using PI controller. The general block diagram of the PI speed controller is shown in figure 3.

The output of the speed controller (torque command) at *n*-th instant is expressed as follows:

$$T_{e(n)} = T_{e(n-1)} + K_p\, \omega_{re(n)} + K_i\, \omega_{re(n)} \quad (22)$$

Where $T_{e\ (n)}$ is the torque output of the controller at the n-th instant, $K_p$ is the proportional gain constants and $K_i$ is the integral gain constant. A limit of the torque command is imposed as

$$T_{e(n+1)} = \begin{cases} T_{e\max}, T_{e(n+1)} \geq T_{e\max} \\ -T_{e\max}, T_{e(n+1)} \leq -T_{e\max} \end{cases} \quad (23)$$

The gains of PI controller shown in can be selected by many methods such as trial and error method, Ziegler–Nichols method and evolutionary techniques-based searching. The numerical values of these controller gains depend on the ratings of the motor.

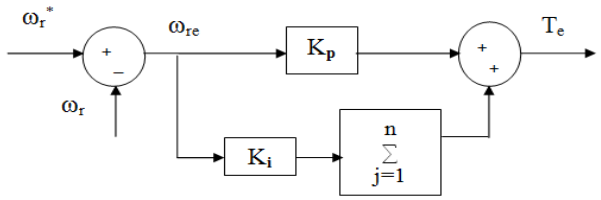


Figure 3. Block diagram of PI speed controller

***Fuzzy Logic Controller:*** The general block diagram of FLC is shown in figure 4. Fuzzy logic control consists of fuzzification process, linguistic rule base, and defuzzification process. The input variables for fuzzy logic controller are speed error and change of speed error. The speed is fed to the fuzzy speed estimator. The speed error and change in speed error are defined as

$$e(k) = \omega(k)^{*} - \omega(k) \quad (24)$$

$$\Delta e(k) = e(k) - e(k-1) \quad (25)$$

The two input variables are e(k), Δe(k) and output variable $T_e$ are divided into different fuzzy segments shown in figures 5, 6 and 7 respectively.

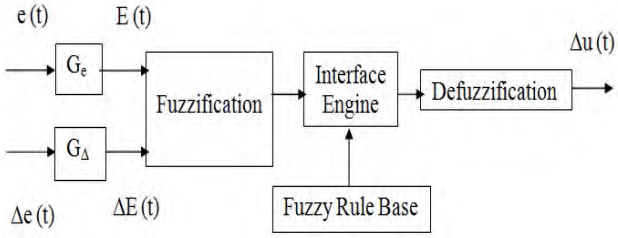


Figure. 4. Block Diagram of Fuzzy Logic Controller

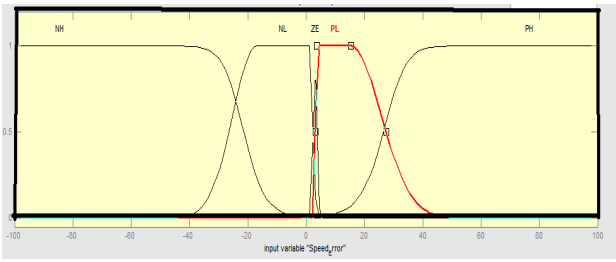


Figure 5.Membership function for speed error

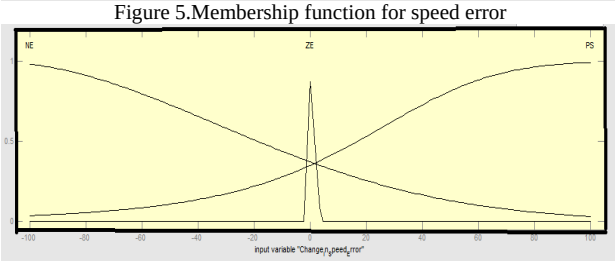


Fig ure 6 .Membership function for change in speed error

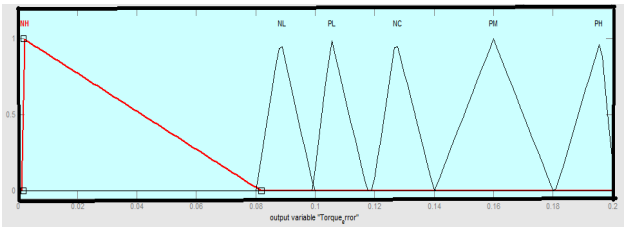


Figure 7 .Membership function for Electromagnetic Torque

For example the rules used for the proposed FLC algorithms are as follows:(i) If $\Delta\omega_r$ is ZE (Zero) and $\omega_r$ is PS (Positive Small) $\Delta T_e$ is PL (Positive Low).(ii) If $\Delta\omega_r$ is ZE (Zero) and $\omega_r$ is ZE (Zero) $\Delta T_e$ is NC (No change) and so on..The complete fuzzy rule base matrix (Mamdani type fuzzy inference) is represented in Table 3. For the proposed drive performance to obtain the optimum switching logic the values of the constants, membership functions, fuzzy sets for the input- output variables and the rules used are selected by trial and error. The membership functions for speed error, change in speed error and electromagnetic torques are shown in figures 5, 6 and 7 respectively.

Table 3 Rule Base Table

| $\omega_e$ \ $\Delta\omega_e$ | NH | NL | ZE | PL | PH |
|---|---|---|---|---|---|
| NE | NH | NL | NC | PM | PH |
| ZE | NH | NL | NC | PM | PH |
| PS | NH | NL | PL | PM | PH |

## 6. Simulation Results

Simulation is carried out using MATLAB/SIMULINK . The SPM drive with specification details mentioned in Table 4 is considered for the study.

Analysis is carried out with different sets of load torques and reference speeds. The electromagnetic torque response, speed response, stator flux response, torque ripple, flux ripple and phase current THD comparison are shown in figures 8 to 22.

At no load condition, when the drive system started with the speed reference set at 1500 rpm (half of the rated speed), it is noticed that the proposed drive with FLC followed the command speed within 0.08 sec without any over shoot, steady state error and with little under shoot (Ref. figure 8) whereas with PI controller the steady state is reached in a slightly longer time (0.2 sec).

When a load torque of 2.3 N-m is applied to the motor shaft in a step wise manner (At t= 0.3 sec) it is observed that the speed momentarily follows load disturbances and immediately reaches to the reference value at 0.4 sec with Fuzzy and in 0.5 sec with PI controller respectively. Whereas the torque response reaches to the steady state value at 0.31 sec in Fuzzy controller and 0.32 sec in PI controller . This is very well depicted in figure 9.

The dynamic analysis of SPM drive (Ref. figure 10 ) is carried out for various load torques applied at different instants with constant set speed (1500 rpm).It is observed with no time and less over shoot the torque response is reaching steady state using Fuzzy controller than PI

Controller. When speed is varied from 500 rpm to 1000 rpm at t=1.59 sec, the torque response is slower and the speed response is faster in reaching the steady state with fuzzy controller shown in figure 11.

From figures 12 and 13 , the torque ripple is 10.2% and flux ripple is 6.81 % for SPM drive with the proposed DTC I using Fuzzy controller for rated speed 3000rpm and load torque 2.0 Nm. The torque ripple, flux ripple comparison for the three space vector DTCs with fuzzy controller for various loads are represented in figures 14 and 15 respectively. For the same load and speed the phase current THD is 1.49 %with fuzzy controller and 2.39% with PI controller. The phase THD comparison with fuzzy controllers for different loads at rated speed 3000rpm are shown in figure 16.The detailed summary of percentage of flux ripples, torque ripples and phase current THDs are given in tables 5, 6 and 7 respectively.

The set speed response, electromagnetic torque response and stator flux response for three space vector DTCs using fuzzy controller with constant speed and constant load are shown from figures 17 to 22. It is concluded that the torque ripple and THD are less with DTC I whereas flux ripple is less with DTCII (little difference compared to DTC I)

Table 4: Specification of SPM

| Parameter Description | Value |
|---|---|
| Rated Output Power | 800 W |
| Rated Speed | 3000 rpm |
| Rated Voltage | 230 V |
| Torque Constant +- 5% | 0.455Nm/A |
| Voltage Constant +- 5% | 31.8 V/Krpm |
| Phase Resistance +- 5% | 19.4 Ohms |
| Phase Inductance +- 5% | 3.82 mH |
| Electric Time Constant | 5.6 ms |
| Mechanical Time Constant | 0.65 ms |
| Rotor Inertia | 1.16 Kgcm2 |

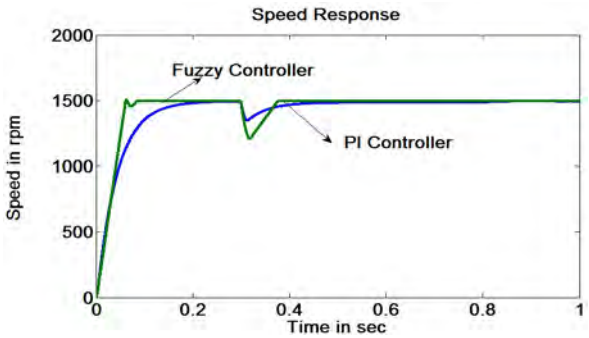


Figure 8: Speed response at no load and when load applied at t= 0.3 sec with DTC I

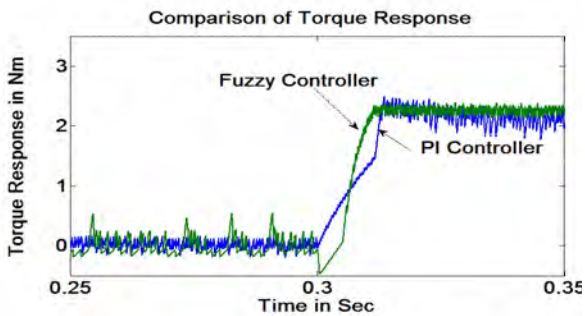


Figure 9: Torque response at no load and when load applied at t= 0.3 sec with DTC I

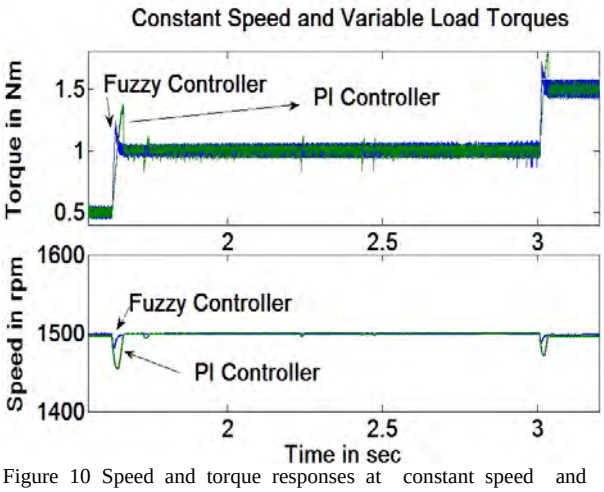


Figure 10 Speed and torque responses at constant speed and variable loads with DTC I

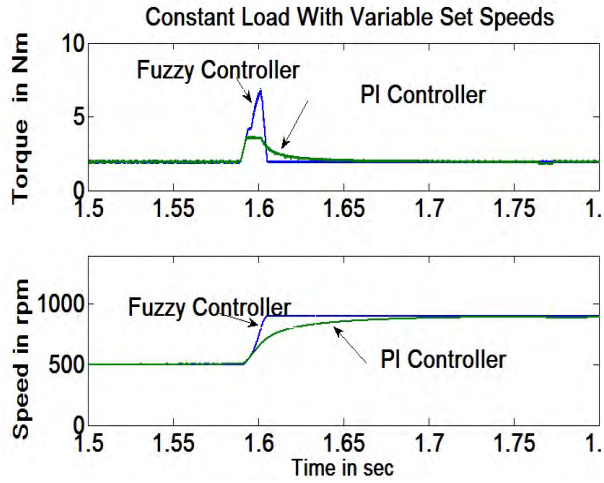


Figure 11 Speed and torque responses at constant Load torque and variable set speeds with DTC I

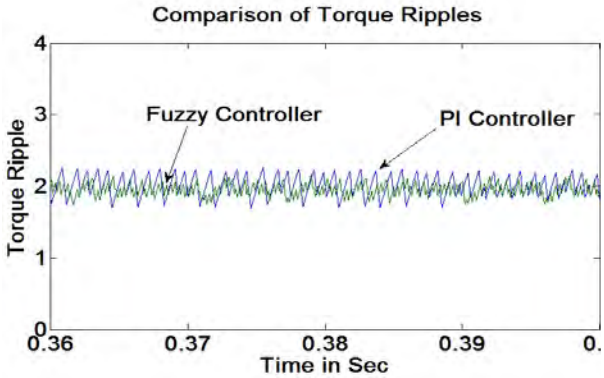


Figure 12. Comparison of torque ripple analysis with DTC I

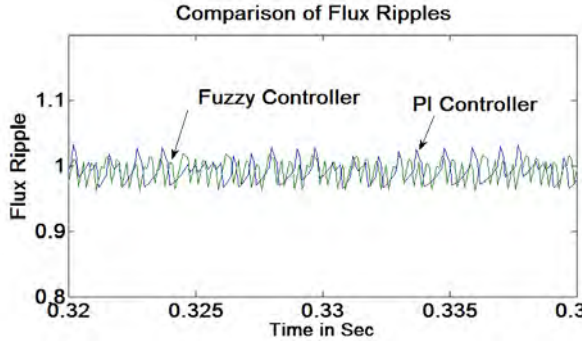


Figure. 13. Comparison of flux ripple analysis with DTC I

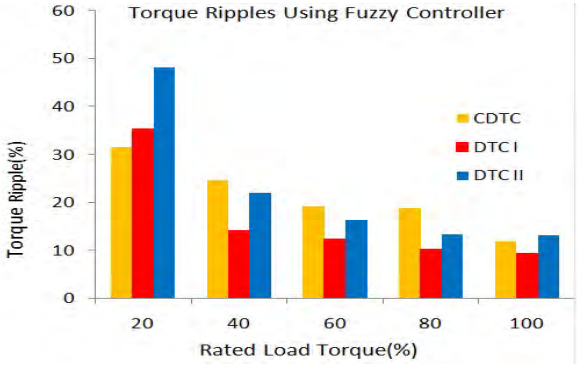


Figure.14. Comparison of torque ripples with CDTC , DTC I and DTC III

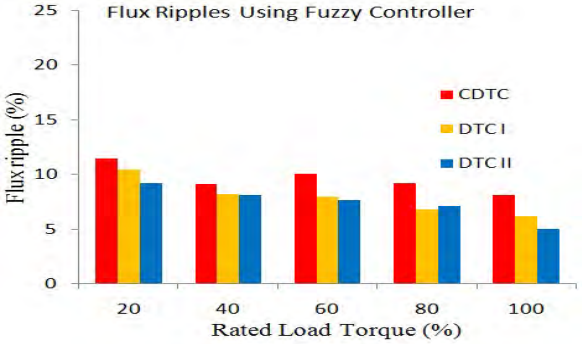


Figure 15. Comparison of flux ripples with CDTC , DTC I and DTC III

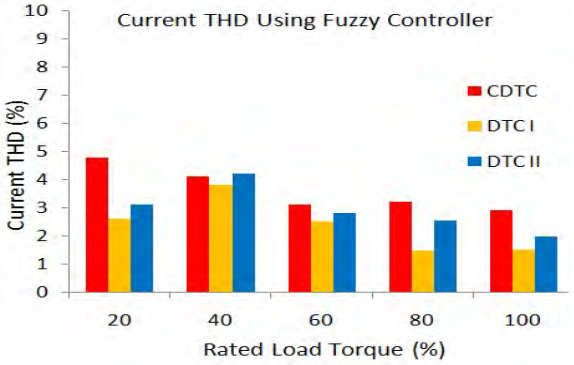


Figure.16. Comparison of phase current THD with CDTC , DTC I and DTC III

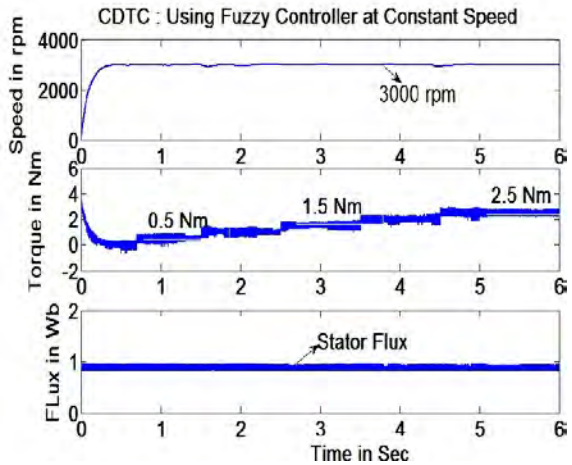


Figure 17. Flux, electromagnetic torque and speed responses for 0.5 Nm to 2.5 Nm load with constant speed = 3000 rpm with CDTC

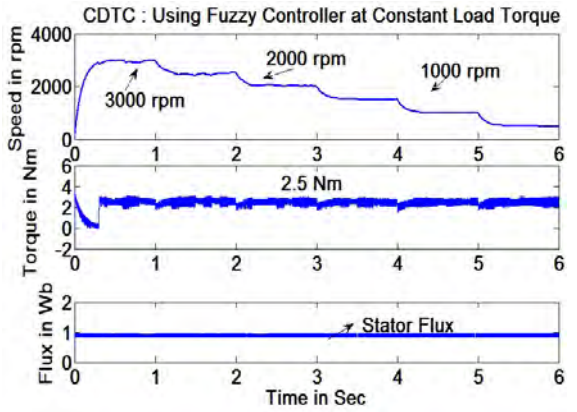


Figure 18. Flux, electromagnetic torque and speed responses for 3000 rpm to 500 rpm as set speeds with constant load = 2.5 Nm with CDTC

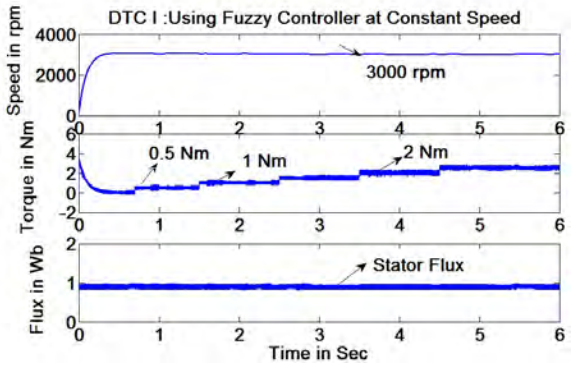


Figure 19. Flux, electromagnetic torque and speed responses for 0.5 Nm to 2.5 Nm load with constant speed = 3000 rpm with DTC I

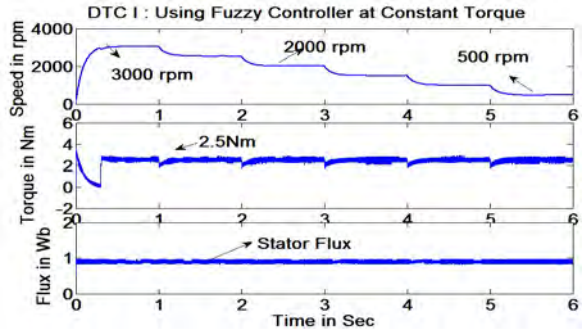


Figure 20. Flux, electromagnetic torque and speed responses for 3000 rpm to 500 rpm as set speeds with constant load = 2.5 Nm with DTC I

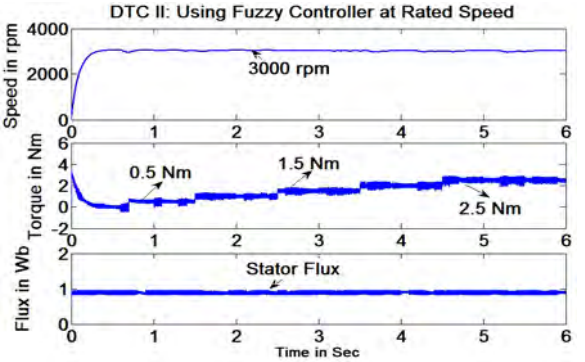


Figure 21. Flux, electromagnetic torque and speed responses for 0.5 Nm to 2.5 Nm load with constant speed = 3000 rpm with DTC II

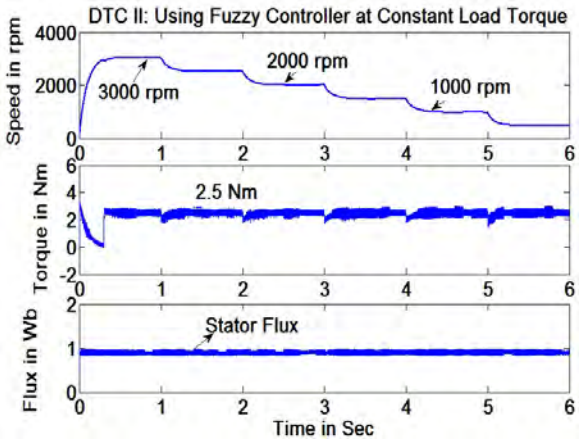


Figure 22. Flux, electromagnetic torque and speed responses for 3000 rpm to 500 rpm as set speeds with constant load = 2.5 Nm with DTC II

Table 5: Torque Ripple, Flux Ripple, THD Analysis for Phase Cureents of the SPM drive using PI and Fuzzy Controllers with CDTC at rated speed= 3000 rpm

| Time at which load is applied (sec) | Load Torque (Nm) | Torque Ripple (%) PI | Torque Ripple (%) Fuzzy | Flux Ripple (%) PI | Flux Ripple (%) Fuzzy | Phase Current (THD) % PI | Phase Current (THD) % Fuzzy |
|---|---|---|---|---|---|---|---|
| 0.7 | 0.5 | 33.33 | 31.5 | 12.45 | 11.42 | 5.1 | 4.8 |
| 1.5 | 1.0 | 25 | 24.7 | 11.52 | 9.1 | 4.79 | 4.12 |
| 2.5 | 1.5 | 22 | 19.2 | 12.2 | 10.02 | 3.71 | 3.12 |
| 3.5 | 2.0 | 21 | 18.8 | 12.04 | 9.21 | 3.63 | 3.21 |
| 4.5 | 2.5 | 14.81 | 12 | 10.63 | 8.12 | 3.26 | 2.9 |

Table 6: Torque Ripple, Flux Ripple, THD Analysis for Phase Cureents of the SPM drive using PI and Fuzzy Controllers with DTC I at rated speed= 3000 rpm

| Time at which load is applied (sec) | Load Torque (Nm) | Torque Ripple (%) PI | Torque Ripple (%) Fuzzy | Flux Ripple (%) PI | Flux Ripple (%) Fuzzy | Phase Current (THD) % PI | Phase Current (THD) % Fuzzy |
|---|---|---|---|---|---|---|---|
| 0.7 | 0.5 | 38.46 | 35.3 | 12.37 | 10.4 | 3.92 | 2.63 |
| 1.5 | 1.0 | 18.18 | 14.2 | 11.45 | 8.2 | 3.83 | 3.82 |
| 2.5 | 1.5 | 16.46 | 12.4 | 11.57 | 7.98 | 3.66 | 2.52 |
| 3.5 | 2.0 | 15.59 | 10.2 | 11.52 | 6.81 | 2.39 | 1.49 |
| 4.5 | 2.5 | 12.21 | 9.3 | 10.41 | 6.2 | 2.13 | 1.52 |

Table 7: Torque Ripple, Flux Ripple, THD Analysis for Phase Cureents of the SPM drive using PI and Fuzzy Controllers with DTC II at rated speed= 3000 rpm

| Time at which load is applied (sec) | Load Torque (Nm) | Torque Ripple (%) PI | Torque Ripple (%) Fuzzy | Flux Ripple (%) PI | Flux Ripple (%) Fuzzy | Phase Current (THD) % PI | Phase Current (THD) % Fuzzy |
|---|---|---|---|---|---|---|---|
| 0.7 | 0.5 | 53 | 48.2 | 10.02 | 9.21 | 4.3 | 3.12 |
| 1.5 | 1.0 | 26 | 22.13 | 9.56 | 8.08 | 3.97 | 4.23 |
| 2.5 | 1.5 | 20.5 | 16.38 | 8.5 | 7.68 | 3.33 | 2.81 |
| 3.5 | 2.0 | 18 | 13.45 | 7.12 | 7.1 | 3.06 | 2.54 |
| 4.5 | 2.5 | 16 | 13.18 | 5.55 | 5.02 | 2.4 | 1.98 |

## 7. Conclusion

The dynamic performance of the drive is tested with two controllers up to the base speed the results showed better dynamic performance of SPM drive when using DTCI-FLC with online stator reference flux as compared with PI controller. It is observed that the proposed Fuzzy logic controller with simple design approach and smaller rule base can provide better performance .From results, it is clear that for steady state analysis PI controller and for transient analysis FLC is recommended. Further scope of study may be extended for Flux Weakening Operation with Model Reference Adaptive System.

## References

[1] Tae-Suk Kwon, Seung-Ki Sul, "Novel Antiwindup of a Current Regulator of a Surface-Mounted Permanent-Magnet Motor for Flux-Weakening Control" IEEE Transactions on industry applications, vol 42, No. 5, pp no: 1293 – 1300 September/October 2006.

[2] Marco Tursini, Enzo Chiricozzi, and Roberto Petrella," Feedforward Flux-Weakening Control of Surface-Mounted Permanent-Magnet Synchronous Motors Accounting for Resistive Voltage Drop "IEEE Transactions on industrial electronics, vol. 57, No 1, pp no 440-448 January 2010.

[3] Bin Wang, Yue Wang and Zhaoan Wang, " A Modified Direct Torque Control of Surface Permanent Magnet Synchronous Motor Drives without a Speed Sensor", IPEMC2009 ,pp no: 1871-1874, 2009.

[4] Adriano Faggion, Nicola Bianchi and Silverio Bolognani, "Ringed-Pole Permanent-Magnet Synchronous Motor for Position Sensorless Drives" IEEE Transactions on industry applications,vol 47, No: 4, pp no 1759-1766, July/August 2011 .

[5] Lin Chen, Kang-Ling Fang, Zi-Fan Hu, " A Scheme of Fuzzy Direct Torque Control for Induction Machine", Proceedings of the Fourth International Conference on Machine Learning and Cybernetics, Guangzhou, 18-21 August 2005, pp no 803-807.

[6] Sheng Zhao and Xiafu Peng, "A Modified Direct Torque Control Using Space Vector Modulation (DTC-SVM) for Surface Permanent Magnet Synchronous Machine (PMSM) with Modified 4-order Sliding Mode Observer", Proceedings of the 2007 IEEE International Conference on Mechatronics and Automation August 5 - 8, 2007, Harbin, China pp no 1207-1212.

[7] Mohsen Siami, S.Asghar Gholamian " Application of Direct Torque Control Technique for Three Phase Surface Mounted AFPM Synchronous Motors" *International Journal of Science and Advanced Technology (ISSN 2221-8386)* Volume 1 No 10, pp no: 15- 20, December 2011

[8] Lixin Tang, Limin Zhong, Muhammed Fazlur Rahman,, Yuwen Hu," A Novel Direct Torque Control for Interior Permanent-Magnet Synchronous Machine Drive With Low Ripple in Torque and Flux—A Speed-Sensorless Approach", IEEE Transactions on Industry Applications, Vol. 39, No. 6, November/December 2003, pp no 1748- 1756.

[9] Md. Selim Hossain and Md. Jahangir Hossain "Performance Analysis of a Novel Fuzzy Logic and MTPA Based Speed Control for IPMSM Drive with variable d- and q-axis Inductances", Proceedings of 2009 12th International Conference on Computer and Information Technology (ICCIT 2009) 21-23 December, 2009, Dhaka, Bangladesh , pp no 361-366.

[10] Ahmad Reza Shafiei, Behzad Mirzaeian Dehkordi, Arash Kiyoumarsi , Caro. Lucas, "A Hybrid Speed Sensorless MTPA Vector Controller for IPMSM Drive Incorporated with Online Parameter

Identification", Proceedings of ICEE 2010, May 11-13, 2010.

[11] I.Zhong; M.F. rahman, w.Y.Hu and K.W. Lim, " Analysis of direct torque control in permanent magnet synchronous motor drives", IEEE Trans. On power Electronics, vol 12 Issue: 3, pp 528- 536, may 1997.

[12] Kalyan Kumar Halder, Naruttam Kumar Roy, B. C. Ghosh " A High Performance Position Sensor less Surface Permanent Magnet Synchronous Motor Drive Based on Flux Angle" 6th International Conference on Electrical and Computer Engineering, ICECE 2010, Dhaka, Bangladesh , pp no 78-81, 18-20 December 2010.

[13] Isao Takahashi and Toshihiko Noguchi, "A New Quick- Response and High-Efficiency Control Strategy of an Induction Motor", IEEE Trans. Ind. Appl., Vol.IA.22, No.5, pp. 820-827, Sep/Oct, 1986.

[14] Sivaprakasam Arumugam, Manigandan Thathan "Novel Switching Table for Direct Torque Controlled Permanent Magnet Synchronous Motors to Reduce Torque Ripple", Journal of Power Electronics, Vol. 13, No. 6, pp. 939-954, November 2013.

**Biographies**

N. Krishna Kumari graduated in Electrical and Electronics Engineering from Sri Venkateswara University, Tirupathi, Andhra Pradesh, India in 1994. Received M.E in Electrical machines from PSG College of Technology, Coimbatore, Bharathiyar University, Tamilnadu, India in 1997. Presently.Pursuing PhD from JNTU, Hyderabad, India. She has presented/ published 16 research papers in national and international conferences and journals. Her research areas include PWM techniques, DC-DC converters, DC to AC converters, AC-AC converters and control of electrical drives. She is a Life Member of ISTE and SAE. She is presently working as Associate Professor in the Electrical and Electronics Engineering Department, Vallurupalli Nageswara Rao Vignana Jyothi Institute of Engineering and Technology, Hyderabad, India.

He was born in the year 1960 in Hyderabad, India and received B.Tech degree in Electrical & Electronics Engineering from J.N.T.U.College of Engineering, Hyderabad, in 1983. He has received M.E.with *Industrial Drives & Control* from O.U College of Engineering, Hyderabad, in 1986. He has received PhD degree from the Indian Institute of Technology, Madras, in 1996. He is having 29 years of teaching and research experience. His Research interests are Power Electronics, Industrial Drives & FACTS Controllers. He has supervised 21 Ph.D. theses and published/presented 151 technical research papers in national and international conferences and journals. Presently supervising 6 Ph.D. scholars. He is a Fellow of Institute of Engineers (India), (FIE), and Fellow of Institute of Electronics and Telecommunication Engineering (FIETE), and Member of IEEE and SESI. He was Vice-Chancellor, Jawaharlal Nehru Technological University Kakinada, Andhra Pradesh (Nov 2011 to Nov 2014). He is presently professor of Electrical & Electronics Engineering in JNTUH College of Engineering, Hyderabad, Telangana, India. He has visited widely including, Singapore, Malaysia, K.S.A.,U.A.E., Srilanka, Thailand, Sweden, France, Finland, U.K. Switzerland, and U.S.A. He has received several awards including State Teachers Award in 2009 by the Government of Andhra Pradesh from the hands of Honorable Chief Minister.

Dr.M.P.Soni graduated in Electrical Engineering and obtained post graduation in control systems from Govt. Engineering collage Jabalpur in 1969 & 1973 respectively. He joined I.I.T Bombay as Senior Research Fellow under the DAE project on Nuclear Power Plant Control Sponsored by BARC. Dr Soni was awarded Ph.D from I.I.T Bombay in 1977.Dr Soni joined Corporate. R&D Division of BHEL Hyderabad and retired as Additional General Manager in April 2007. Dr.Soni had distinguished career at BHEL. He headed the Transmission & Protection lab and guided the Research team for the development of various products. These are namely, Numerical Relays for Substation Protection, Fitter-bank protection for National HVDC Project, 400 KV 5F6 CT, Substation SCADA, AVR for Turbo Generator .During his tenure he published more than 20 papers in National & International conferences. His Ph.D work has been published in IEEE transaction on Nuclear Science. He has also authored a Chapter in the Handbook of Switchgear published by TATA Mc Graw Hill, 2004. Presently he is working as a Professor & Head of the Department of Electrical & Electronics Engineering in Muffakham Jah College of Engineering and Technology, Hyderabad, India.

www.icgst.com

# Effect of Multiple Particles and Collisions in a 3-Phase Gas Insulated Bus Duct under Switching Impulse Voltage

Ranuva Nageswara Rao, S.S Tulasi Ram
*G. Narayanamma institute of technology & science ,Hyderabad, AP, INDIA*
*Dept. of EEE,JNT university, Hyderabad, AP, INDIA*

## Abstract

Gas Insulated Substations have to withstand for lightning and switching surges without breakdown of Insulation. In this paper a three Phase Gas Insulated Bus duct with inner diameter of each conductor 64 mm and diameter of enclosure 500 mm is considered. Three particle of different sizes assumed to be rest at a position. Switching Impulse Voltage of 1050 kV is superimposed on Power frequency voltages of 245 kV, 300 kV ,400 and 450 kV are applied to Three Phase GIS bus

The motion of the three particles are simulated for different voltages using MATLAB. Effect of the three particles for Switching Impulse Voltage super imposed on power frequency on particle movement are analyzed and time of collisions of the particle at first time is determined for various voltages. And also the horizontal and vertical distances at which the particles collide are determined for Particles of aluminum of 10 mm in length and 0.1 mm radius, 10 mm length and 0.15 mm radius and 7 mm and 0.15 radii. The results show that the three particle collide at different points depending on the particles position , the velocity and direction of the particle changes after collisions . The max displacement of the particles without collision are compared with the max radial displacements by considering the collisions. The results show that the max displacement of particles is higher as compared with without collisions.

***Keywords:*** *Multiple particles , Gas Insulated Substations, Particle Contamination, MATLAB.*

## 1. Introduction

Compressed Gas Insulated Substations (GIS) consists basically of a conductor supported by insulator inside an enclosure, filled with SF6 gas. Basic components of the GIS bay are circuit breakers, disconnectors, earthing switches, bus ducts, current and voltage transformers, etc. The inner live parts of GIS are supported by insulators called spacers, which are made of alumina filled epoxy material. The GIS enclosure forms an electrically integrated, rounded enclosure for the entire substation. Even though SF6 exhibits very high dielectric strength, the withstand voltage of SF6 within the GIS is drastically reduced due to the presence of particles or defects like Free particles on the inner surface of the enclosure, Protrusion on the high voltage (HV) bus,

Protrusion on the inner surface of the enclosure and narrow gaps between the spacer and the electrode are due to imperfect casting and imperfect mechanical strength, The presence of contamination can therefore be a problem with gas-insulated substations operating at high fields [1, 2].

Free conducting particles are most dangerous to GIS. These free conducting particles may have any shape or size,

may be spherical or filamentary (wire like) or in the form of fine dust. Particles may be free to move or may be fixed on to the surfaces. wire like particles made of conducting material are more harmful and their effects are more pronounced at higher gas pressures. As given by the authors [2-5], the presence of atmospheric dust containing conducting particles, especially on the cathode, reduces the breakdown voltage

The present work deals with considering three different particles on the inner surface of the bus duct at a position, and using the basic equations for the movement of these metallic particles. Switching Impulse Voltage of 1050 kV is superimposed on Power frequency voltages of 245 kV, 300 kV ,400 and 450 kV are applied to Three Phase GIS bus.

In this paper a Three Phase Gas Insulated Bus duct with diameter of each conductor 64mm and enclose diameter of 500mm is considered for analysis . Particles of aluminium of 10 mm in length and 0.1 mm radius, 10 mm length and 0.15 mm radius and 7 mm and 0.15 radius are considered for simulation with MATLAB

## 2. Modelling of Gas Insulated Bus duct

A typical horizontal Three-phase bus duct shown in Figure (a) has been considered for the analysis. It consists of three inner conductors spaced equilaterally in a metal enclosure, filled with SF6 gas. Particles are assumed to be rest at some position on the enclosure surface, until a voltage sufficient enough to lift the particles and move in the field is applied. After acquiring an appropriate charge in the field, the particles lift and begin to move in the direction of the field after overcoming the forces due to its own weight and drag. For particles on bare electrodes, several authors have

suggested expressions for the estimation of charge on both vertical/horizontal wires and spherical particles. The equations are primarily based on the work of Felici[5].

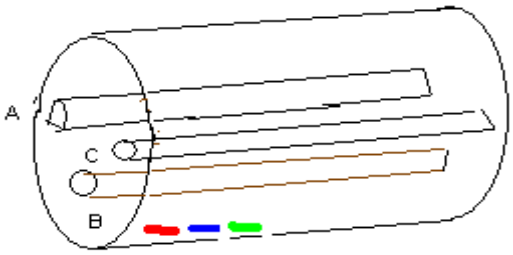


Figure 1. Typical three phase gas insulated bus

Conducting particles in motion in an external electric field will be subjected to a collective influence of several forces. The forces are : -
-Electrostatic force (Fe)
- Gravitational force (mg)
- Drag force (Fd)
The motion equations for the three particles are given by [10][11]

$$m_1 \frac{d^2 y_1}{dt^2} = F_{e1} - m_1 g - F d_1 \quad (1.a)$$

$$m_2 \frac{d^2 y_2}{dt^2} = F_{e2} - m_2 g - F d_2 \quad (1.b)$$

$$m_3 \frac{d^2 y_3}{dt^2} = F_{e3} - m_3 g - F d_3 \quad (1.c)$$

where m1,m2,m3 = mass of the particles
y = displacement in vertical direction
Fe = Electrostatic force
g = gravitational constant

Switching Impulse voltage is superimposed on power frequency voltage and is given by

(1) Switching impulse of 250/2500 micro sec

$$V = V_0(e^{-at} - e^{-Bt}) \quad (A)$$

Where $V_0$=1050 KV
a= 0.3585 x 103
b= 0.7429 x 104

(2) Super imposed Switching impulse on power frequency

$$V = (Vm.\sin w(t - t_0) + V_0(e^{-at} - e^{-Bt}) \quad (B)$$

Where $t_0$=time at which it is superimposed

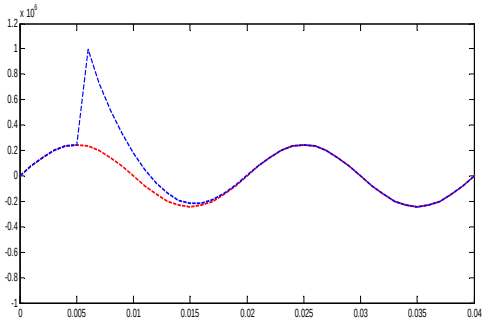


Figure 2. Switching impulse super imposed on ppower frequency voltage

The charges acquired by a vertical wire particles respectively in contact with a naked enclosure can be expressed as:

$$Q_1 = \frac{\pi \in_0 l_1^2 E(t0)}{\left(\ln(\frac{2l_1}{r_1}) - 1\right)} \quad (2.a)$$

$$Q_2 = \frac{\pi \in_0 l_2^2 E(t0)}{\left(\ln(\frac{2l_2}{r_2}) - 1\right)} \quad (2.b)$$

$$Q_3 = \frac{\pi \in_0 l_3^2 E(t0)}{\left(\ln(\frac{2l_3}{r_3}) - 1\right)} \quad (2.c)$$

where Q1 Q2 Q3 are the charges on the particles until the next impact with the enclosure, l1 l2 l3 are the particle length, r1 r2 r3 are the particle radii respectively , E(t0) is the ambient electrical field at t = t0. The charge carried by the particle between two impacts has been considered constant in the simulations.

The electric field in a coaxial electrode system at position of the particles can be written as:

$$E = \sqrt{E_x^2 + E_y^2}$$

$$E_x = 48.64 \times 10^3 \left[\cos 0^0 \left(\frac{1}{0.125 - x}\right) + (\cos 120^0 + \cos 240^0)\left(\frac{\cos\theta_2}{R_1}\right)\right] \quad (3)$$

$$E_y = 48.64 \times 10^3 \left[\sin 0^0 \left(\frac{1}{0.125 - x}\right) + (\sin 120^0 + \sin 240^0)\left(\frac{\cos\theta_2}{R_1}\right)\right]$$

where $R_1$ = Distance between the conductor B and particle
$\theta_2$ = Angle between the vertical axis and $R_1$
x = Position of the particle within the enclosure
$V_m$ = 200 Kv/ph $V_{rms}$ = 245 Kv (line to line)
h = Distance between the centre of the conductor and the enclosure
r = Radius of the conductor

The electrostatic force on each particle is given by

$$F_{e1} = K\, Q_1\, E(t) \quad (4.a)$$

$$F_{e2} = K\, Q_2\, E(t) \quad (4.b)$$

$$F_{e3} = K\, Q_3\, E(t) \quad (4.c)$$

Where K is a corrector and is a factor less than unity. However, for length-to-radius ratios greater than 20 the correction factor, K, is close to unity

The drag forces are given by:

$$F_{d1} = \dot{y}\, \pi r_1 \left(6\mu K_d (\dot{y}) + 2.656 \left[\mu \rho_g l_1 \dot{y}\right]^{0.5}\right)$$

$$F_{d2} = \dot{y}\, \pi r_2 \left(6\mu K_d (\dot{y}) + 2.656 \left[\mu \rho_g l_2 \dot{y}\right]^{0.5}\right) \quad (5)$$

$$F_{d2} = \dot{y}\, \pi r_3 \left(6\mu K_d (\dot{y}) + 2.656 \left[\mu \rho_g l_2 \dot{y}\right]^{0.5}\right)$$

where y is the velocity of the particle, $\mu$ is the viscosity of the fluid (SF6 : 15.5_10−6kg/m_s at 200C), r1 r2 r3 are the particle radius, $\rho_g$ is the gas density, l1 l2 l3 are the particle lengths, Kd(y) is a drag coefficient.
The influence of gas pressure on the drag force is given by empirical formula.

$$\rho_g = 7.118 + 6.332P + 0.2032P^2 \quad (6)$$

where $\rho_g$ = density p = Pressure of the gas and 0.1 < p < 1mboxMPa.
The restitution coefficient for copper and aluminum particles seem to be in the range of 0.7 to 0.95:R = 0.8 implies that 80% of the incoming impulse of the particle is preserved when it leaves the enclosure.

The motion equation (1a) ,(1b),(1c) using all forces can therefore be expressed as

$$m\ddot{y}(t) = \frac{\pi \in_0 I^2 E(t_0)}{\ln\left(\frac{2l}{r}\right)-1} x\ 48.64\ x10^3 \left[\left(\frac{1}{0.125-x}\right) + \left(\frac{Cos\theta_2}{R_1}\right)\right] Sin\omega t \quad (7)$$

$$- mg - \dot{y}(t)\,\pi r\,(6\mu K_d(\dot{y}) + 2.656\,(\mu r_g\ ly\ (t)^{0.5})$$

In the above equation, the parameters m,l,r can be replaced by m1,l1,r1 and motion of the particle 1 can be obtained . similarly for paricles 2 and 3 motions can be obtained. The above equation is a second order non-linear differential equation and in this paper, the equation are solved using MATLAB
In order to determine the random behavior of moving particles, the calculation of movements in axial and radial directions was carried at every time step using rectangular random numbers. The above simulation yields the particle movement in the radial and axial directions. The random movement can be adequately simulated by Monte-Carlo method. In order to determine the randomness, it is assumed that the particle emanates from its original site at any angle less than φ, where φ/2 is half of the solid angle subtended with the vertical axis.

## 3. Results and Discussions

The particle 1 has 10 mm in length and 0.1 mm radius, particle 2 has 10 mm length and 0.15 mm radius and particle 3 has 7 mm and 0.15 radius.
Table 1 shows the radial movement of the particles in a 3-Phase Gas Insulated Bus duct in Electric Field for switching impulse voltage superimposed on voltages of 245KV ,300 kV ,400 KV and 450 KV respectively.
Table 2 (a) and 2 (b) shows the time at which particle collide for first time Tc and Vertical height of the particle at collisions in mm velocity of the particle at just before the collision (mm /sec) . In Table 3 the velocity of the particles after collision are shown determined by calculating the angle of collisions at Tc by MATLAB .Figure 1 to Figure 4 shows the movement patterns of aluminum particles in Electric Field for switching impulse voltage superimposed on voltages applied voltages of 245KV ,300 kV ,400 KV and 450 KV respectively

Figure 7 to Figure 10 shows the collision of particles in the bus ducts. It is observed that the three particle are started at same position and probability of collision at different points also shown in figures 7 to 10. It is seen that as the voltage varies from 245 KV to 450 KV maximum radial movement also varies as shown in Table1 and also the particles collide at different intervals. The collisions of the particles for the first time both time and height of collision also shown in Table 2. At this point of collisions (from fig 7 to 10 ) the particle moves randomly and its velocity and direction also changes which gives the actual maximum radial displacement would be more than the maximum radial displacement when no collision takes place.
The axial movements of particles and collision points are shown in figures 11 to 14 for the applied voltages of 245 KV,300 KV,400 KV and 450 KV respectively.
The vertical velocity and angle of collision of the particles are calculated by simulation results for different voltages 245 KV,300 kv,400 kv,450 KV respectively by knowing angle of collisions , the velocity of the particles 1, 2 and 3 after collisions are calculated as given in Appendix.

In the table 3 ,the velocity of the particles just the instant after collision for different voltages is given. It is seen from the table 2 that the velocity of the particles 2 and 3 ( Gree and red colours in the plot) are abruptly changes its velocity after collision. If the particles continue to move with its new velocity the maximum height of the particle would be more than that when particles are considered individually without collision as given in Table 4(a) and 4(b).
In Table 4(a) and 4(b) , it is shown that the maximum expected radial displacements of the particles after collision. For the particle 3 its expected radial displacements for 300 KV is almost 1.25 time as that when no collisions are assumed to take place. For the superimposed voltages of 245 KV ,400 KV and 450 KV ,the collision of particles take place after the switching impulse have been elapsed so the radial displacements after collision at the Time Tc are slightly changed. These values are very much less than max. radial displacements .hence for only voltages 300 kv the max radial displacement changes.

| Voltage KV | Max. Radial Movement of particle 1 (mm ) | Max. Radial Movement of particle 2 (mm ) | Max. Radial Movement of particle 3 (mm ) |
|---|---|---|---|
| 245 | 77.1367 | 35.8078 | 29.7986 |
| 300 | 82.4341 | 47.0803 | 41.2123 |
| 400 | 86.7683 | 54.3026 | 43.2723 |
| 450 | 88.4441 | 62.6838 | 51.8091 |

Table:1 Radial movement of aluminum particles with Monte-Carlo technique for various voltages assuming no collisions

| Voltage KV | Time at which particle collide first time Tc | Vertical height of the particle at collisions (mm ) | | |
|---|---|---|---|---|
| | | Particle1 (blue) | Particle2 (green) | Particle3 (Red) |
| 245 | 0.17 | NC | 2.5 | 2.5 |
| 300 | 0.065 | NC | 38.5 | 38.5 |
| 400 | 0.18 | NC | 14.5 | 14.5 |
| 450 | 0.17 | NC | 23.2 | 23.2 |

Table:2.(a) Vertical height and time of particle collisions for various voltages

| Voltage KV | Velocity of the particle at just before the collision (mm /sec) | | |
|---|---|---|---|
| | Particle 1 (blue) | Particle2 (green) | Particle3 (Red) |
| 245 | -243.6 | **-632.8** | **264.2** |
| 300 | 787.3 | **370** | **304.8** |
| 400 | -2094 | **-1301.4** | **-1261.8** |
| 450 | -5517.2 | **-331.3** | **-403.3** |

Table:2.(b) velocities of the particles at just before the collision for various voltages.

| Voltage KV | Velocity of the particle after the collision (mm /sec) | | |
|---|---|---|---|
| | Particle1 (blue) | Particle2 (green) | Particle3 (Red) |
| 245 | NC | **105.9221** | **--791.0779** |
| 300 | NC | **316.3047** | **381.5047** |
| 400 | NC | **-1268.8** | **-1308.4** |
| 450 | NC | **-390.5954** | **-318.5954** |

Table:3. velocities of the particles at just after the collision for various voltages.

| s.no | Max Radial displacements without considering collisions | | |
|---|---|---|---|
| Voltage KV | Max. Radial Movement of particle 1 (mm ) | Max. Radial Movement of particle 2 (mm ) | Max. Radial Movement of particle 3 (mm ) |
| 245 | 77.13 | 35.80 | 29.79 |
| 300 | 82.43 | **47.08** | **41.21** |
| 400 | 86.76 | 54.3 | 43.27 |
| 450 | 88.44 | 62.68 | 51.8 |

Table:4.(a) Max Radial displacements without collision

| s.no | Max Radial displacements with collisions | | |
|---|---|---|---|
| Voltage KV | Radial Movement of particle 1 | Radial Movement of particle 2 (mm ) | Radial Movement of particle 3 (mm ) |
| 245 | 77.13 | 35.80 | 29.79 |
| 300 | 82.43 | **40.24** | **51.63** |
| 400 | 86.76 | 29.11 | 43.27 |
| 450 | 88.44 | 35.91 | 51.80 |

Table:4.(b) Expected Max Radial displacements with collision

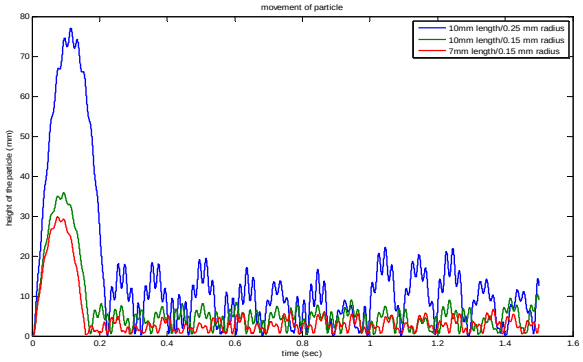


Figure:3 Radial Movement for Al/ 245 KV / 64mm - 500mm Enclosure

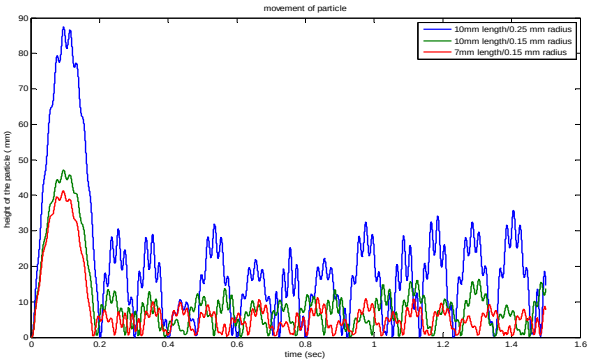


Figure:4 Radial Movement for Al/ 300 KV / 64mm - 500mm Enclosure

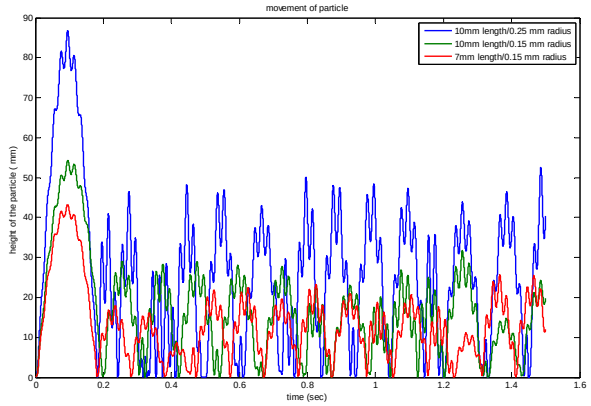


Figure:5 Radial Movement for Al/ 400 KV / 64mm - 500mm

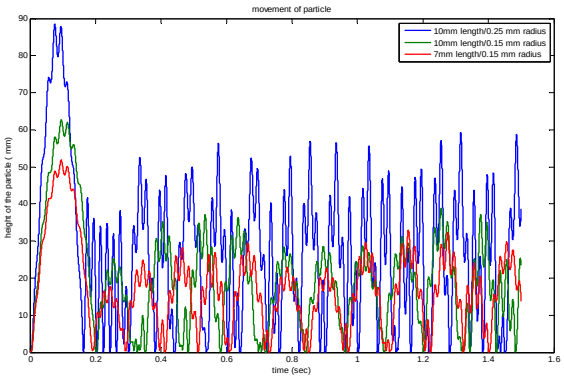


Figure:6 Radial Movement for Al/ 450 KV / 64mm - 500mm Enclosure

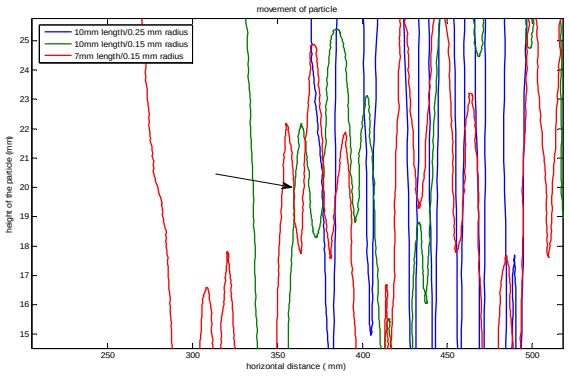


Figure:10 Particle collisiont for Al/ 450 KV / 64mm - 500mm Enclosure

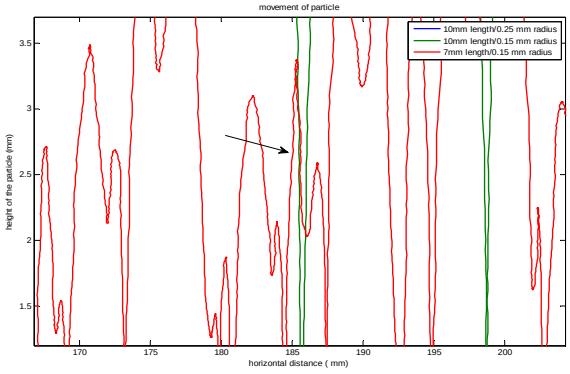


Figure:7Particles collision for Al/ 245 KV / 64mm - 500mm Enclosure

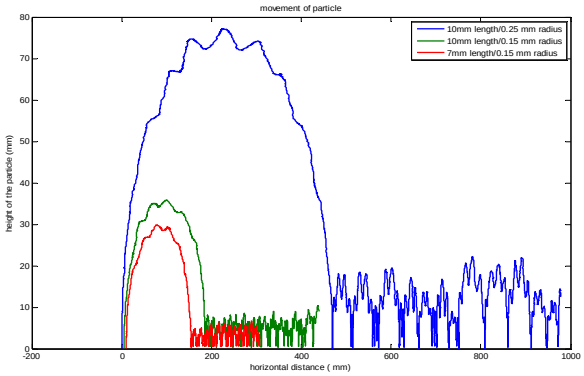


. Figure:11 Axial Movement for Al/ 245 KV / 64mm - 500mm Enclosure

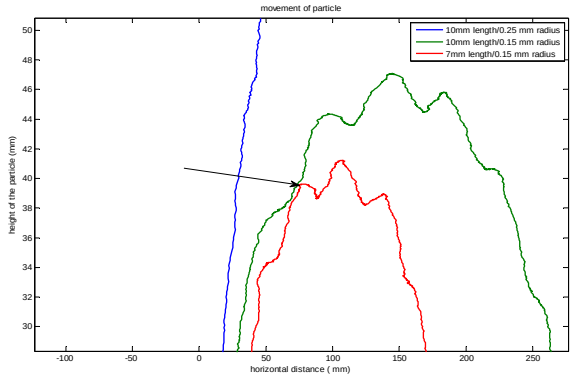


Figure:8 Particles collision for Al/ 300 KV / 64mm - 500mm Enclosure

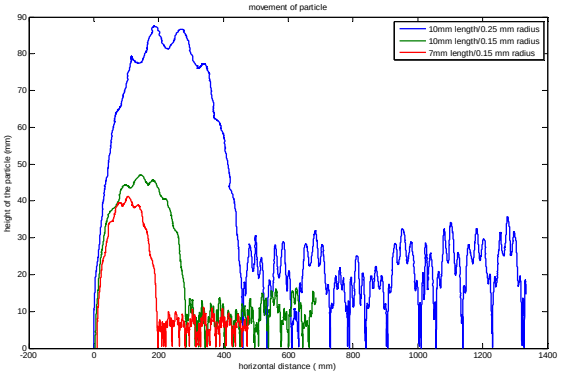


Figure:12 Axial Movement for Al/ 300 KV / 64mm - 500mm Enclosure

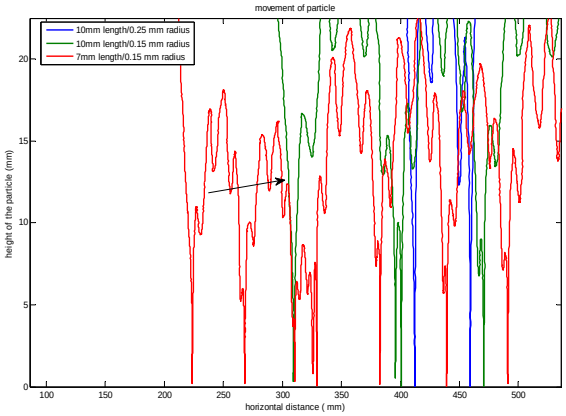


Figure:9 Particle collisiont for Al/ 400 KV / 64mm - 500mm Enclosure

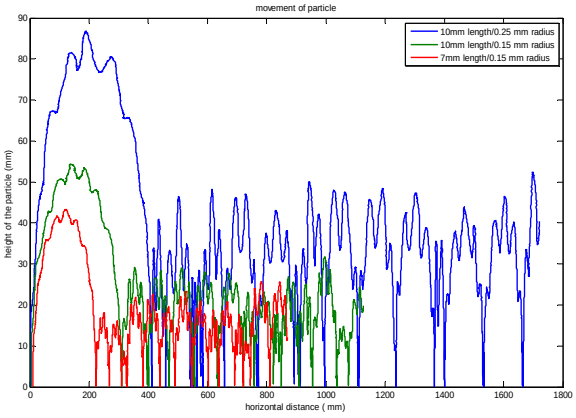


Figure:13 Axial Movement for Al/ 400 KV / 64mm - 500mm Enclosure

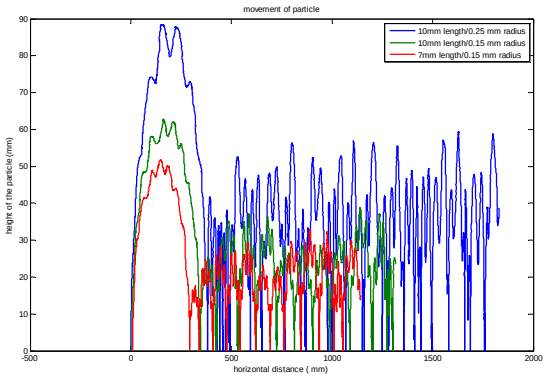


Figure:14 Axial Movement for Al/ 450 KV / 64mm - 500mm Enclosure

## 4. Conclusions

For the superimposed voltages of 245 KV ,400 KVand 450 KV the collision of particles take place after the switching impulse have been elapsed where as the For the superimposed voltages of 300 KV the collision takes place before the switching impulse have been elapsed

It is shown that the probability of a flashover occurs at smaller size of the particle and at higher voltages but due to the particle collisions particles move randomly and its velocity and direction also changes which leads to flash over even at low voltages. If the calculations, as described above, are performed at a different voltage levels by considering a single particle at a time as no collisions takes place, max height of the particle and chances of flash over would be low. The results obtained from the calculations show that additional information about the particles collision and time at which first time collision takes place should be considered to estimate the flash over chances. However the collision of the particles in the gap will increase the chances of flashover.

## Appendix: Two- dimensional Collision of particles

Consider two particles, denoted by subscripts 1 and 2. Let $m_1$ and $m_2$ be the masses, $v_1$ and $v_2$ the velocities before collision. For the case of two colliding bodies in two dimensions, the overall velocity of each body must be split into two perpendicular velocities: one tangent to the common normal surfaces of the colliding bodies at the point of contact, the other along the line of collision. Since the collision only imparts force along the line of collision, the velocities that are tangent to the point of collision do not change. The final velocities can then be calculated from the two new component velocities and will depend on the point of collision.

In a center of momentum frame at any time the velocities of the two bodies are in opposite directions, with magnitudes inversely proportional to the masses. In an elastic collision these magnitudes do not change. The directions may change depending on the shapes of the bodies and the point of impact.

Assuming that the second particle is at rest before the collision, the angles of deflection of the two particles, $v_1$ and $v_2$ , are related to the angle of deflection $\theta$ in the system of the center of mass by

$$\tan \nu_1 = \frac{m_2 \sin \theta}{m_1 + m_2 \cos \theta} \qquad (8)$$

$$\nu_2 = \frac{\pi - \theta}{2}$$

The velocities of the particles after the collision are:

$$\nu_1' = \nu_1 \frac{\sqrt{m_1^2 + m_2^2 + 2 m_1 m_2 \cos \theta}}{m_1 + m_2} \qquad (9)$$

$$\nu_2' = \nu_1 \frac{2 m_1}{m_1 + m_2} \sin \frac{\theta}{2}$$

where $v_1$ and $v_2$ are the scalar sizes of the two original speeds of the objects, $m_1$ and $m_2$ are their masses, $\theta$ *is the* movement angle,

## Acknowledgements

The authors are thankful to the managements of G.Narayanamma Institute of Technology and science ,Hyderabad and JNT University, Hyderabad, for providing facilities and to publish this work.

## 5. References

[1] L. G. Christophorou, J. K. Olthoff, R. J. Van Brunt, "SF6 and theElectric Power Industry", IEEE Electrical Insulation Magazine,DEIS, 1997, pp. 20

[2] A.H. Cookson, P.C. Bolin, H.C. Doepken, R.E. Wootton, C.M. Cooke and J.G. Trump, "Recent Research in the United States on the Effect of Particle Contamination Reducing the Breakdown Voltage in Compressed Gas Insulated System", Int. Conf. On Large High Voltage System; Paris, 1976.

[3] H.Anis and K.D. Srivastava, "Breakdown Characteristics of Dielectric Coated Electrodes in Sulphur Hexafluoride Gas with Particle contamination", Sixth Intern. Sympos High Voltage Engineering, Paper No. 32.06, New Orleans, LA, USA. 1989.

[4] J. Amarnath, B. P. Singh, C. Radhakrishna and S. Kamakshiah, "Determination of particle trajectory in a Gas Insulated Busduct predicted by Monte-Carlo technique", IEEE Conf. Electr. Insul.Dielectr. Phenomena (CEIDP), Texas, Austin, USA, 1991 Vol. 1, pp. 399-402,1991.

[5] N. Felic. Forces et charges de petits objects en contact avec une electrode affectee d'un champ electrique. Revue generale de I' electricite, 1996, 1145–1160.

[6] M.Ramya Priya, G.V.Nagesh Kumar, Member, IEEE, J.Amarnath and R.Prabha Devi Effect of Various Design Parameters ofGas Insulated Bus Duct in the Performance of Gas Insulated Sub-Stations.

[7] G.V. Nagesh Kumar, J. Amarnath, B.P. Singh and K.D. Srivastava “Electric Field Effect on Metallic Particle Contamination in aCommon Enclosure Gas Insulated Busduct” IEEE Transactions on Dielectrics and Electrical Insulation Vol. 14, No. 2; April 2007

[8] IL. Rajasekhar Goud, K.B.Madhu Sahu, 'J. Amarnath, , 3B.P. Singh and 4K.D. Srivastava “Deternination of Random Movement of Particle in Gas Insulated Busduct”

[9] S.Luding , “ Collisions and contact between two particles “ institute of computer Aplications.

[10] Ranuva Nageswara Rao,Dr S S tulasi Ram , “Effect of simultaneous movement of multiple particles under electric field in a Single Phase Gas Insulated Bus duct” Int. Journal of Engineering Research and Applications ISSN : 2248-9622, Vol. 4, Issue 10( Part - 3), October 2014

[11] Ranuva Nageswara Rao,Dr S S tulasi Ram ,” Effect of movement of multiple particles and collisions in a 3- Phase Gas Insulated Bus duct ” “International conference on High Voltage Engineering & Technology” (ICHVET2015), during January 29-30, 2015 at Hyderabad,

## Biographies

Ranuva Nageswara Rao received the M.Tech degree in electrical and electronics engineering from Sri venkateswara University college of Engineering, Tirupathi, Andhra Pradesh , India in 2000. Ccurretly he is an associate professor at G.N.I.T.S, Hyderabad, INDIA he is doing Ph D in the area of High voltage Engineering his interesting areas are Power system control, High voltage engineering.

Dr S.S. Tulasiram received his ph.D degree in High Voltage Engineering, JNTU in 1995. At present he is professor in the department of Electrical and electronics Engineering, JNT university Hyderabad. His research interests are insulation protection studies of High Voltage Equipment, SR motors, SiC and power semiconductors



www.icgst.com

# An Exotic Robust Performance of PI-Fuzzy Controller Fed BLDC Drive

J.E.Muralidhar and P.Varanasi
Associate Professor, EED, Muffakham Jah college of Engineering & Technology, Hyderabad
Rtd.Professor, Department of Electrical & Electronics Engineering, BRECW, Hyderabad, India
jmuralidhar@yahoo.com,

## Abstract
Brushless DC motors are promptly increased popularity because of its more efficiency & attain control characteristics with high accuracy speed. Need some digital controllers for sensing & regulating the disturbances by utilizing the several control logic units. The obstacles of formal PI controller for the speed control can be regulated by Fuzzy+PI control units with affordable stability factor. This paper highlights the design of the six switch converter fed BLDC drive with Fuzzy+PI controller supports the dynamically renew the parameters of formal PI controller. The intended control units have very moderate structures because of hybrid fuzzy rule in the rule based system is relevant to ease design using computer simulations. Simulation results are conferred satisfactorily in transient & steady states, low error values and with a high stability factor.

***Keywords:*** *BLDC Drive; Six Switch Converter Topology, PI Proportional Integral Controller, Fuzzy Controller, Hybrid Fuzzy Controller.*

***Nomenclatur:*** *BLDC – Brushless DC, FLC – Fuzzy Logic Control, EMF- Electro Magnetic force.*

## 1. Introduction
Brushless DC motors offer the imperative advantageous over brushed type, embraces the more torque/weight-watt ratio, appreciate reliability, low noise, high lifetime, deducting the ionizing sparks from the commutator, low EMI. However, composite control strategies for BLDC current/speed regulation can be acute to parameter variations, uneven disturbances, which make the total system to be less reliable. Utilization of BLDC drives in domestic applications, where variations in system parameters to be more frequent, need to regulate the parameters using digital control units. Major considerations for the implementation of robust control units for maintaining high stability factor, when the drive is operating under sudden disturbances, load torque adoptions. Due to the preferment of digital logic units is very appropriate to control the drive characteristics, which can be preferred in aerospace, robotics and many precise applications [1]. Formally several speed control methodologies are utilized for BLDC drive applications such as PI, PID controlled themes are presented in [2]. Due to the non-linear characteristics of BLDC drive, need a non-linear type control unit is merely preferred such as Fuzzy Logic Unit are used for better speed regulation. Fuzzy is a multi-variable with capable control algorithm with a very simple structure and good robustness, there were some deficiencies at tuning the high precision and expeditious speed of system static & dynamic performance. A modern terminology is acquainted for tuning & designing of scaling gains of classical fuzzy logic control (FLC) unit based on its amply tuning of linear counterparts. The classical FLC unit with a linear rule based is very similar to its linear counterpart. This fuzzy logic can be used to control-over the process that the human can control manually with expertise gained depends from his experience [3]. The base value is exactly analogous to its linear counterpart.
Cognately, classical two term controller has fuzzy integral & fuzzy proportional gains with a linear rule [4]. Among them FLC had good processing ability for non-linear ascertain systems, moreover suitable for the control of non-linear highly disturbed BLDC drive system. By incorporating the individual fuzzy rules for tuning the PI parameters, the controlled objectives attain good dynamic steady performance. The formal fixed gain values are not ideal for a huge range of torque/speed application. So as to obtain the foremost performance of BLDC drive [5], these parameters have to be dynamically tuning with reference speed value at which the drive is operating. This may lead to the new dimension of FUZZY+PI controller is dynamically updated the parameters with respect to torque/speed changes for optimal performance of BLDC drive.
The operated elements of the proposed Fuzzy+PI controller are depicted in Figure 2. This drive system comprises of three phase six switch inverter topology with a speed sensing device and regulation of speed using Fuzzy+PI controller. The PI controller variables are dynamically adjusted with in a specific speed coming from the drive from hall sensors which are built into the BLDC drive system. Here ωr* is the set speed & ω_actual is the actual speed of the drive both will be composed achieves error values and a controller sense that error signal and disposes that error values may get a

reference PWM signal and same is interfaced to a logic sequencer circuit. The main intension of this paper is presenting a novel multiloop approach with the allowed decoupling factor of emulating mechanical vibrations and hence minimizing the torque ripple for that dynamically evaluated by using computer simulated software package and simulation results are conferred with a better dynamic performance with merely real time industrial applications.

## 2.Principle of Operation:

Basically there are two major types of permanent magnet-type machines like sinusoidal back EMF type & trapezoidal back EMF type. With that trapezoidal motor have a higher torque ratio compared to other types. The back EMFs induced in the stator windings has trapezoidal type and its phases must be supplied with quasi-square wave currents for ripple free operation [6].

### *A. Mathematical Model of the PMBLDC Motor*

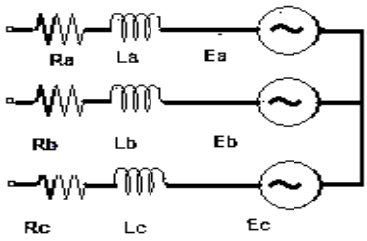


**Figure 1 Motor Circuit Model**

The voltage equations of the BLDC motor are as follows

$$V_a = R_a i_a + \frac{d}{dt}(L_{aa} i_a + L_{ba} i_b + L_{ac} i_c) + \frac{d\lambda_{ar}(\theta)}{dt}$$

$$V_b = R_b i_b + \frac{d}{dt}(L_{ba} i_a + L_{bb} i_b + L_{bc} i_c) + \frac{d\lambda_{br}(\theta)}{dt}$$

$$V_c = R_c i_c + \frac{d}{dt}(L_{ca} i_a + L_{cb} i_b + L_{cc} i_c) + \frac{d\lambda_{cr}(\theta)}{dt}$$

In balanced system the voltage equation becomes

$$\begin{bmatrix} V_a \\ V_b \\ V_C \end{bmatrix} = \begin{bmatrix} R & 0 & 0 \\ 0 & R & 0 \\ R & 0 & R \end{bmatrix} \begin{bmatrix} i_a \\ i_b \\ i_c \end{bmatrix} + \frac{d}{dt} \begin{bmatrix} L_a & L_{ba} & L_{ca} \\ L_{ba} & L_b & L_{ca} \\ L_{ca} & L_{cb} & L_c \end{bmatrix} \begin{bmatrix} i_a \\ i_b \\ i_c \end{bmatrix} + \begin{bmatrix} e_a \\ e_b \\ e_c \end{bmatrix}$$

$$L_a = L_b = L_c = \mathrm{L}$$

$$L_{ab} = L_{bc} = L_{ac} = \mathrm{M}$$

Assuming constant self and mutual inductance, the voltage equation becomes

$$\begin{bmatrix} V_a \\ V_b \\ V_C \end{bmatrix} = \begin{bmatrix} R & 0 & 0 \\ 0 & R & 0 \\ R & 0 & R \end{bmatrix} \begin{bmatrix} i_a \\ i_b \\ i_c \end{bmatrix} + \frac{d}{dt} \begin{bmatrix} \mathrm{L-M} & 0 & 0 \\ 0 & \mathrm{L-M} & 0 \\ 0 & 0 & \mathrm{L-M} \end{bmatrix} \begin{bmatrix} i_a \\ i_b \\ i_c \end{bmatrix} + \begin{bmatrix} e_a \\ e_b \\ e_c \end{bmatrix}$$

In state space form the equation is arranged as

$$\frac{d}{dt} \begin{bmatrix} i_a \\ i_b \\ i_c \end{bmatrix} = -\frac{R}{L} \begin{bmatrix} i_a \\ i_b \\ i_c \end{bmatrix} - \frac{1}{L} \begin{bmatrix} e_a \\ e_b \\ e_c \end{bmatrix} + \frac{1}{L} \begin{bmatrix} V_a \\ V_b \\ V_C \end{bmatrix}$$

The electromagnetic torque is given as

$$T_e = (e_a i_a + e_b i_b + e_c i_c)/\omega_r$$

The equation of motion is given as

$$\frac{d}{dt}\omega_r = (T_e - T_L - B\omega_r)/J$$

The proposed trapezoidal type motor drives are more attractive for industrial applications because of simplicity, lower price, and high efficient operation compared to sinusoidal type, this may require complex hardware & software tools for sensing the rotor position. BLDC drives exist in many more configurations but the three phased motor is most valuable type due to affordable features. Offers a good interaction between precise control and number of switching devices are required to control over the stator currents. Detection of rotor position is usually implemented by utilizing three hall sensing devices that detects the presence of small magnets are distributed to the rotor shaft.

The phase conductance for each interval is 120° by electrical angle. Each interval should be started with the stator & rotor fields lines of 120° apart & ends when 60° apart. Maximum torque is attained when the intended field lines are perpendicular nature. The commutation phase sequence is AB; AC; BC; BA; CA; CB, respective conduction stage is known as one step. However, only two-phases are conducted at any time leaving the third to be floating one. So as to generate maximum torque the inverter is commutated under every 60° then current is in-phased with back EMF [7]. Commutation timing is evaluated by the rotor position, which can be detected by hall sensors & switches as a IGBT valves depicted in above figure. Table I shows the switching sequence for the current direction and the positioned signals.

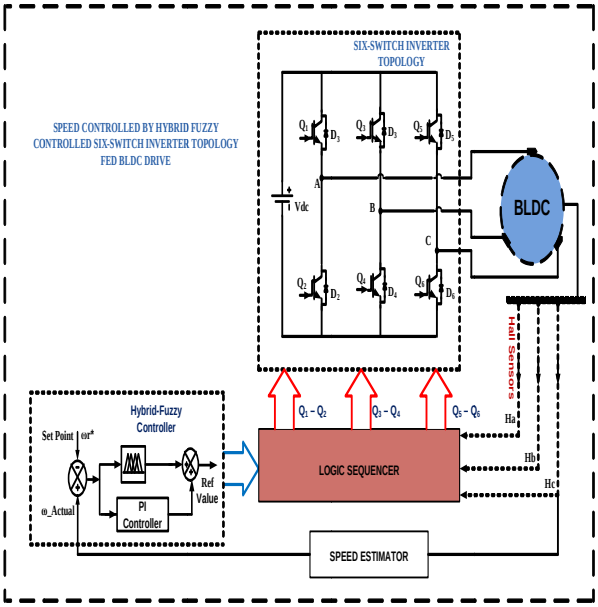


Figure 2 Overall Schematic Diagram of Hybrid Fuzzy Controlled Six-Switch Inverter Topology Fed BLDC Drive

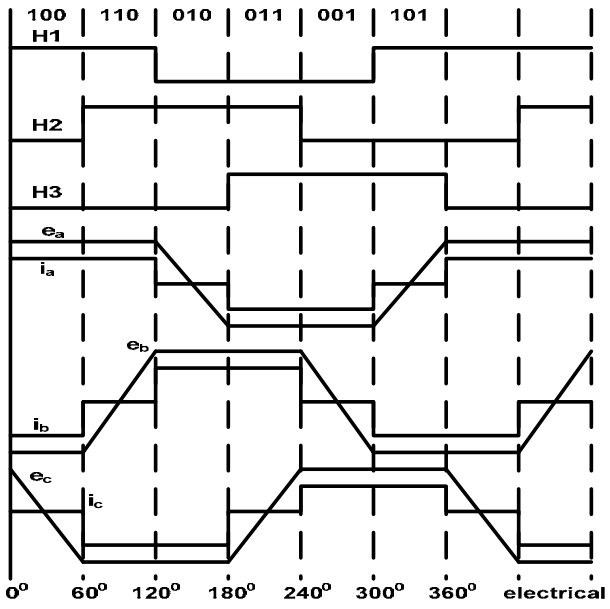


Figure 3 Ideal Back-Emf's, Phase Currents, and Position Sensor Signals.

Table I Switching Sequence & Sensing Signals

| Switching Interval (deg) | Seq. Number | Hall Sensors | | | Switch Closed | | Phase Current | | |
|---|---|---|---|---|---|---|---|---|---|
| | | H1 | H2 | H3 | | | A | B | C |
| 0-60 | 0 | 1 | 0 | 0 | Q1 | Q4 | + | - | 0 |
| 60-120 | 1 | 1 | 1 | 0 | Q1 | Q6 | + | 0 | - |
| 120-180 | 2 | 0 | 1 | 0 | Q3 | Q6 | 0 | + | - |
| 180-240 | 3 | 0 | 1 | 1 | Q3 | Q2 | - | + | 0 |
| 240-300 | 4 | 0 | 0 | 1 | Q5 | Q2 | - | 0 | + |
| 300-360 | 5 | 1 | 0 | 1 | Q5 | Q4 | 0 | - | + |

## 3. Proposed Closed Loop Control Technique

Many industrial applications such as robotics, automation systems, require precise control action of position and speed. Digital control a system allows easy set and accommodates the speed of the drive. An efficient designed feedback controller acquires the system insensible to pertaining disturbances and changes of the parametric variations.

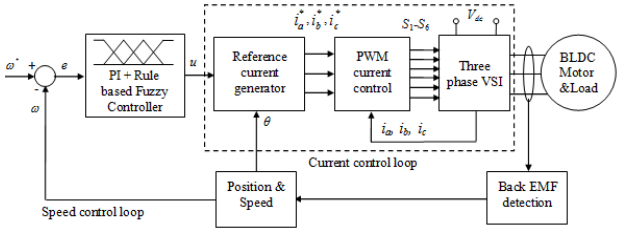


Figure 4 Block diagram for closed loop Scheme

***Formal PI Controller:***

Implementation of closed loop speed sensing devices has accurate response, but because more expensive due to the importance of feedback components like sensors, comparators, control actuators. Speed controller evaluates the actual speed of the system and compare to reference speed may get error value, which is fed to PI controller. PI controllers comprise of a proportional gain that supports a proportional action to the input error and an integrated to achieve the steady state error value to be zero for a step change in the input. Calculation of PI gain values is a two-term control action. Meticulously, these values can be implicated in terms of time; on that *P* depends on present error; *I* support the accumulation of past errors due to the current rate of change. The weighted summing of these two actions is merely used for optimal tuning of process via position control element. Due to these non-linear characteristics of PI gains merely used intelligence control actions to attain perfect control features.

***Fuzzy Controller:***

Fuzzy logic control action is extensively preferred in many control logic applications. The term "Fuzzy" bears the fact of logic involved can deal with the concept of "true" or "false" but rather as "partial true" cases. However, alternative methods such as such as genetic evolves, neural networks can predominate as well as fuzzy in many specific applications [8],[9]. Fuzzy logic has the specific advantage that the solution for this problem can be cast in the nature of human operators to be understood, based on that utilized design for a new controller to this BLDC drive system is more valuable. The imperative membership functions are depicted in Figure 5.

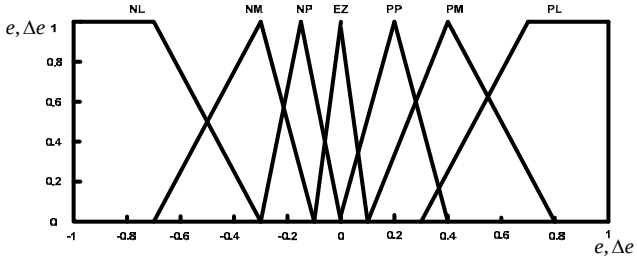


Figure 5. Membership Functions of FLC

Table II. The Decision Table of FLC

| e / Δe | NL | NM | NS | EZ | PS | PM | PL |
|---|---|---|---|---|---|---|---|
| NL | NL | NL | NL | NL | NM | NS | EZ |
| NM | NL | NL | NL | NM | NS | EZ | PS |
| NS | NL | NL | NM | NS | EZ | PS | PM |
| EZ | NL | NM | NS | EZ | PS | PM | PL |
| PS | NM | NS | EZ | PS | PM | PL | PL |
| PM | NS | EZ | PS | PM | PL | PL | PL |
| PL | NL | NM | NS | EZ | PS | PM | PL |

As seen from above table II, each interval of each input or output variable are divided into seven membership functions; NB-Negative Big value, NM- Negative Medium Value, NS- Negative Small Value, Z- Zero Value, PS-Positive Small Value, PM- Positive Medium Value, PB-Positive Big value.

***Hybrid Fuzzy Controller:***

The exotic intended control technique is implemented so as to control over the BLDC parameters effectively. As before we developed PI or Fuzzy individually, here authors prefer a combination of both controller acts as a PI+Fuzzy controller. For these control actions, PI

minimizes the steady state error values & Fuzzy take over the change in error value. Hence called as Hybrid-Fuzzy controller is applicable to motion control system, it has more valuable features compared to formal techniques and applications in many industrial sectors.

## I. MATLAB/SIMULINK MODELING & RESULTS

Simulation is carried out for verifying the effectiveness of the Fuzzy+PI controller. The simulation results are compared with PI controller and found a tangible improvement in the performance characteristic. The constant & variable speed response of BLDCM at 2000 rpm with PI controller, Fuzzy and Fuzzy+PI controller is presented. The controller makes the speed of a motor to a desired level. Here simulation is evolved as various cases, 1. Performances of BLDC drive Operating under PI Controller. 2. Performance of BLDC Drive Operating under Fuzzy Controller. 3. Performance of BLDC Drive Operating under Fuzzy+PI Controller.

*Case 1: Performances of BLDC drive Operating under PI Controller*

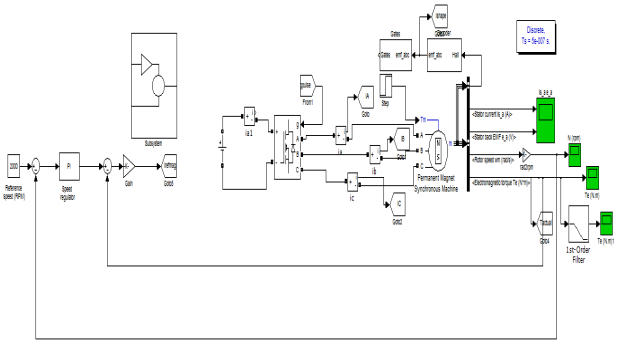

Figure 6 Matlab/Simulink Model of Proposed BLDC drive Operating under PI Controller with Six Switch BLDC Drive

Figure 6 shows the matlab/simulink model of proposed bldc drive operating under pi controller with six switch bldc drive using computer simulation tool.

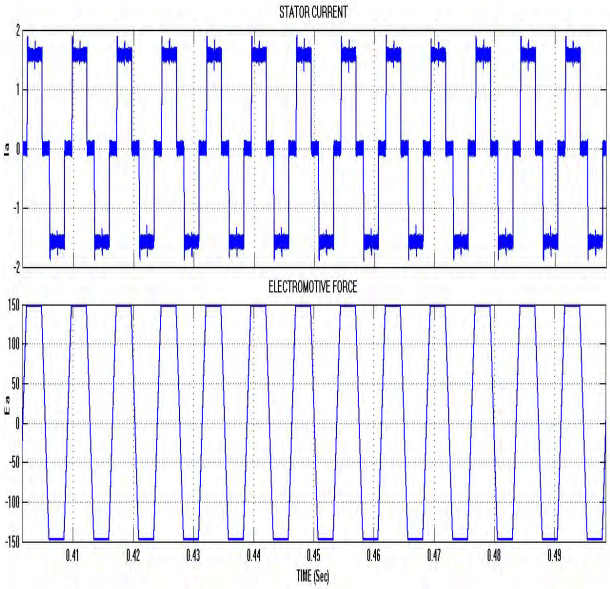


(a) Stator Current & Back EMF

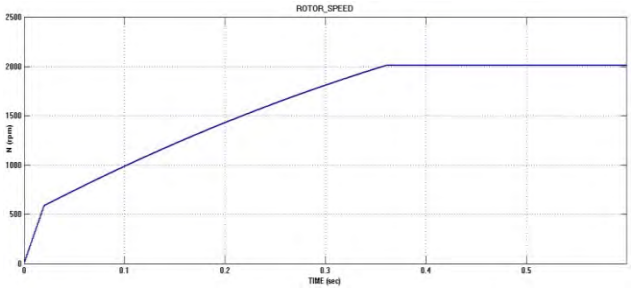


(b) Rotor Speed

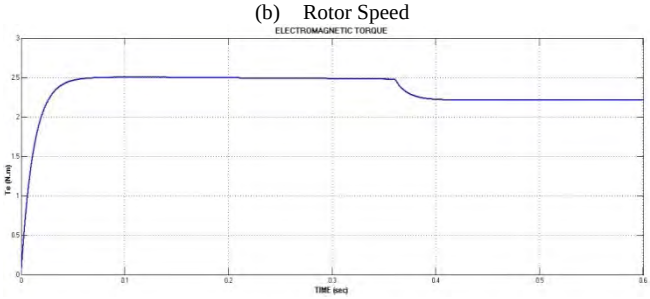


(c) Electromagnetic Torque

Figure 7 (a) Stator Current & Back EMFs, (b) Rotor Speed, (c) Electromagnetic Torque of the BLDC Drive operating under constant speed condition with PI control design.

Figure 7 shows the (a) stator current & back EMF of the BLDC drive, here back EMF as a trapezoidal shape with alignment of stator current operated under 120 (deg) mode, (b) Rotational speed of the BLDC drive at constant speed with PI regulator, due to non-linear gains attains some of error in steady state value merely 0.35 sec need the response to achieve the system in stable region, (c) Electromagnetic torque of the BLDC machine operated under constant torque condition with PI control design, because of non-linear characteristics of conventional system has quite displaced in time frame.

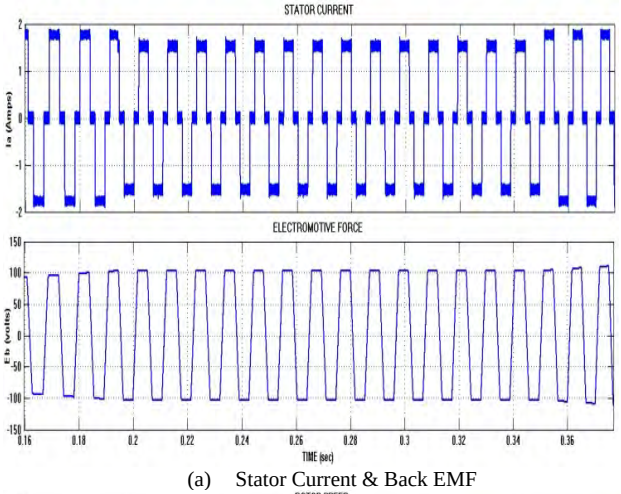


(a) Stator Current & Back EMF

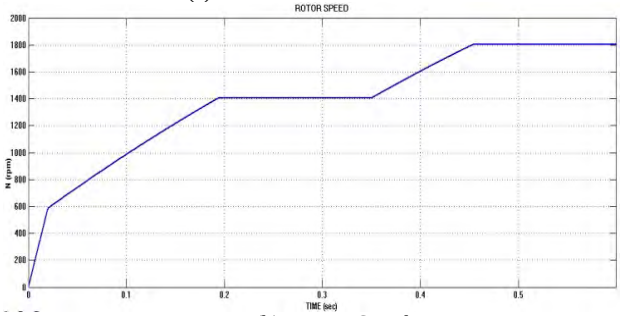


(b) Rotor Speed

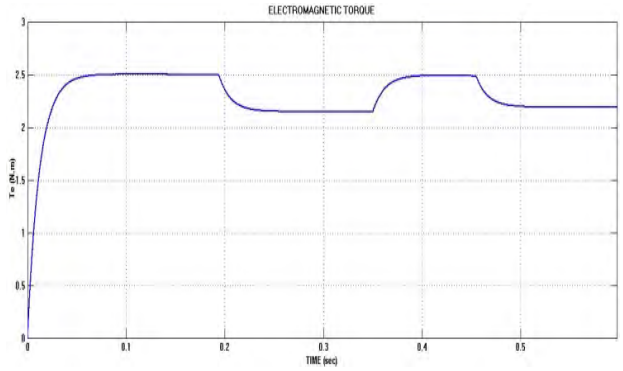


(c) Electromagnetic Torque

Figure 8 (a) Stator Current & Back EMFs, (b) Rotor Speed, (c) Electromagnetic Torque of the BLDC Drive operating under variable speed condition with PI control design.

Figure 8 shows the (a) stator current & back EMF of the BLDC drive, here back EMF as a trapezoidal shape with alignment of stator current operated under 120 (deg) mode at variable speed condition and these parameters also varied within a specified period, (b) Rotational speed of the BLDC drive at variable speed with PI regulator, due to non-linear gains attains some of error in steady state value merely 0.15 to 0.2 sec, need the response to achieve the system operation stable region, variable speed comes at 0.2 to 0.35 and 0.45 to 0.6 sec, (c) Electromagnetic torque of the BLDC machine operated under variable torque condition with PI control design, because of non-linear characteristics of conventional system has quite displaced in time frame.

*Case 2: Performance of BLDC Drive Operating under Fuzzy Controller*

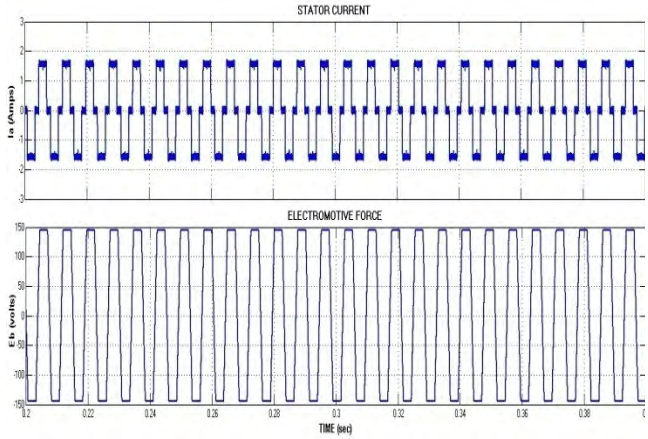


(a) Stator Current & Back EMFs

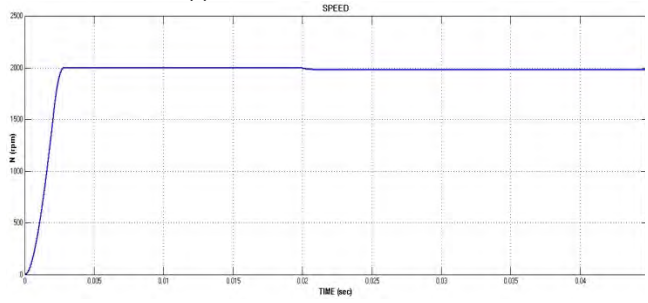


(b) Rotor Speed

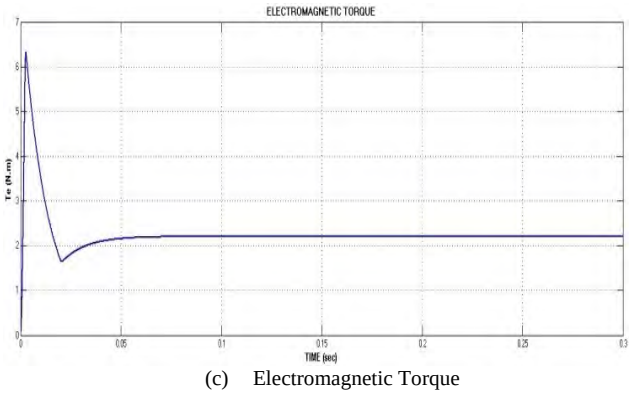


(c) Electromagnetic Torque

Figure 9 (a) Stator Current & Back EMFs, (b) Rotor Speed, (c) Electromagnetic Torque of the BLDC Drive operating under constant speed condition with Fuzzy control design.

Figure 9 shows the (a) stator current & back EMF of the BLDC drive, here back EMF as a trapezoidal shape with alignment of stator current operated under 120 (deg) mode, (b) Rotational speed of the BLDC drive at constant speed with Fuzzy controller, due to supportive gains system attains some of minimized error in steady state value merely 0.02 sec need the response to achieve the system in stable region, (c) Electromagnetic torque of the BLDC machine operated under constant torque condition with Fuzzy control design, because of optimal characteristics of classical Fuzzy system has quite displaced in time frame.

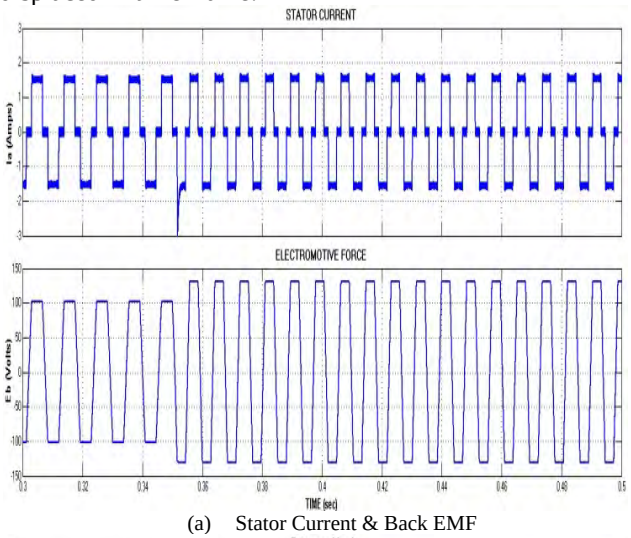


(a) Stator Current & Back EMF

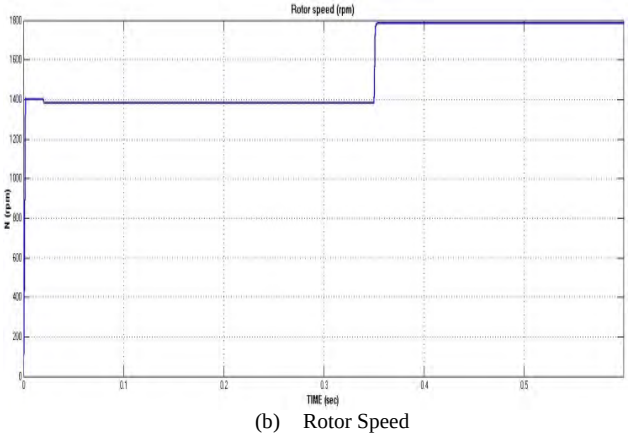


(b) Rotor Speed

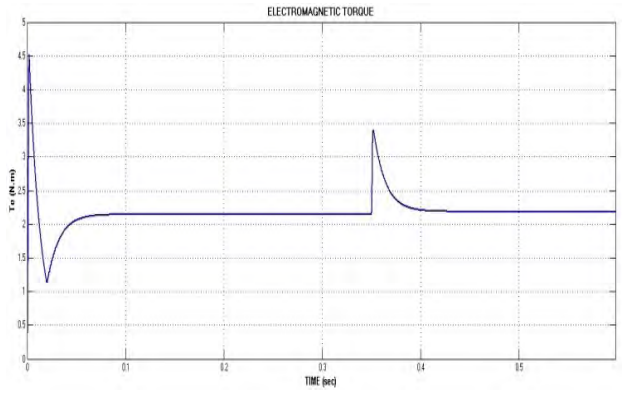


(c) Electromagnetic Torque

Figure 10 (a) Stator Current & Back EMFs, (b) Rotor Speed, (c) Electromagnetic Torque of the BLDC Drive operating under variable speed condition with Fuzzy control design.

Figure 10 shows the (a) stator current & back EMF of the BLDC drive, here back EMF as a trapezoidal shape with alignment of stator current operated under 120 (deg) mode at variable speed condition and these parameters also varied within a specified period, (b) Rotational speed of the BLDC drive at variable speed with Fuzzy regulator, due to non-linear gains attains some of error in steady state value merely 0.1 sec, need the response to achieve the system operation stable region, variable speed comes at 0.2 to 0.35 and 0.45 to 0.6 sec, (c) Electromagnetic torque of the BLDC machine operated under variable torque condition with Fuzzy control design, because of optimal characteristics of conventional system has quite displaced in time frame.

*Case 3: Performance of BLDC Drive Operating under Fuzzy+PI Controller*

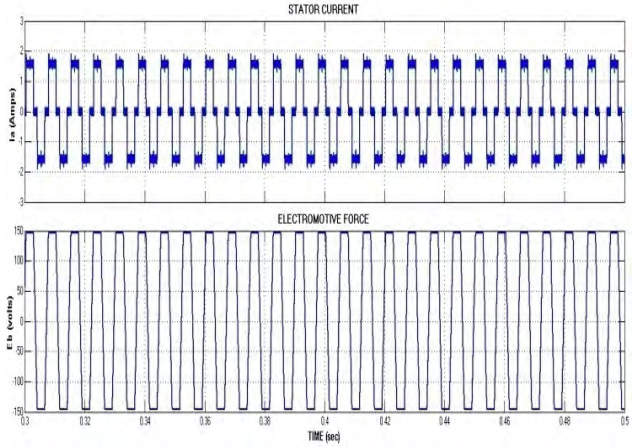


(a) Stator Current & Back EMFs

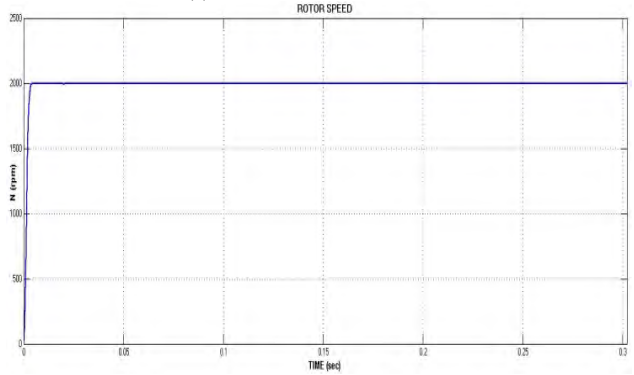


(b) Rotor Speed

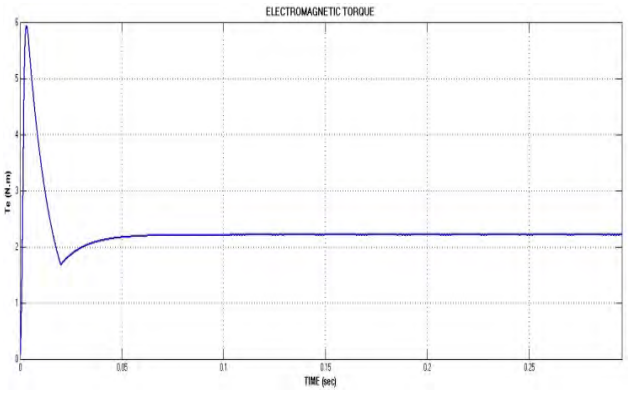


(c) Electromagnetic Torque

Figure 11 (a) Stator Current & Back EMFs, (b) Rotor Speed, (c) Electromagnetic Torque of the BLDC Drive operating under variable speed condition with Fuzzy+PI control design.

Figure 11 shows the (a) stator current & back EMF of the BLDC drive, here back EMF as a trapezoidal shape with alignment of stator current operated under 120 (deg) mode, (b) Rotational speed of the BLDC drive at constant speed with Fuzzy+PI controller, due to supportive gains system attains some of minimized error in steady state value merely 0.005 sec need the response to achieve the system in stable region, (c) Electromagnetic torque of the BLDC machine operated under constant torque condition with PI+Fuzzy control design, because of optimal characteristics of proposed PI+Fuzzy system has quite displaced in time frame.

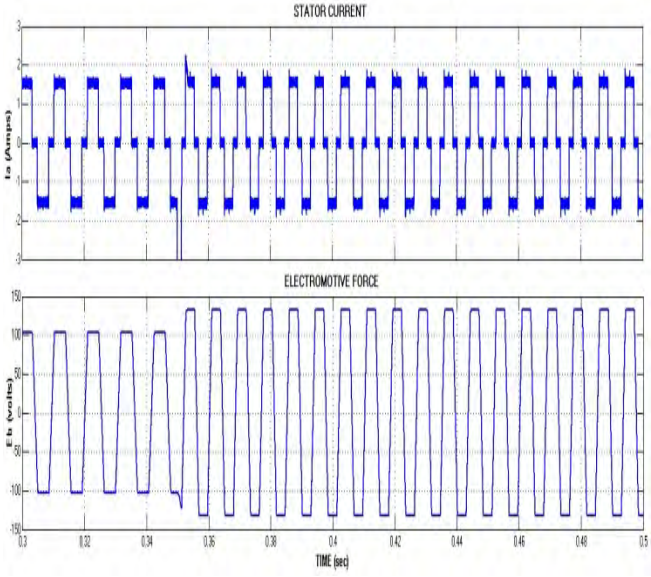


(a) Stator Current & Back EMFs

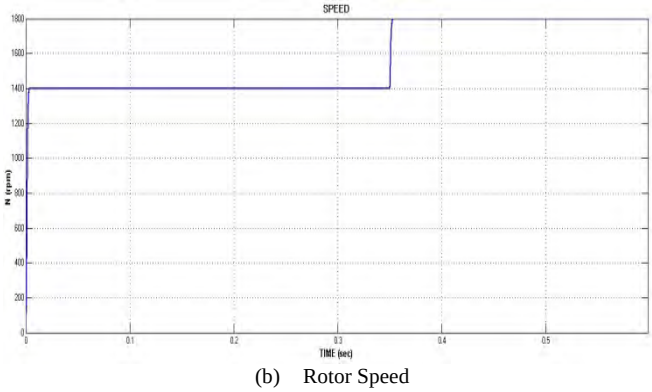


(b) Rotor Speed

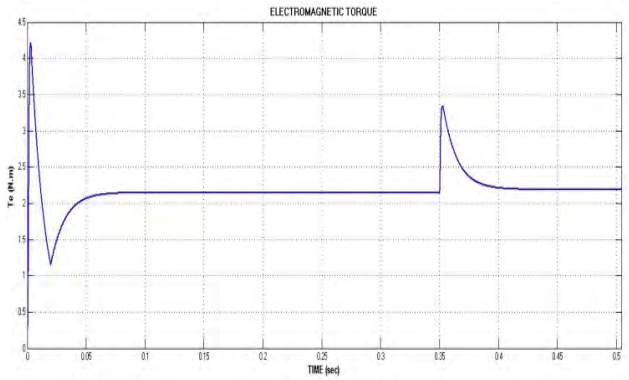


(c) Electromagnetic Torque

Figure 12 (a) Stator Current & Back EMFs, (b) Rotor Speed, (c) Electromagnetic Torque of the BLDC Drive operating under variable speed condition with Fuzzy+PI control design.

Figure 12 shows the (a) stator current & back EMF of the BLDC drive, here back EMF as a trapezoidal shape with alignment of stator current operated under 120 (deg) mode at variable speed condition and these parameters also varied within a specified period, (b) Rotational speed of the BLDC drive at variable speed with Fuzzy+PI regulator, due to imperative gains system attains minimized error in steady state value merely 0.05 sec compare to formal methods, need the response to achieve the system operation at stable region, variable speed comes at 0.2 to 0.35 and 0.45 to 0.6 sec, (c) Electromagnetic torque of the BLDC machine operated under variable torque condition with Fuzzy+PI control design, because of optimal characteristics of intended system has quite displaced in time frame.

Table III
Comparative analysis of formal PI controller, Fuzzy controller & PI+Fuzzy Controller of six switch converter fed BLDC drive operating under constant & variable speed condition

| S.No | Type of Controller | Constant Speed Condition | Variable Speed condition |
|---|---|---|---|
| 1 | Conventional PI Controller | 0.35 sec | 0.15 sec |
| 2 | Classical Fuzzy Controller | 0.02 sec | 0.1 sec |
| 3 | Proposed Fuzzy+PI Controller | 0.005 sec | 0.05 sec |

As table III depicts the Comparative analysis of formal PI controller, Fuzzy controller & PI+Fuzzy Controller of six switch converter fed BLDC drive operating under constant & variable speed condition. Compared to classical methods, proposed control strategic has better features about steady state condition, low settling time, low error values, with high stability factor would be applications to many industrial sector.

## 4.Conclusions

This paper highlights the double-layer closed loop control scheme of the six switch converter fed BLDC drive controlled by utilizing an extensive PI+Fuzzy controller with the help of powerful simulation tool operating under constant & variable speed range applications. By simulation results, PI controller has the features of more overshoot, high steady state error value to 0.35 sec obtain the dynamic response for constant speed condition, 0.15 for variable speed range, fuzzy controller has the features of average steady state values with a 0.02 sec for constant speed condition, 0.1 sec for variable speed range condition. This PI+Fuzzy controller reacts quickly with high static precision. Using this PI+Fuzzy controller accelerates the speed response of the BLDC drive. The optimal control characteristics of PI+Fuzzy fed BLDC drive have been optimized due to the profound significance for attaining high accuracy control actions.

## 5. References

[1] Park. S.J, Park. H.W, Lee. M. H and Harashima. F, " A new Approach for Minimum-Torque Ripples Maximum Efficiency Control of BLDC Motor", IEEE Trans. Ind. Electron., vol. 47, no. 1, pp. 109-114, Feb. 2000.

[2] Aghili. F, Buehler. M, Hollerbach. J. M, " Experimental Characterization and Quadratic Programming-Based Control of Brushless-Motors", IEEE Trans. Control Syst. Technol., vol. 11, no. 1, pp. 139-146.

[3] Murai. Y, Kawase. Y, Ohashi. K and Okuyamz. K " Torque Ripple Improvement for Brushless DC Miniature Motors" IEEE Trans. Ind. Appl., vol. 25, no. 3, pp. 441-449, May/Jun.1989.

[4] Delecluse. C and Grenier. D, " A Measurement Method of the Exact Variations of the Self and Mutual Inductances of a Buried Permanent Magnet Synchronous Motor and its Application to the Reduction of Torque Ripples" in Proc 5th International Workshop Adv. Motion Control, Coimbra, 1998, pp.191-197.

[5] Wallace. R. S, and Taylor. D.G, "Low Torque-Ripple Switched Reluctance Motors for Direct-Drive Robotics," IEEE Trans. Robot. Autom., vol. 7, no.6, pp.733-742, Dec. 1991.

[6] Newman. W.S and Patel. J.J, "Experiments in Torque Control of the Adept One Robot," in Proc, IEEE Int. Con. Robot. Atom, Sacramento, CA, Apr. 1991, pp. 1867-1872.

[7] Filicori. F, Bianco. C.G.L and Tonielli. A, "Modeling and Control Strategies for a Variable Reluctance Direct Drive Motor" IEEE Trans. Ind. Electron., vol.40, no.1. 105-115, jan 1993.

[8] Han-Xiong Li, "A Comparative Design and Tuning for Conventional Fuzzy Control", IEEE Trans on Systems, man, Cybernetics, part-B; vol. 27, no.5, Oct 1997.

[9] Wang. Y, Yali. Yu, G. Zhang, A. Sheng, " Fuzzy Auto-Adjust PID Controller Design of Brushless DC Motor", ICMPBE Elsevier Physics Proceedia, vol.33, 2013, pp. 1533-1539.

[10] J.EMuralidhar and Dr. P.Varanasi "Torque Ripple Minimization & Closed Loop Speed Control of BLDC Motor with Hysteresis Current Controller" SecondInternational Conference on Devices,Circuits and Systems (ICDCS'14) , March-2014 , pp.121-127

## Biographies

**J. E. MURALIDHAR** is working as Associate Professor in the Electrical Engineering Department, MuffakhamJah College of Engineering & Technology, Hyderabad. His research area includes Power Electronics and Drives.

**Dr. P. VARANASI** received his Doctorate from IIT Delhi. He worked as Professor in RIT Jamshedpur.
His research area includes Power Electronics and Drives, Digital Control of Motor Drives.